2015

# Study of UHF and VHF Compact Antennas

Abraham Loutridis
*Technological University Dublin*


# Study of UHF and VHF Compact Antennas

Abraham Loutridis

Doctor of Philosophy

Supervisors:
Prof. Max J. Ammann
Dr. Matthias John

Dublin Institute of Technology
School of Electrical & Electronic Engineering

July 2015

# Abstract

This thesis presents and describes designs of small antennas that operate in UHF and VHF frequency bands. The proposed antennas are designed for integration into small volumes, therefore low profile, compact size and good radiation properties are the key parameters in this work. A further investigation on miniaturization techniques, as well as the ground plane effects on the general performance, is also made.

The main objective is the design of novel compact sized geometries, lightweight and cost efficient, operating in the lower UHF and VHF frequency bands. The groundplane size and the antenna position with respect to it, are two parameters which are investigated and contribute to optimum design performance. Compact solutions are realised in this work based on folded, meander-line and inverted-F geometries providing broadband operation and omnidirectional radiation properties.

The investigation of broadband properties of a dual band folded monopole led to a controllable frequency-ratio with wide range, operating in the WLAN frequency spectrum. The proposed solution offers high efficiency and gain and stable omnidirectionality across the operating frequency band.

The study also deals with planar inverted-F antennas (PIFA) operating in the LTE frequency bands. The two highly efficient broadband antennas provide compactness, gain

stability and are fabricated using low-cost materials. By configuring an optimised position of the PIFA on the groundplane, the impedance bandwidth, the gain and the total efficiency can be significantly improved. A more compact solution of a dual band PIFA structure is provided with omnidirectional radiation characteristics and large frequency ratio for machine-to-machine applications.

A novel tuneable meander line structure operating over the frequency range of 412 − 475 MHz is designed for integration into smart meter devices. The resonant frequency of this antenna can be tuned using a sliding via connector. A matching stub is introduced into the proposed geometry to improve the impedance matching and to shift the resonant frequency to lower values. This innovative solution overcomes material loading problems when installed on a concrete wall, as well as the $S_{11}$ characteristic are not impaired with the small sized ground plane.

Finally, a dual band meander line folded monopole antenna in the lower UHF and VHF frequency bands is proposed for smart metering and Wireless M-Bus applications. The miniaturization of the proposed solution is based on a double-sided meandering structure which also offers good isolation between the two sections and an easily controlled large frequency-ratio. The introduction of a shunt lumped inductor improves the impedance matching at both frequencies. The antenna despite its compact size offers high total efficiency and gain across the operating frequency bands.

# Declaration

I certify that this thesis which I now submit for examination for the award of PhD, is entirely my own work and has not been taken from the work of others, save and to the extent that such work has been cited and acknowledged within the text of my work.

This thesis was prepared according to the regulations for postgraduate study by research of the Dublin Institute of Technology and has not been submitted in whole or in part for another award in any other third level institution.

The work reported on in this thesis conforms to the principles and requirements of the DIT's guidelines for ethics in research.

The Institution has permission to keep, to lend or to copy this thesis in whole or in part, on condition that any such use of the material of the thesis be duly acknowledged.

Signature: _____ Date _____

Abraham Loutridis

# Acknowledgements

I am sincerely thankful to my supervisors, Professor Max J. Ammann and Doctor Matthias John, for the guidance they provided me during the elaboration of my work. I would also like to thank them for the patience, the support and the encouragement shown to me all this time.

I thank all my colleagues at the Antenna and High Frequency Research Centre for their support and interesting discussions. In particular, I am very grateful to Giuseppe and to Kansheng for their assistance and our discussions regarding to issues related to antenna miniaturization techniques. I also wish to express my gratitude to my colleagues Padraig, Antoine, Xiulong, Afshin, Oisin, Adam and Domenico with whom I had the great pleasure to work and socialize for the last four years.

I thank my colleagues at the Centre for Telecommunications Value-Chain Research group for the extraordinary learning experience we shared those years. I am also very grateful to Science Foundation Ireland for supporting my research work.

My heartfelt thanks to all my friends here in Dublin and back in Greece for their invaluable company has been always greatly supportive and valuable to me.

Very special thanks go to my housemates Panos for our countless hours of philosophising and Rasa for making me feel at home all the time and for the great fun we had altogether during the last year of my studies.

I would like to express all my gratitude to my close family back in Greece for their lasting love. Finally, I dedicate this thesis to my parents, to my sister to my grandmother and to my brother in law for their support and love that they showed me all these years.

# Abbreviations

| | |
|---|---|
| AMR | Automatic Meter Reading |
| AUT | Antenna Under Test |
| CDMA | Code Division Multiple Access |
| CST | Computer Simulation Technology GmbH |
| ECC | Electronic Communication Committee |
| EIRP | Equivalent Isotropically Radiated Power |
| ESA | Electrically Small Antenna |
| FIT | Finite Integration Technique |
| GPRS | General Packet Radio Service |
| GSM | Global System for Mobiles |
| IEEE | Institute of Electrical and Electronic Engineers |
| LTE | Long Term Evolution |
| MWS | *CST* Microwave Studio |
| M2M | Machine-to-Machine |
| PCB | Printed Circuit Board |
| PCS | Personal Communication System |
| PIFA | Planar Inverted-F Antenna |
| RF | Radio Frequency |
| SGH | Standard Gain Horn |
| VNA | Vector Network Analyzer |
| VSWR | Voltage Standing Wave Ratio |
| WLAN | Wireless Local Area Network |

# Contents

# List of Figures

# List of Tables

# 1. Introduction

The rapid evolution of wireless cellular communications started with the deployment of the 1st generation of mobile networks in the early 1980s and led to the requirement for compact terminal antennas. The new communication systems and newly introduced applications operating at frequencies in the ultra-high frequency (UHF) and super-high frequency (SFH) bands (Table 1.1) set strict requirements for the antenna in terms of size and efficiency. The portability and mobility of wireless technology demands compact and handheld devices with small enough size to be easily carried, of light weight and with low cost.

Dipole and monopole antennas were the two most practically used antennas types for wireless communication systems in the early stage of their development. The broadband radiation characteristics and manufacturing simplicity made monopoles the most widely used antennas for portable devices such as mobile and cordless phones, laptops, wireless metering devices, etc. The introduction of Global System for Mobiles (GSM), General packet radio service (GPRS) and other mobile services such as Wireless Local Area Network (WLAN), Bluetooth, ad-hoc networks, etc. (Table 1.2) as well the availability

of the frequency spectrum generated further specifications and requirements for antenna designers.

In 1889, Heinrich Hertz was the first developer of a wireless communication system in which he forced an electrical spark to occur in the gap of a dipole antenna. For the receiver he used a loop antenna. By 1901, Marconi was transmitting data across the Atlantic Ocean by using several vertical wires attached to the ground. Across the Atlantic Ocean, the receive antenna was a 200 meter wire held up by a kite [1]. Since then, an extensive evolution of electrically small antennas (ESA) and compact integrated antennas followed making it one of the important elements that make modern wireless devices possible.

Modern mobile communication applications require large available channel capacity, large quantities of transmitting data, high efficiency, flexibility and capability to handle multiband frequencies. Modern mobile terminals define additional requirements for the antennas used, like compact size, low profile and low-cost, omnidirectional radiation characteristics, adopted low and safe levels of Specific Absorption Rate (SAR) values [2, 3] for devices operating within close proximity to the human body as specified in [4]. The trend in universal wireless access connectivity and the compatibility of different devices drive the motivation for miniaturization of antennas able to work well across a broadband bandwidth with good efficiency.

Nowadays, wireless communication technology (Fig. 1.1) has replaced the wired networks in an efficient way, increasing the distance beyond the capabilities of typical cabling. Wireless communication technology is used to meet many needs such as:

- To provide a backup connection in case of network failure,
- To link portable or temporary workstations,
- To overcome problems where cabling is difficult or financially impractical,
- To remotely connect mobile users or networks.

A large range of wireless applications involves home security systems, Wi-Fi, cellular phones, wireless power transfer, wireless sensors and smart meters. The implementation and optimization of existing wireless technology can be addressed also in automotive, airborne and medical applications offering reliability and low operating cost.

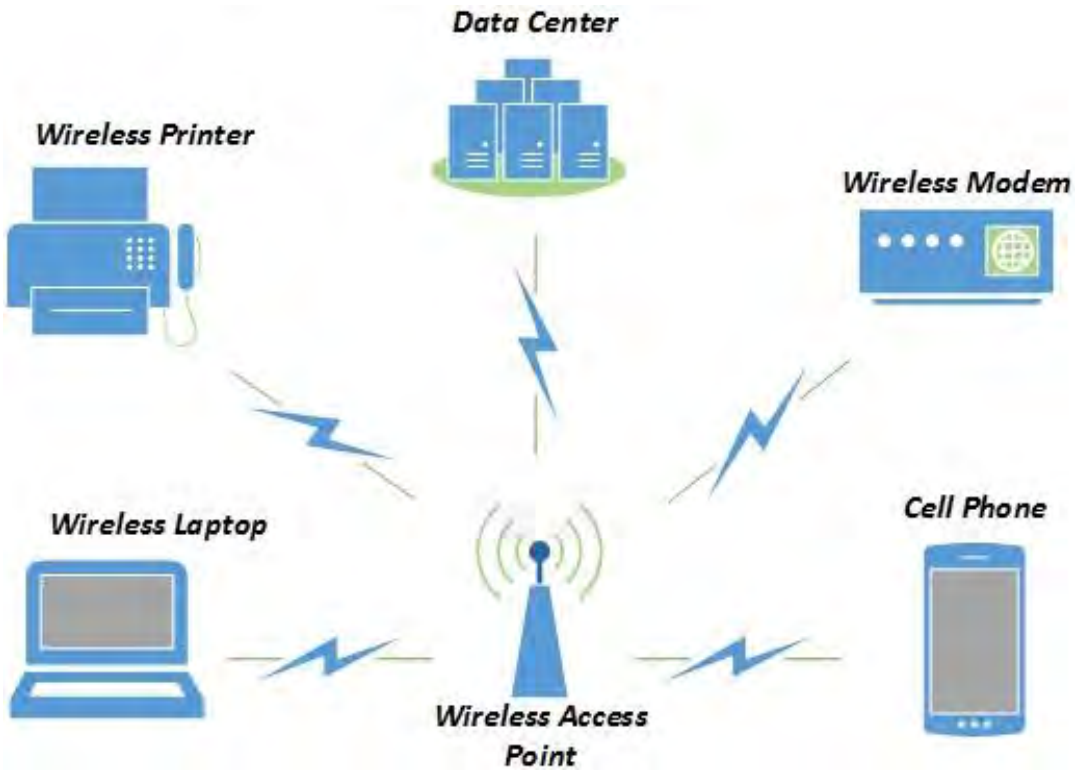


**Figure 1.1. Wireless Communication Technology.**

**Table 1.1. The frequency spectrum.**

| Band | Frequencies | | Wavelengths* | |
|---|---|---|---|---|
| VLF | 3 kHz | 30 kHz | 100 km | 10 km |
| LF | 30 kHz | 300 kHz | 10 km | 1 km |
| ML | 300 kHz | 3 MHz | 1 km | 100 m |
| HF | 3 MHz | 30 MHz | 100 m | 10 m |
| VHF | 30 MHz | 300 MHz | 10 m | 1 m |
| UHF | 300 MHz | 3 GHz | 1 m | 10 cm |
| SHF | 3 GHz | 30 GHz | 1 cm | 1 mm |

*Wavelength: $\lambda(m) = 300/f(MHz) \Rightarrow \lambda(cm) = 30/f(GHz)$

**Table 1.2. Wireless Communication Frequency Spectrum.**

| Wireless System | Frequency Range |
|---|---|
| AM/FM Radio | 535-1605 KHz/88-108 MHz |
| Broadcast TV (Ch. 2-6) | 54-88 MHz |
| Broadcast TV (Ch. 7-13) | 174-216 MHz |
| ISM Band (LPD433) | 433.05-434.79 MHz |
| DVB-T/TVWS (UHF) | 470-862 MHz |
| 1G/2G Cell Phones | 806-902 MHz/1.85-1.99 GHz |
| 3G UMTS | 746-798 MHz, 814-894 MHz |
| 3G UMTS | 1.7-1.85 GHz, 2.5-2.69 GHz |
| Satellite Digital Radio | 2.32-2.325 GHz |
| 4G LTE | 690-960 MHz, 1.7-2.69 GHz |
| ISM Band (Bluetooth, 802.11b WLAN) | 2.4-2.4835 GHz |
| 5.8 GHz ISM Band | 5.725-5.875 GHz |
| Digital Broadcast Satellite | 12.2-12.7 GHz |
| Local Multipoint Distribution Service (LMDS) | 27.5-29.5 GHz, 31-31.3 GHz |
| Fixed Wireless Services | 38.6-40 GHz |

## 1.1 ELECTRICALLY SMALL ANTENNAS

In according to Harold A. Wheeler, a small antenna is one in which the maximum dimension is less than the "radianlength". The radianlength is equal to 1/2π wavelength [5]. Another expression to define a compact antenna is that it fulfils the condition $ka<1$, which $k=2\pi/\lambda$ where, $a$ is the radius of the minimum sphere (radiansphere) [6] that encloses the antenna (Fig. 1.1). For over 60 years, extensive research took place on the theoretical and practical field of fundamental limitations and small antennas by Chu [7], Wheeler [5, 6], Harrington [8], Fano [9] and other pioneers providing facts and results which are invaluable for the antenna engineers.

Over the years new miniaturization techniques have been documented to reduce the size of an antenna for a given frequency. Using high dielectric constant substrates enables more miniaturization as more of the antenna fields are coupled in the substrate [1, 10]. A variety of different folded [11, 12, 13, 14], spiral [15, 16], fractal [17, 18, 19, 20] and meander line [21, 22, 23, 24] geometries are reported in order to reduce the antenna size.

Antenna designers also employ lumped elements (capacitors and inductors) and varactor diodes [25, 26, 27, 28, 29] to improve impedance matching and antenna bandwidth as well to control the resonant frequency. Lumped elements can be used to achieve a good impedance matching to the source but they introduce additional losses into the antenna system. On the other hand, incomplete matching is more critical and has stronger impact on the antenna total efficiency than inserted losses from lumped elements. Despite of this disadvantage, these kind of compact antennas with external matching networks exist in many real applications because of their simple design methodology.

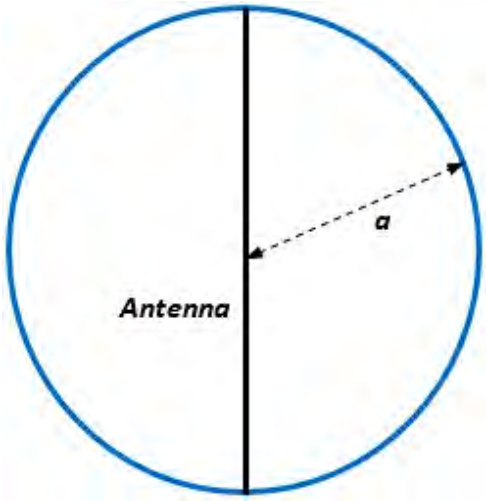


**Figure 1.2. The radiansphere.**

## 1.2 Antenna Requirements for Wireless Communication Systems

Monopole antennas have been used as the best choice for various portable and mobile equipments. The simplicity of the antenna design, the fulfilment of the performance specifications, particularly with respect to bandwidth and efficiency, are the basic criteria for the antenna designers to create electrically small antennas that are compatible with modern wireless technology, which will also operate on a small ground plane.

The ongoing evolution of wireless communication and the demand for high speed and high quality data transfer using portable and personal communication (PCS) services [30, 31] has led to the need for a reorientation of antenna design specifications as a basic part of any wireless system. The modern handheld devices require antennas which are embedded on a small area, a relatively short distance from a user body tissue operating in accordance with Electromagnetic Compatibility (EMC) Regulations.

Modern wireless units tend to have small and compact size, low-cost manufacturability, flexibility to integrate with the wireless communication system and an omnidirectional radiation performance in at least one plane. The consideration of frequency of operation, impedance matching, broadband or wideband operation, high gain and efficiency, omnidirectional radiation pattern, ground plane size and Specific Absorption Rate (SAR) are the fundamental electrical characteristics that drove the designers to introduce a wide variety of antenna structures and topologies to balance the particular demands for modern wireless communication systems.

## 1.3 MOTIVATION FOR ELECTRICALLY SMALL ANTENNAS

At its resonant frequency $f_0$, the length $L$ of the half-wavelength (λ/2) dipole is equal to a half of the wavelength $\lambda_0$. The quarter-wavelength (λ/4) vertical monopole consists of one arm of a half-wavelength (λ/2) dipole, placed on a horizontal ground plane (Fig. 1.3).

Monopoles and dipoles have good radiation properties but for a 4G mobile phone which operates at 800 MHz, a quarter-wavelength (λ/4) is almost 9.4 cm, hence a typical dipole would not be suitable to embed in a modern portable device.

Moreover, some constrains such as the narrow bandwidth (up to 10% FBW) performance, as well as the balanced feeding, (need for baluns in some cases) and the protrusive and extended structure make them less attractive solutions for compact designs especially for low frequencies.

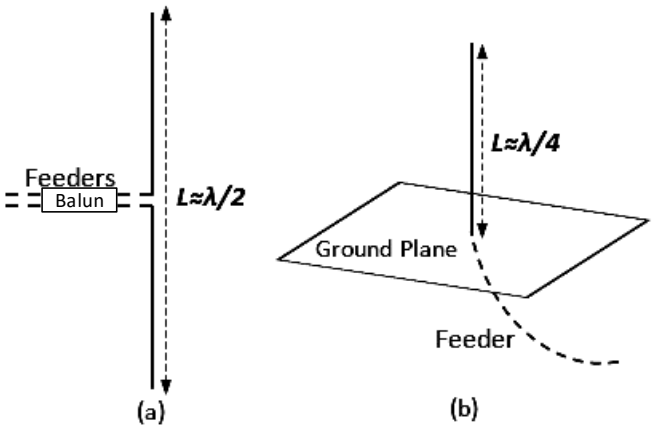


**Figure 1.3. (a) λ/2 dipole, (b) λ/4 monopole on a ground plane.**

Miniaturization techniques and methods enable antenna designers to enclose monopole antennas with large electrical length into a compact physical size. Electrically small and compact antennas including monopoles, dipoles, normal-mode helix antennas [32, 33], planar inverted-F antennas (PIFA's) [34, 35, 36, 37, 38], microstrip patches [39, 40] and meander line antennas [21, 22, 23, 24] used mostly for small terminals and handheld units. Additionally, miniaturization techniques give more freedom to the available space and allow the integration of other components on the same Printed Circuit Board (PCB). The low manufacturing cost is favoured from this integration.

This thesis presents an investigation of electrically small and compact antennas and the use of miniaturization techniques. A variety of topologies that include folded and meander-line monopoles and Planar Inverted-F Antennas (PIFA's) are designed and studied, as well an extensive investigation of the ground plane size which is an integral part of the electrically small antennas. Miniaturisation techniques are analysed and

developed for application to antennas which are ready to be integrated into different types of mobile and compact units.

## 1.4 Outline of the Thesis

Initially, in Chapter 2 an overview of dipole, monopole, PIFA and meander line antennas is provided. A theoretical background on the operation principle of antennas is also presented. The simulation software, prototyping method, measurement setup and techniques used in the thesis are introduced and described.

A printed folded monopole antenna for WLAN applications is investigated in Chapter 3. The effects of key geometrical parameters of the monopole and the role of the ground plane size in the general performance of the antenna are studied.

In Chapter 4, two LTE Planar Inverted-F Antennas (PIFAs) for M2M application are introduced. Both configurations are optimised and developed for better impedance matching and bandwidth. The PIFA position on the ground plane and the ground plane size are investigated.

Chapter 5 deals with the design of a novel tuneable meander line monopole operating in the lower UHF band. A parametric study of the ground plane size is made and the antenna is optimised for impedance matching. The installed performance of the monopole embedded in a plastic housing and placed on a concrete wall is investigated.

A dual-band meander-line monopole operating in VHF and lower UHF bands for smart meters is presented in Chapter 6. The proposed design is optimised in both frequency bands for impedance matching. A geometrical parametric investigation is made

and the frequency-ratio performance is also reported. The radiation and total efficiency of proposed antenna is measured based on the Wheeler Cap Method providing good agreement with the simulated results.

Chapter 7 gives conclusions and outlines as well as possibilities for future work. A List of Journal and Conference Publications are listed in chronological order given in Appendix A.

The novelty which is provided in this work is summarized in the following paragraph. A compact low profile dual band folded monopole for WLAN applications enable to control large frequency ratio with more than 90% efficiency and 2 dBi gain across the two bands is presented. In an effort to move to lower frequencies and to maintain the compact size of the design, two LTE PIFAs with large and easily controlled frequency ratio ranges are provided with more than 80% efficiency and 2 dBi gain across the operating frequency range. A novel forked feed is introduced providing compactness. A tuneable novel UHF meander line monopole for M2M applications with very compact size and with good and stable efficiency (21%-24%) across the tuneable band is proposed. The tuneability of the antenna is based on a novel tuneable sliding via connector which controls the antenna electrical length offering adjustability to its radiation performance. Finally, the first dual band printed meander line monopole antenna is presented operating at 169 MHz and 433 MHz offering more than 20% and 50% efficiency at the first and second resonant frequencies, respectively.

# 2. Background

An antenna can be defined as an electrical device which converts electric power into radio waves and vice versa [41]. The IEEE defines the antenna as a means for radiating or receiving radio waves [42]. In this chapter the definitions of fundamental parameters and performance metrics of an antenna are given.

The design and software simulation tools used in this work are presented. Additionally, facilities used for the analysis, fabrication and measurement of the proposed antennas are described.

## 2.1 Antenna Theory

### 2.1.1 Dipole and Monopole Antennas

A dipole antenna is the simplest and most widely used antenna type which consists of two identical conductive wires. Between the two halves of the dipole, a current source is applied, connected to the two adjacent ends. Dipole antennas are resonant, with the current flowing back and forth between the ends of the two elements. A half-wave dipole has two wire elements of approximately a quarter wavelength long (λ/4). In Fig. 2.1 a half

wave and a full wave dipole with their voltage and current distribution along the two structures is shown.

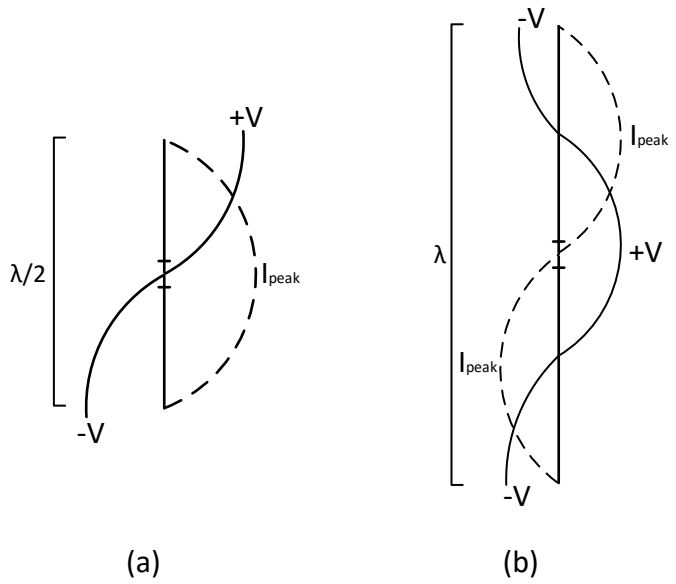


**Figure 2.1. Voltage and Current distribution of (a) half wave and (b) full wave dipole.**

The basic principle of a conventional quarter wavelength (*λ/4*) monopole mounted over a ground plane is that the length *L,* is equal to a quarter of the wavelength *λ/4* at its fundamental resonant frequency $f_0$ ($L_0 = \lambda_0/4, f_0 = 1/\lambda_0 \Rightarrow \lambda_0 = 1/f_0$) [1]. Fig 2.2 below shows the corresponding voltage and current distribution along a quarter wavelength monopole structure. The reflections from the ground plane produce a virtual identical monopole below it (mirror effect) and the monopole antenna can be evaluated in much the same way as dipole antenna.

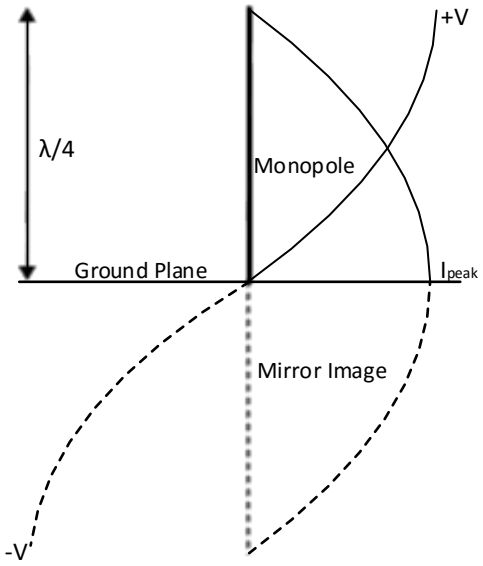


**Figure 2.2. Voltage and Current distribution of quarter wave monopole.**

The radiation pattern for the monopole antenna is strongly affected by a finite sized ground plane while its impedance is minimally affected [43]. Whereas a ground plane with diameter of 10λ or larger (infinite size) has a fairly small effect on the feed-point impedance of a monopole antenna [44].

### 2.1.2 PLANAR INVERTED-F ANTENNAS

Planar Inverted-F Antennas (PIFAs) are a widely used terminal antenna type with many advantages which make them suitable for integration in portable and compact devices [45]. The evolution of the PIFA design [46, 47, 48] can be started from a quarter wavelength (λ/4) wire monopole (Fig. 2.3 (a)) which is placed above a ground plane and it is folded by 90° as it shown in Fig. 2.3 (b). By connecting the monopole to the ground plane through a shorting pin, a significant impedance matching improvement can be

achieved. The overall height is reduced while the antenna maintains the good performance.

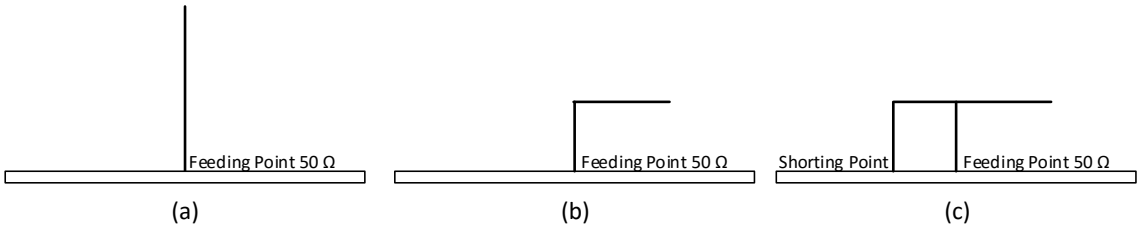


**Figure 2.3. The evolution of the PIFA design.**

Finally, the bandwidth of the antenna can be improved if the wire is replaced by a planar radiating patch, as it shown in Fig. 2.4.

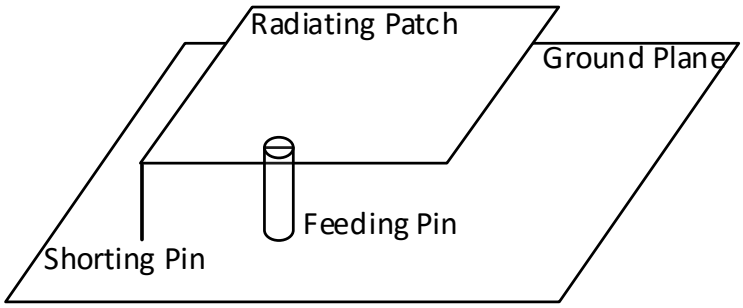


**Figure 2.4. Planar Inverted-F Antenna (PIFA) structure.**

### 2.1.3 MEANDER LINE ANTENNAS

Meander Line Antennas [49, 50, 51] are a type of monopole antenna which can achieve miniaturization in size. The starting evolution point of the basic meander

monopole design is achieved by folding the conductor back and forth, decreasing the overall height of the antenna and introducing more wire into the structure (Fig. 2.5).

A meander line monopole is a set of horizontal and vertical wires which form turns. For a fixed wired length, as the number of turns increases, the antenna volume decreases and as the separation between the wires increases, the resonant frequency decreases [23].

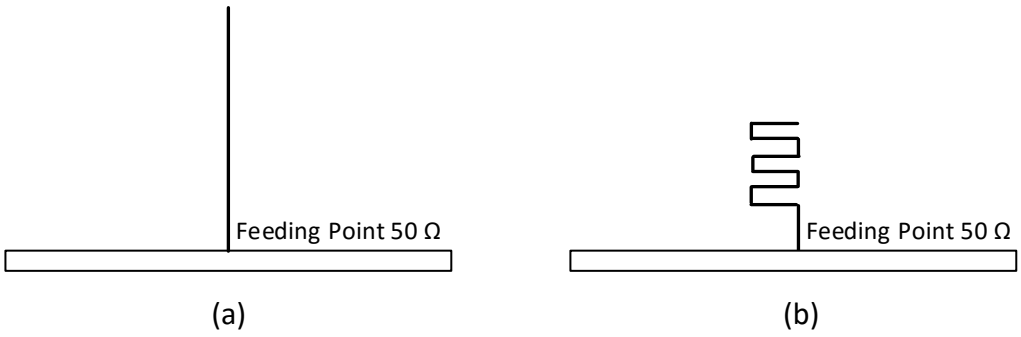


**Figure 2.5. Meander Line Monopole Antenna structure.**

## 2.1.4 INPUT IMPEDANCE

The antenna input impedance $Z_i(f)$ relates the voltage and current at the antenna input port. The real part $R_i(f)$ of the input impedance represents the power that the antenna radiates or absorbs. The imaginary part $jX_i(f)$ of the input impedance represents the power that is stored in the near field of the antenna. The input impedance is frequency dependent [52]:

$$Z_i(f) = R_i(f) + jX_i(f) \tag{2.1}$$

### 2.1.5 Return Loss and Bandwidth

The return loss is the ratio that compares the power reflected $P_r$ at the antenna port to the power $P_i$ that is fed into the antenna from the transmission line. It is usually expressed as a ratio in decibels (dB):

$$RL(dB) = 10 \log P_i/P_r \tag{2.2}$$

The return loss is also expressed as the negative of the magnitude of the reflection coefficient in dB,

$$RL(dB) = -20 \log|\Gamma|, \tag{2.3}$$

where the reflection coefficient is given by

$$\Gamma = \frac{Z_i - Z_0}{Z_i + Z_0} \tag{2.4}$$

The return loss is related to the voltage standing wave ratio (VSWR) and expressed by the following equation:

$$VSWR = \frac{1 + |\Gamma|}{1 - |\Gamma|} \tag{2.5}$$

The impedance bandwidth (BW) is another fundamental antenna parameter. It describes the frequency range over which the antenna has a return loss remains below −10 dB (VSWR 2:1). For electrically small antennas which operate at relatively low frequencies, a return loss below −6 dB (VSWR 3:1) is acceptable. The fractional bandwidth (FBW) is the ratio of the bandwidth divided by the centre frequency and is given by:

$$FBW = \frac{f_u - f_l}{f_0} \times 100\%, \quad (2.6)$$

where $f_u$ is the upper frequency and $f_l$ is the lower frequency.

## 2.1.6 RADIATION PATTERN

The radiation pattern of an antenna is the three dimensional spatial distribution of radiated energy as a function of the antenna position along a constant radius [1]. Radiation properties include radiation intensity, field strength, phase and polarization.

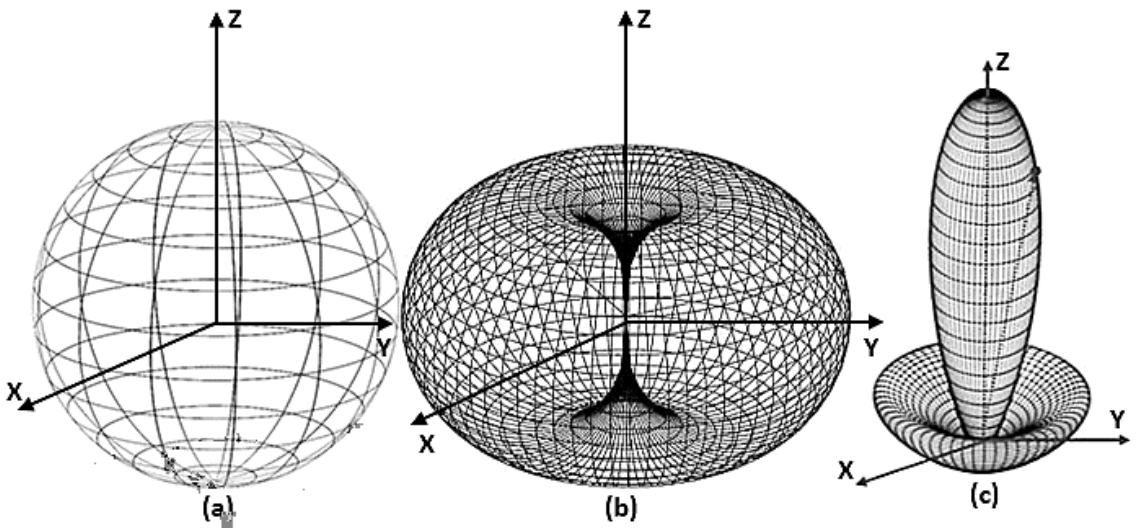


**Figure 2.6. The three radiation pattern types (a) isotropic, (b) omnidirectional and (c) directional [1].**

An antenna with isotropic radiation pattern is an ideal antenna having equal radiation in all directions. A directional antenna radiates more effectively in some directions than in others. Some antennas may also be described as omnidirectional which have an

isotropic radiation pattern in a single plane. An example of omnidirectional antenna is the dipole antenna (Figure 2.6 (b)).

### 2.1.7 DIRECTIVITY AND GAIN

The antenna directivity $D$ is defined the ratio of the radiation intensity in a certain direction to the radiation intensity of an isotropic radiator [1]:

$$D = \frac{U}{U_0} = \frac{4\pi U}{P_{rad}}, \tag{2.7}$$

where $U$ is the radiation intensity, $U_0$ is the radiation intensity of the isotropic radiator and $P_{rad}$ is the total radiated power.

The antenna gain $G$ is related to directivity $D$ and to the radiation efficiency $\eta$ of an antenna [1]

$$G(\theta, \varphi) = \eta \times D(\theta, \varphi) \tag{2.8}$$

The antenna gain is usually expressed in dBi and signifies the ratio of radiated power in a given direction relative to that of an isotropic radiator which is radiating the electrical power uniformly in all directions.

According to the IEEE standards, gain does not include losses arising from impedance and polarization mismatches [53]. The term realized gain is used when mismatch effects are included.

### 2.1.8 ANTENNA EFFICIENCY

The antenna radiation efficiency $\eta$ is defined as the ratio of radiated power $P_{rad}$ to the power delivered (input power) $P_{input}$ to the antenna:

$$\eta = \frac{P_{radiated}}{P_{input}} \tag{2.9}$$

An efficient antenna radiates most of the input power. An inefficient antenna has more of the power absorbed as losses within the antenna. The losses can be due to limited conductivity of the antenna or due to dielectric losses.

The Total Efficiency $\eta_T$ of an antenna is the Radiation Efficiency $\eta$ multiplied by the impedance mismatch loss $(1 - |\Gamma|^2)$ of the antenna:

$$\eta_T = (1 - |\Gamma|^2) \times \eta \tag{2.10}$$

For electrically small antennas, 40 to 50% (−3.9 to −3 dB) of Total Efficiency is usually the acceptable level in the design phase and it is challenging to obtain a fully embedded antenna.

### 2.1.9 FUNDAMENTAL LIMITATIONS OF ELECTRICALLY SMALL ANTENNAS

In recent years there has been some emphasis on establishing a link between the volume occupied by an electrically small antenna and the Quality Factor (Q) and its bandwidth (BW). Early studies on the fundamental limitations and performance of small antennas were published by Harold Wheeler [5, 6]. Chu determined the lowest possible Quality Factor Q (2.11) of a linearly-polarized omnidirectional antenna and introduced the concept of maximal and practical gain [7]:

$$Q > \frac{1}{k^3a^3} + \frac{1}{ka}, \tag{2.11}$$

where $k$ is the wave number in free space, $k=2\pi/\lambda$ and $a$ is the radius of the minimum sphere that encloses the antenna.

Following Chu's work and same principle for a circularly-polarized antenna, McLean obtains the smallest possible Q [53]:

$$Q = \frac{1}{2}\left[\left(\frac{1}{ka}\right)^3 + \frac{2}{ka}\right], \tag{2.12}$$

In 1958, Harrington [8] extended Chu's previous obtained results and defined the natural gain limit for a practical antenna:

$$G_{max} = (ka)^2 + (ka), \tag{2.13}$$

Based on the theory of the evaluation of the energy stored around the antenna, Fano [9], Collin [55] and Fante [56] derived expressions for the radiation Q which verify Chu's earlier results.

The theoretical investigation on the fundamental limits of an electrically small antenna expands to the relationship between the bandwidth (BW) which is an important parameter for antennas and the Quality Factor (Q). Considering the antenna as a resonant RLC circuit, the Fractional Bandwidth (FBW) can be defined by:

$$FBW = \frac{1}{Q} \tag{2.14}$$

In practice, an antenna's Fractional Bandwidth is also defined in terms of VSWR. The relationship between Q and VSWR is given by:

$$Q = \frac{VSWR - 1}{FBW\sqrt{VSWR}} \tag{2.15}$$

Fano introduced an expression for the maximum Fractional Bandwidth that can be achieved with a lossless matching network that matches to a resonant circuit (antenna) [9].

$$FBW = \frac{27}{Q}\frac{1}{RL}, \tag{2.16}$$

where RL is the desired return loss.

### 2.1.10 WHEELER CAP METHOD

One of the simplest, cheapest and most accurate methods to determine the antenna radiation efficiency is the Wheeler Cap method which was presented by H. A. Wheeler in 1959 [6]. Harold Wheeler presented a method for measuring the efficiency of electrically small antennas (ESAs) and it is more accurate compared with other methods, such as, gain comparison, radiometric and pattern integration.

The wheeler cap method is based on the "radiansphere" concept which defines the boundary between the near field and the far field of any small antenna (Fig. 2.7). The distance between the Antenna Under Test (AUT) and the walls of wheeler cap is called "radianlength" and it is λ/2π. The measurement procedure separates into two parts which are without cap (measurement in free space) and with cap and they will respectively determine the radiation resistance and loss resistance (Fig. 2.7). The cap consists of a conducting radiation metal shield.

Wheeler suggested that the placement of the antenna within a conductive cavity would reduce the radiation in the far-field without affecting the losses of the antenna. The method is based on the assumption that the placement of the antenna into the cavity shorts the radiation resistance $R_{rad}$, while the losses $R_{loss}$ remains constant. Wheeler indicates that the size of the cavity must be very large to avoid the excitations of the near-field and small enough to prevent the emergence of resonances at the frequency of measurement.

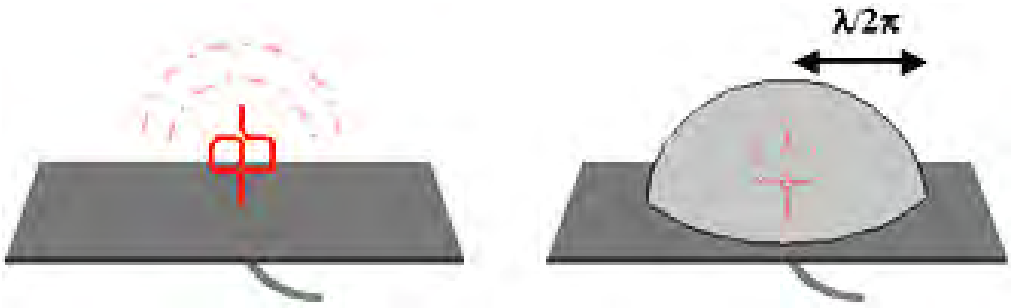


**Figure 2.7. Measurement Wheeler Cap method [57].**

In the practice, there are many factors that influence the measurement accuracy, such as the thickness of the shield and the reflections by walls, floor and ceiling of the room if the measurements is made indoors. Otherwise, the choice of material and shape of the caps will affect results during measurement.

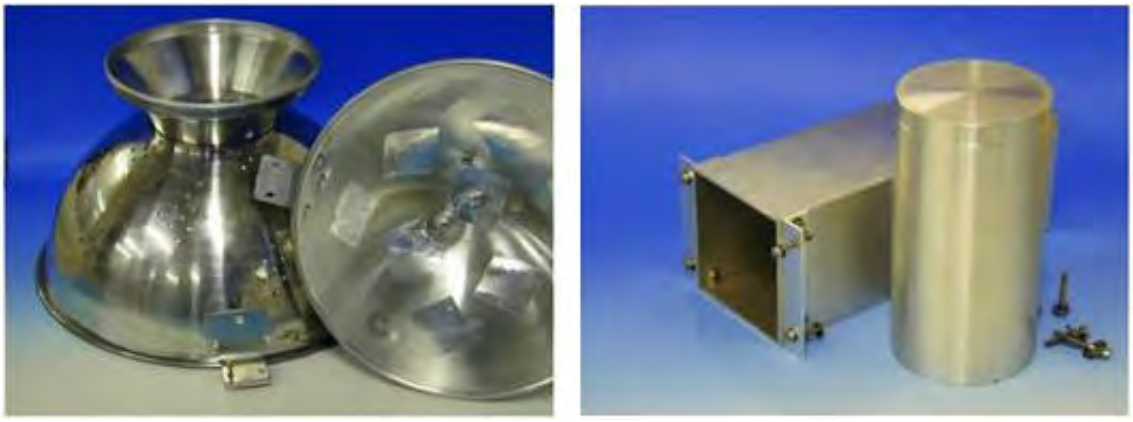

**Figure 2.8. Different shapes of shields is used in the Wheeler Cap method [57].**

- ***The Constant Power Loss Method***

The radiation efficiency can be defined as radiated power is directly proportional to input power, where input power is the sum of radiated power and loss power. Thus the radiation efficiency, $\eta$, is given by:

$$\eta = \frac{P_{rad}}{P_{rad}+P_{loss}} = \frac{I^2 R_{rad}}{I^2 R_{rad}+I^2 R_{loss}} = \frac{R_{rad}}{R_{rad}+R_{loss}}, \quad (2.17)$$

where

$P_{rad}$ is radiation power of antenna

$P_{in}$ is input power

$P_{loss}$ is loss power (reflection power)

$I$ is the input current

$R_{rad}$ is radiation resistance of antenna

$R_{loss}$ is loss resistance.

With the Wheeler Cap on, the radiation resistance is zero and the antenna reflection coefficient is measured and referred to as $\boldsymbol{S_{11WC}}$.

$$\frac{P_{loss}}{P_{in}} = 1 - S^2_{11WC} \tag{2.18}$$

Without the Wheeler Cap the radiation resistance is that of the antenna radiating into free space and the antenna reflection coefficient is measured and referred to as $S_{11FS}$.

$$\frac{P_{rad}+P_{loss}}{P_{in}} = 1 - S^2_{11FS} \tag{2.19}$$

The antenna efficiency becomes

$$\eta = \frac{P_{rad}}{P_{rad}+P_{loss}} = \frac{(1-|S_{11FS}|^2)-(1-|S_{11WC}|^2)}{(1-|S_{11FS}|^2)} = \frac{|S_{11WC}|^2-|S_{11FS}|^2}{1-|S_{11FS}|^2} \tag{2.20}$$

- ***The Constant Loss Resistor Method***

Also, the antenna reflection coefficient $S_{11WC}$ can be represented as

$$S_{11WC} = (R_{loss}-R_s)/(R_{loss}+R_s) \tag{2.21}$$

The antenna reflection coefficient $S_{11FS}$ can be represented as

$$S_{11FS} = ((R_{rad}+R_{loss})-R_s)/((R_{rad}+R_{loss})+R_s), \tag{2.22}$$

where $R_s$ is the source resistance.

Equations (2.17), (2.21) and (2.22) are transposed to become

$$R_{loss}/R_s = (1+S_{11WC})/(1-S_{11WC}) \tag{2.23}$$

$$((R_{rad}+R_{loss}))/R_s = (1+S_{11FS})/(1-S_{11FS}) \tag{2.24}$$

The radiation efficiency now is

$$\eta = \frac{R_{rad}}{R_{rad}+R_{loss}} = \frac{\left(\frac{1+S_{11FS}}{1-S_{11FS}}\right)-\left(\frac{1+S_{11WC}}{1-S_{11WC}}\right)}{\left(\frac{1+S_{11FS}}{1-S_{11FS}}\right)} = 1-\frac{(1-S_{11FS})(1+S_{11WC})}{(1+S_{11FS})(1-S_{11WC})} \tag{2.25}$$

### 2.1.11 Comparison with Other Methods

The most common method used to measure the radiation efficiency of an antenna is the Gain /Directivity method which is based on anechoic chamber measurements [58]. The advantage of G/D method is the ability for accurate measures. However, this method has some limitations, such as requiring large space for installation [59]. In order to reduce the costs of design and development of an antenna, a simpler and quicker method, such as the Wheeler Cap method, was used [60].

Another method to determine small antennas efficiency in multipath environment is the reverberation chamber (RC) method [61]. A reverberation chamber is a screened room with a maximum of reflections of electromagnetic energy. It operates as a multi-mode cavity with one or two mechanical stirrers to perturb the boundary conditions of the electromagnetic environment or stir the inevitable standing waves. Inside the chamber, two antennas can be allocated; a transmit antenna which excites the chamber and an antenna under test (AUT) with a radiation efficiency which is to be determined [62].

The Wheeler Cap method was used due to the ease to implement, the fast accurate results which are in a very good agreement with simulations.

## 2.2 Software Simulation and Modelling Tools

CST Microwave Studio (CST MWS) [63] is a 3D electromagnetic software simulation tool which is used to design and to simulate the antennas presented in this work. In a comprehensive design environment (CAD interface), CST MWS allows modelling of the antenna geometry, the properties of the materials and the surrounding space. The

electromagnetic behaviour of the design can be analysed. The simulation delivers a variety of parameters including far field radiation pattern, gain, the total and radiation efficiency, S-parameter information and VSWR. Electric and magnetic field as well the surface current distribution are also available. The time domain and frequency domain solver are mainly used for the simulations. A unique meshing and sub-gridding technique (Tetrahedral or Hexahedral mesh type) is used for every antenna structure (Fig. 2.9).

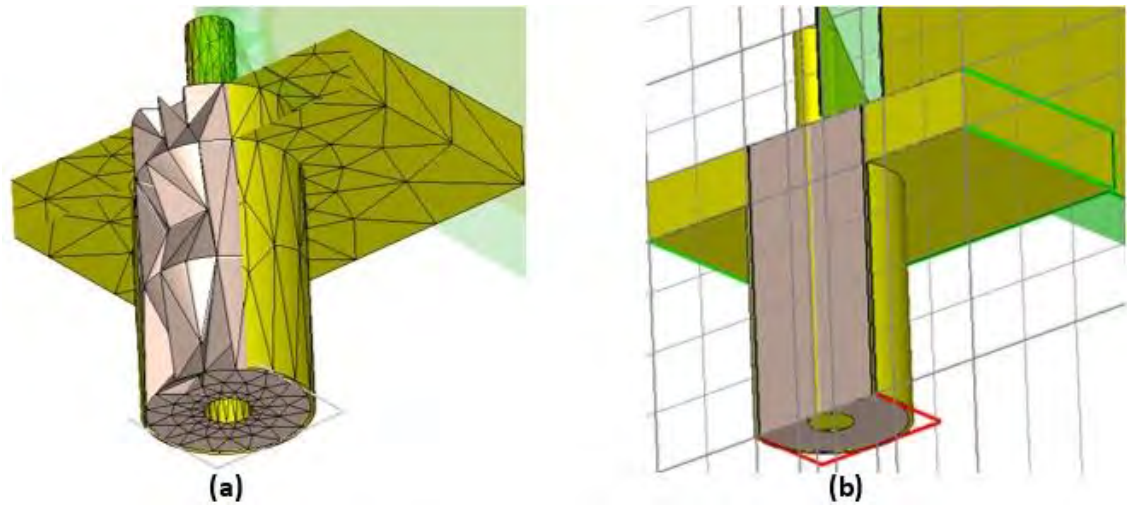


**Figure 2.9. The (a) Tetrahedral and the (b) Hexahedral mesh type.**

CST MWS also allows exporting of parameter data for further analysis and processing and the geometry data in a format readable by the circuit board plotter software used to prototype the antennas.

### 2.2.1 TIME & FREQUENCY DOMAIN SOLVER

The Time Domain Solver (TDS) calculates the electromagnetic fields through time at discrete locations and at discrete time samples. It calculates the transmission of energy between various ports or other excitation sources of the designed structure to the boundaries. A Time Domain Solver (TDS) is efficient for High Frequency structures such as connectors, transmission lines and antennas obtaining the broadband frequency behaviour of the simulated device.

The Frequency Domain Solver (FDS) calculates by using a broadband frequency sweep (frequency by frequency) in order to derive the full broadband spectrum from a relatively small number of frequency samples. Frequency Domain Solver (FDS) is suitable for compact structures or devices with a high Quality Factor (Q) value.

CST MWS is based on the Finite Integration Technique (FIT) which was proposed in 1977 by Thomas Weiland [64] and it is a spatial discretization numerical method to solve electromagnetic field problems in time and frequency domains. It delivers the spatial properties of the continuous equations such as conservation of charge and energy.

The basis of this approach is to apply Maxwell equations in integral form suitable for complex geometries. The Finite Integration Technique (FIT) is a method with high flexibility in geometric modelling and boundary handling as well as incorporation of arbitrary material distributions and material properties such as anisotropy, non-linearity and dispersion. Additionally, the use of a three-dimensional (3D) Cartesian mesh combined with a time integration scheme leads to efficient calculation algorithms, which allow simulating real world electromagnetic field problems [65].

## 2.3 PROTOTYPING

For the manufacturing of prototypes, a LPKF ProMat C60 Circuit Board (PCB) plotter was used to mill prototype designs from a PCB material layer. The substrates used are single or double-sided FR4 laminates with specific properties [66] (Table 2.1). Additionally, thin layers of Brass were used as main components of some prototypes. To facilitate measurements 50 Ω SMA (Sub Miniature version A) connectors were used to excite the prototypes providing good performance from DC to 18 GHz and also good mechanical durability.

**Table 2.1. Properties of FR4 and Brass used for antenna prototyping.**

| Properties | FR4 | Brass |
|---|---|---|
| $\varepsilon_r$ | 4.2-4.5±0.2 (1 GHz) | - |
| $\mu$ | 1 | 1 |
| tanδ | 0.02 (1 MHz) − 0.014 (1 GHz) | - |
| Electric Conductivity | - | $2.74 \times 10^7$ S $m^{-1}$ |
| Thermal Conductivity | 0.3 K m $W^{-1}$ | 109 K m $W^{-1}$ |
| Thickness | 1.52 mm | 0.15 mm |
| Copper Layer Thickness | 0.035 mm | - |

## 2.4 MEASUREMENT SETUP

The accuracy of the measurement results are due to the use of the measurement setup which consists of a partially anechoic chamber, the Antenna Under Test (AUT) and a Standard Gain Horn Antenna (SGH) which are both mounted in the chamber (Fig. 2.10).

The Antenna Under Test is placed on the top of a fiberglass mast which is centred on the turntable base which rotates by 360° in Azimuth. Both antennas are connected to a vector network analyzer. The turntable and measurement data from the vector network analyzer are gathered, processed and plotted in a PC using software which controls both devices. The measured radiation patterns are obtained in far field conditions (Fig. 2.11).

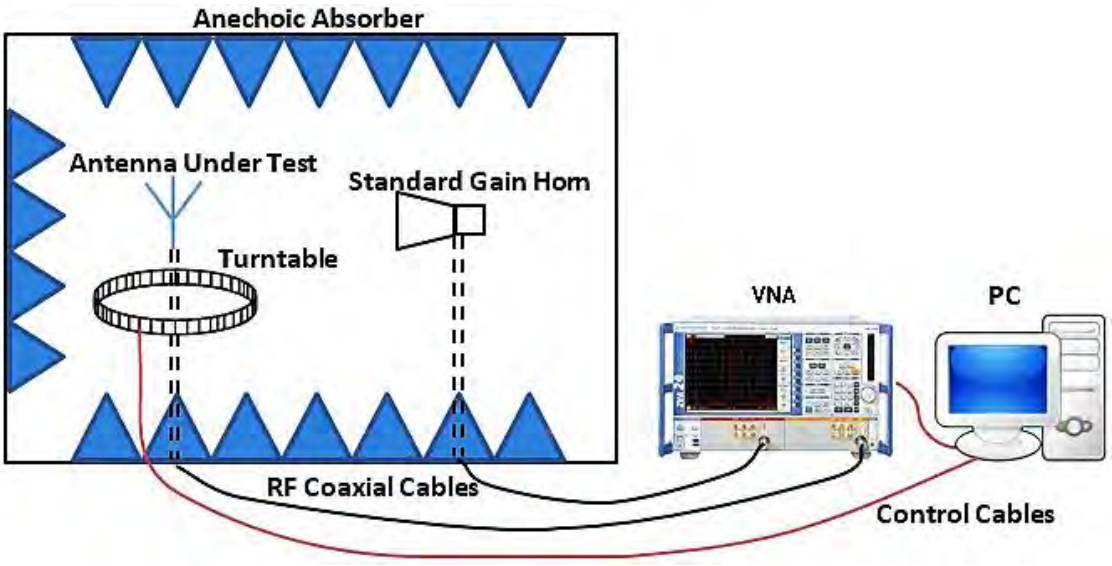


**Figure 2.10. Measurement setup.**

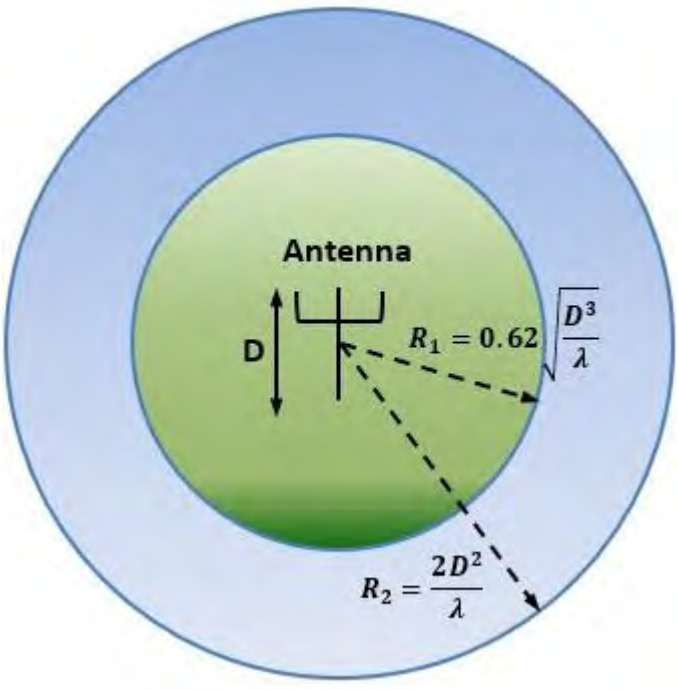


**Figure 2.11. Near R1 and Far R2 field boundaries.**

### 2.4.1 VECTOR NETWORK ANALYZER (VNA)

For measuring the performance of the prototype antennas a Vector Network Analyzer (VNA) *Rohde&Schwarz ZVA 24* is used [67, 68]. A Vector Network Analyzer measures the amplitude and phase of the wave quantities and uses these values to calculate a complex S-parameter, VSWR as well as Smith Chart. The real and the imaginary part of the impedance are also available.

The VNA is connected to a PC and can be controlled since all its functions are available to the PC via a network. Proprietary software controls the measurement of radiation pattern.

### 2.4.2 ANECHOIC CHAMBER

A radio frequency anechoic chamber is an electromagnetic shielded space whose walls are covered with absorbing materials that can absorb almost all of the incident electromagnetic radiation, providing an approximate free space environment. The partial anechoic chamber used in the measurement setup has absorbing materials which were placed in strategic positions on the walls to absorb the incident power and to degrade the signal reflections from the antenna that could impair and affect the accuracy of the measurement results.

The absorbing material used in the partial chamber is *EMERSON & CUMING ECCOSORB* VHP-18 pyramidal carbon loaded urethane foam absorber of 45.7 cm total height and a maximum reflectivity of −30 dB at 500 MHz, −40 dB at 1 GHz, −45 dB at 3 GHz and −50 dB above 5 GHz [69].

### 2.4.3 STANDARD GAIN ANTENNA (SGA)

Horn antennas of known gain and S-parameters value have been used as reference antennas to measure and to calculate the gain of the antennas under test. The measurement setup uses two standard gain horn antennas, one covering from 1 GHz (3.8 dBi) to 10 GHz (17.7 dBi) and the other from 500 MHz (5.3 dBi) to 2.9 GHz (11.1 dBi). The manufacturer is *SCHWARZBECK* [70].

The calculation of the AUT's gain is made by the Friis transmission equation [1], which relates the power $P_r$ which is delivered to the receiver to the input power of the transmitter $P_t$:

$$(G_{AUT})_{dB} = 20\log\left(\frac{4\pi R}{\lambda}\right) + 10\log\left(\frac{P_r}{P_0}\right) - (G_{SGH})_{dB}, \quad (2.26)$$

where $(G_{SGH})_{dB}$ is the known gain of the horn antenna and $R$ is the distance between the two antennas.

## 2.4.4 COORDINATE SYSTEM

Based on the IEEE Standard Test Procedures for Antennas [71], the antenna's coordinate system presented in the following Figure 2.5. The radiation pattern of an antenna under test which located at the centre of the spherical coordinate system is dependent on the two angular coordinates Θ and Φ. The distance $R$ from the antenna under test (AUT) to the measuring point (SGH) is fixed and only the two angular coordinates (Θ, Φ) are variables in a given radiation pattern.

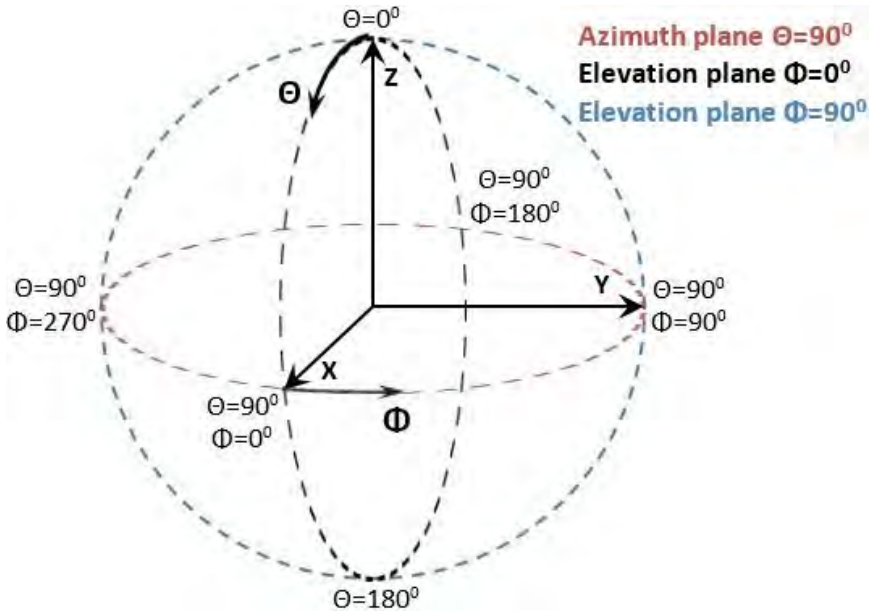


**Figure 2.12. Standard Spherical Coordinate System.**

# 3. Printed Folded Monopole Antenna

Printed Folded Monopole Antennas [11, 12, 13, 14] are designed with the main advantage of the low profile size and ease of integration to compact size devices, offering a very easy and a low cost prototyping and fabrication.

In this chapter a probe-fed printed folded monopole antenna placed on a conventional rectangular ground plane for WLAN applications is presented and discussed. The dual band antenna is operating at 2.45 GHz and 5.8 GHz. It is a low profile size antenna with omni-directional radiation characteristics in both bands. A parametric study of key geometrical parameters is reported as well as the effect of the ground plane size on the radiation performance.

## 3.1 Antenna Design

The evolution of the folded monopole design can be started from a conventional quarter wavelength (λ/4) PIFA antenna placed on a ground plane. By reducing the length of the extended horizontal arm of the PIFA as it shown in Fig. 3.1 a folded monopole antenna shorted to the ground plane, with dual band performance can be achieved.

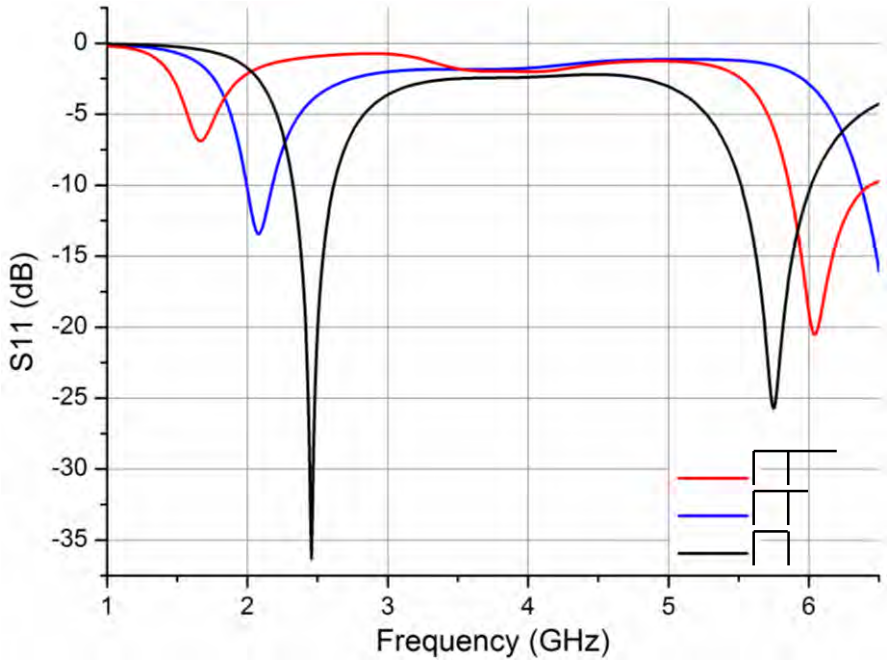


**Figure 3.1. Evolution of the folded monopole antenna.**

A 70 mm × 70 mm brass ground plane (Table 2.1) was used. The folded monopole with perimetric length of 53.38 mm (≈ $0.44\lambda_0$ with $\lambda_0$ = 122.4 mm at 2.45 GHz) and height of $h$ = 20.2 mm (≈ $0.165\lambda_0$) is printed on a single-side FR-4 substrate (Table 2.1) with dimensions 22.2 mm × 17 mm. The width of the shorting and the feeding strip is $s$ =0.5 mm and $f$ = 1.98 mm respectively. The length ($l$) of the horizontal arm of the antenna is $l$ = 10.5 mm and the width $a$ = 3.57 mm. The monopole is fed via a 50 Ω SMA connector through the ground plane (Fig. 3.2).

From the fabrication point of view, the FR-4 substrate is touched on the metallic ground plane and does not affect the measured and simulated results. The connection between the two parts (FR-4 substrate and ground plane) is via shorting strip which is soldered to it.

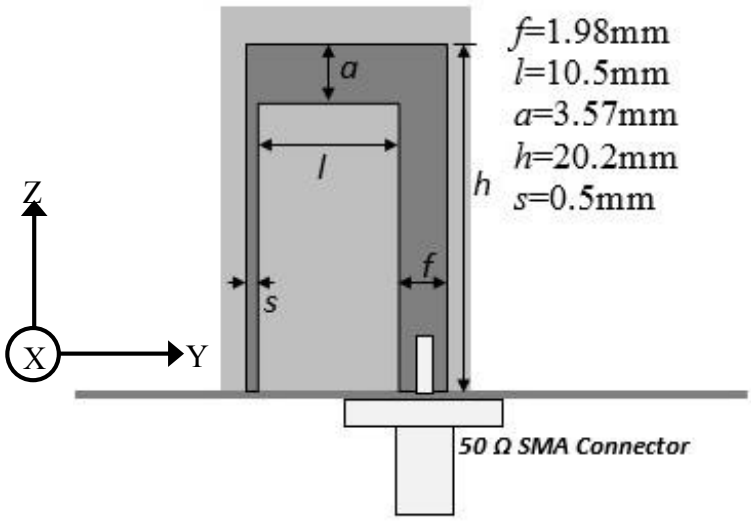


**Figure 3.2. Antenna geometry.**

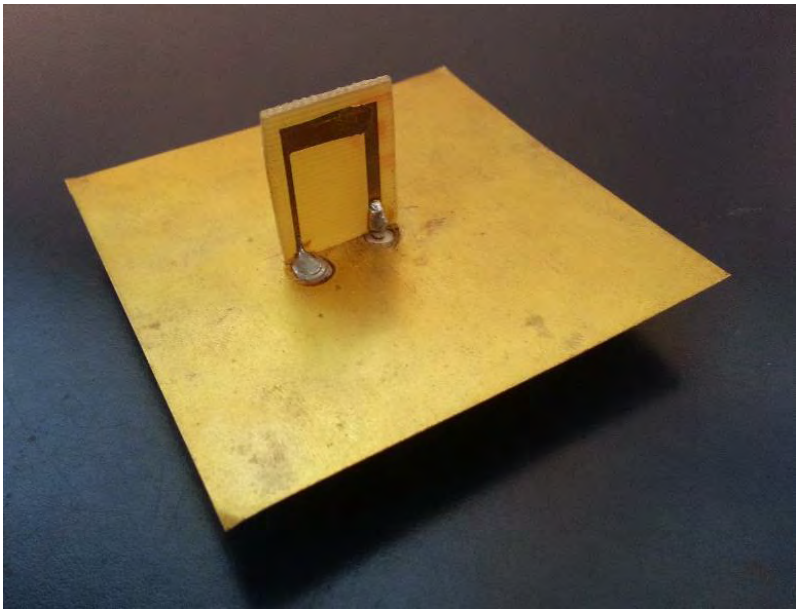

**Figure 3.3. Manufactured folded monopole antenna prototype.**

## 3.2 PARAMETRIC STUDY

A parametric investigation of the variation of $S_{11}$ with respect to four geometric parameters of the printed folded monopole shown in Fig. 3.2 is made.

The frequency of operation of the monopole is strongly dependant on its height ($h$). The height ($h$) of the monopole was varied from 16.2 mm to 22.2 mm in 2 mm increments. Fig. 3.4 shows the simulated $S_{11}$ for different values of height ($h$) of the antenna. The results indicate that as the height ($h$) is increased both resonant frequencies shifted upwards with a significant impedance matching improvement for the second resonance. By selecting the proper value of $h$ = 20.2 mm can be tuned both resonances to the desired values.

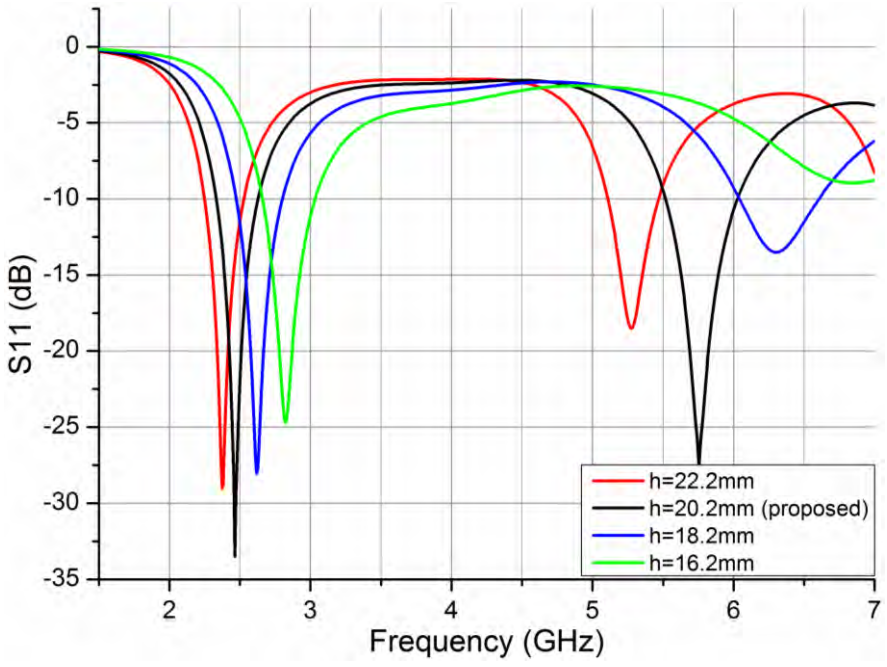


**Figure 3.4. The simulated $S_{11}$ dependence on the height ($h$) of the monopole.**

The width ($a$) of the horizontal strip of the monopole was found to have a significant influence on the frequency-ratio range of the antenna. The width ($a$) of the horizontal strip was varied from 0.57 mm to 5.07 mm in 1.5 mm increments. From the graph (Fig. 3.5) it is clearly visible that increasing the value ($a$) shifts the second resonance upwards with little effect on the lower resonance. The frequency-ratio between the upper and the lower resonance $F_r = f_u/f_l$ continuously increases from 1.88 to 3.82 as the value of ($a$) changes from 0.57 mm to 5.07 mm. The desirable frequency-ratio for the proposed antenna is 2.36.

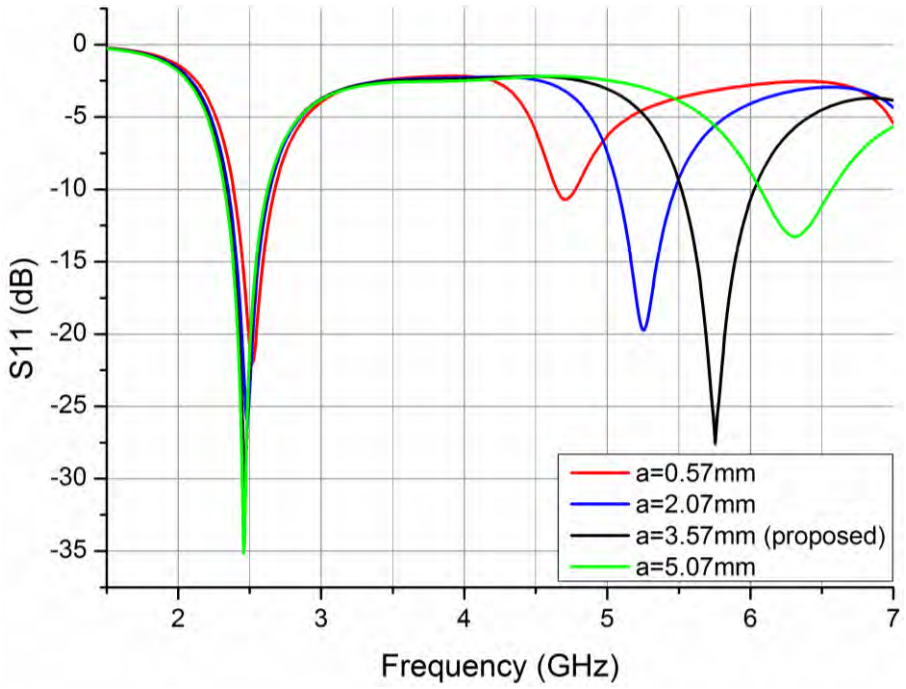


**Figure 3.5. The simulated $S_{11}$ dependence on the width ($a$) of the horizontal strip of the monopole.**

The horizontal arm length (*l*) is one of the geometrical parameters which is also investigated and varied from 2.5 to 12.5 mm with a step size of 4 mm. The results (Fig. 3.6) clearly indicate that as the length (*l*) increases the lower resonance shifts upwards while in the upper resonance a significant impedance matching improvement occurs as well as a frequency shifting. In that case the proposed value is 10.5 mm.

The dependence of the $S_{11}$ on the width of the feeding (*f*) strip was investigated for the two bands. The results are shown in the following Fig. 3.7. The width of the feeding strip as increased from 0.98 mm to 3.98 mm an upward shift of the first resonance with little effect of the impedance matching on both resonances occurred.

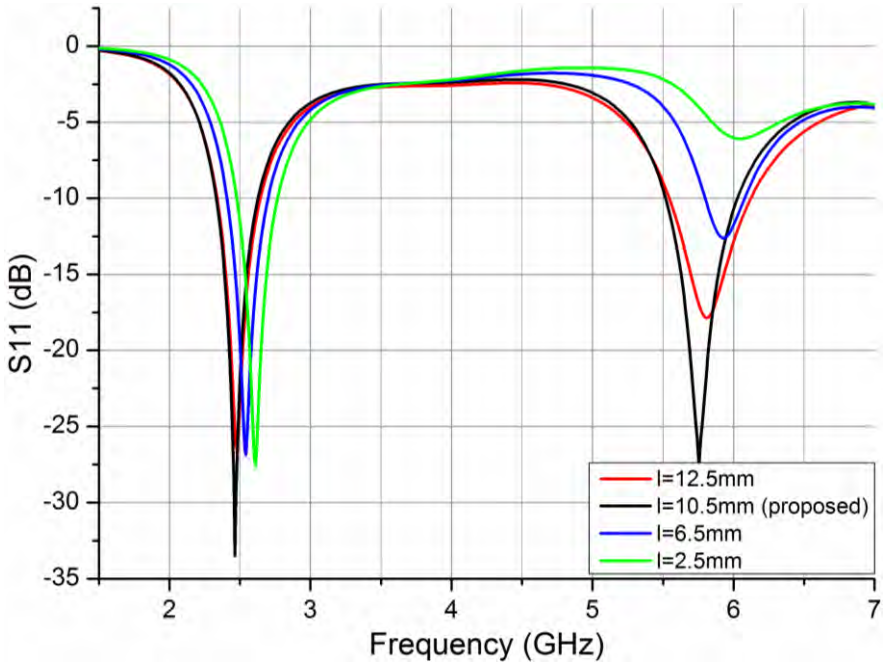


**Figure 3.6. The simulated $S_{11}$ dependence on the length (*l*) of the monopole.**

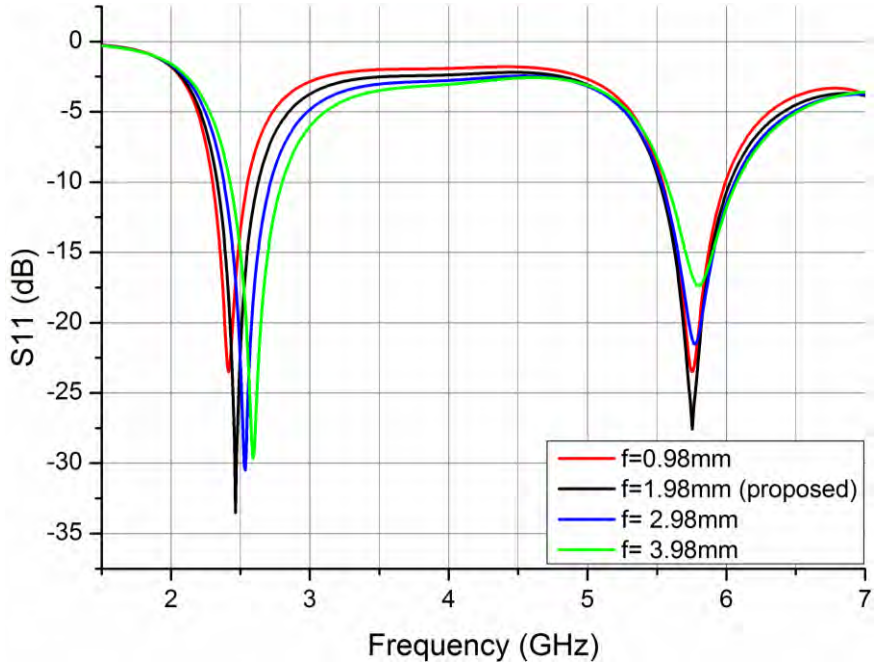


**Figure 3.7. The simulated $S_{11}$ dependence on the width (*f*) of the feeding strip of the monopole**

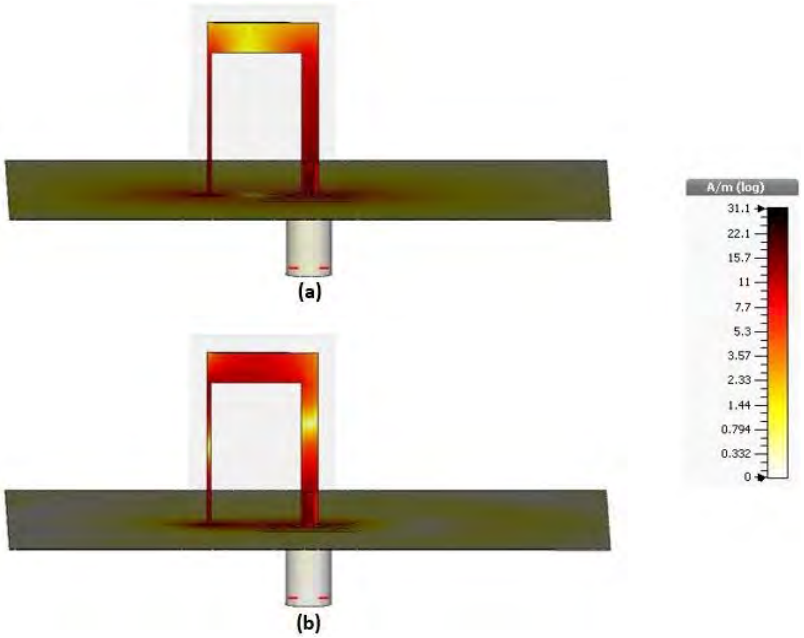


**Figure 3.8. The current distribution at (a) 2.45 GHz and (b) 5.8 GHz.**

The current distribution at both frequencies is shown in Fig. 3.8. For the first resonant frequency (Fig. 3.8(a)) the main part of the monopole which resonates is the feeding and the shorting strips. The electrical length of the two strips is almost 33 mm and it is slightly over $\lambda_0/4$ at 2.45 GHz ($\lambda_0/4$ = 30.6 mm). The distance between the horizontal strip and the ground plane is less than $\lambda_0/4$ and due to the mirror effect, there is a current cancelation between the two parts. For the second resonance (Fig. 3.8(b)) the main current distribution comes from the horizontal part of the monopole and partially from the two vertical strips where the current is strong but with opposite phase. The length of the horizontal strip is almost 13 mm which is slightly over $\lambda_0/4$ at 5.8 GHz (≈ 12.9 mm) and the distance from the ground plane (≈ 16.63 mm) allows the contribution given by these currents to radiation to become dominant.

## 3.3 Ground Plane Investigation

The size of the ground plane was found to have a significant influence on the radiation performance of the folded monopole antenna. A parametric study of the ground plane size was made and simulations were carried out for ground plane sizes of 30 × 30 $mm^2$ to 90 × 90 $mm^2$. Fig. 3.9 shows a plot of the simulated $S_{11}$ results as a function of ground plane size. From the results it becomes obvious that the lower resonant frequency can be effectively controlled (impedance matching and frequency shifting) by the size of the ground plane. The upper resonance is unaffected by the ground plane size which is electrically large and almost twice wavelength (99 mm ≈ $2\lambda_0$) at 5.8 GHz ($\lambda_0$ ≈ 51.7 mm).

Fig. 3.10 shows a plot of the simulated total efficiency (%) for various ground plane sizes. The efficiency for the lower resonance is very high (more than 92%) for its centre frequency $f_0$ for each ground plane size. For the upper resonance the total efficiency is stable without notable changes. The simulated maximum value of the total efficiency at 2.45 and 5.8 GHz is 98% and 90% respectively for ground plane size of 70 × 70 mm.

Radiation patterns cuts (x-y, z-x and z-y) were simulated using CST MWS and are presented in Figs. 3.11 and 3.12 for both frequencies in 10 dB/division scaled plots. The patterns are shown for ground plane sizes of 30 × 30 mm$^2$, 50 × 50 mm$^2$, 70 × 70 mm$^2$ and 90 × 90 mm$^2$.

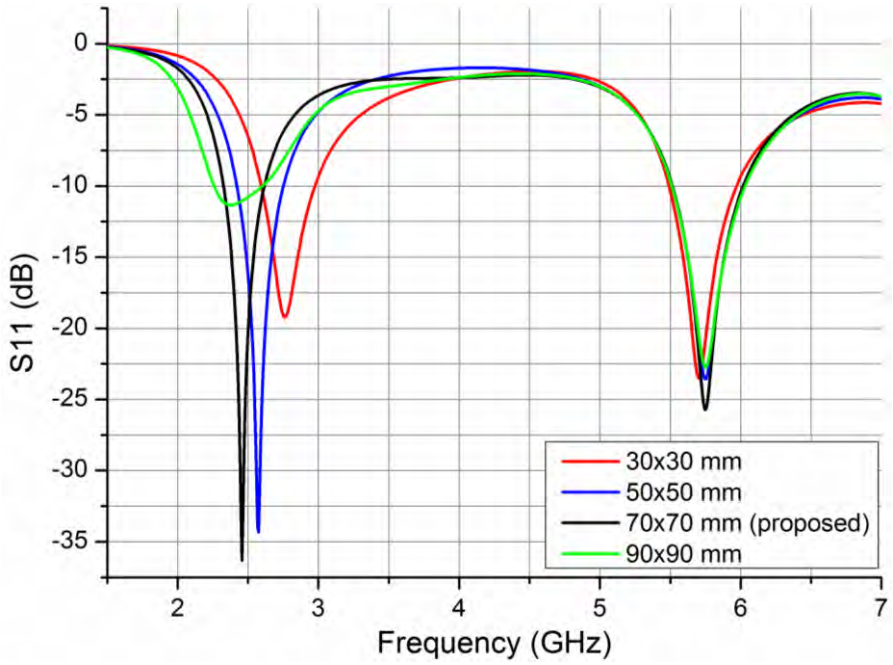


**Figure 3.9. The simulated $S_{11}$ dependence on the size of the ground plane.**

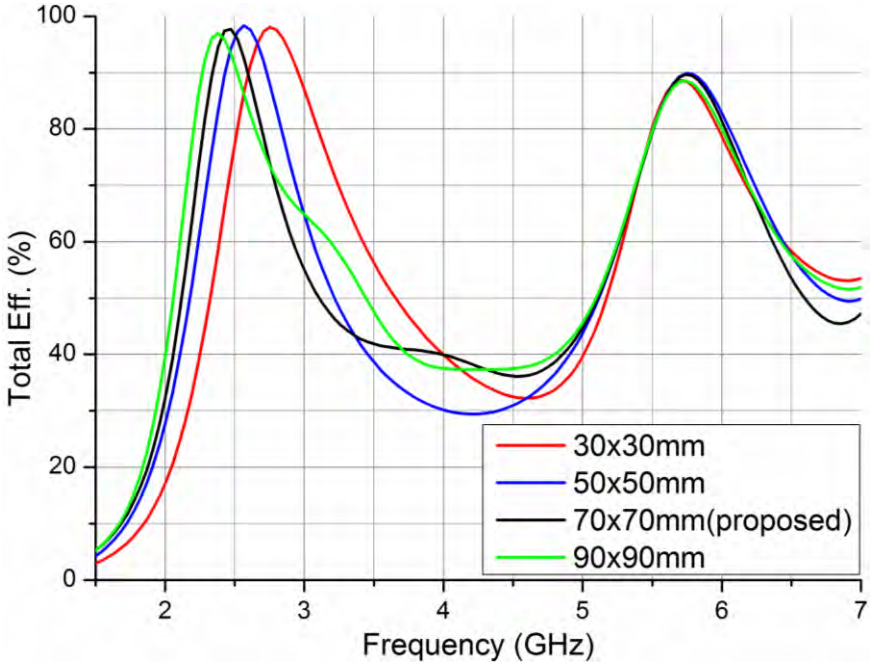


**Figure 3.10. Simulated Total Efficiency for various ground plane sizes.**

For the azimuth plane (x–y) the radiation patterns are omnidirectional for both frequencies with a small variation of gain as the ground plane size varies. The two elevation radiation patterns (z–x) and (z–y) at the lower resonant frequency are found to be more dipole-like with two visible nulls at $\theta = 0°$ and $\theta = 180°$ as the ground plane size is increased from 30 mm × 30 mm to 90 mm × 90 mm.

As the size of the ground plane is increased the gain at $\theta = 30°$ and $\theta = 330°$ is increased. For the upper resonant frequency, in both elevation planes (z–x) and (z–y) (Fig. 3.12) the gain below the ground plane ($\theta = 180°$) is decreased and respectively increased above the ground plane ($\theta = 0°$) as the size increases.

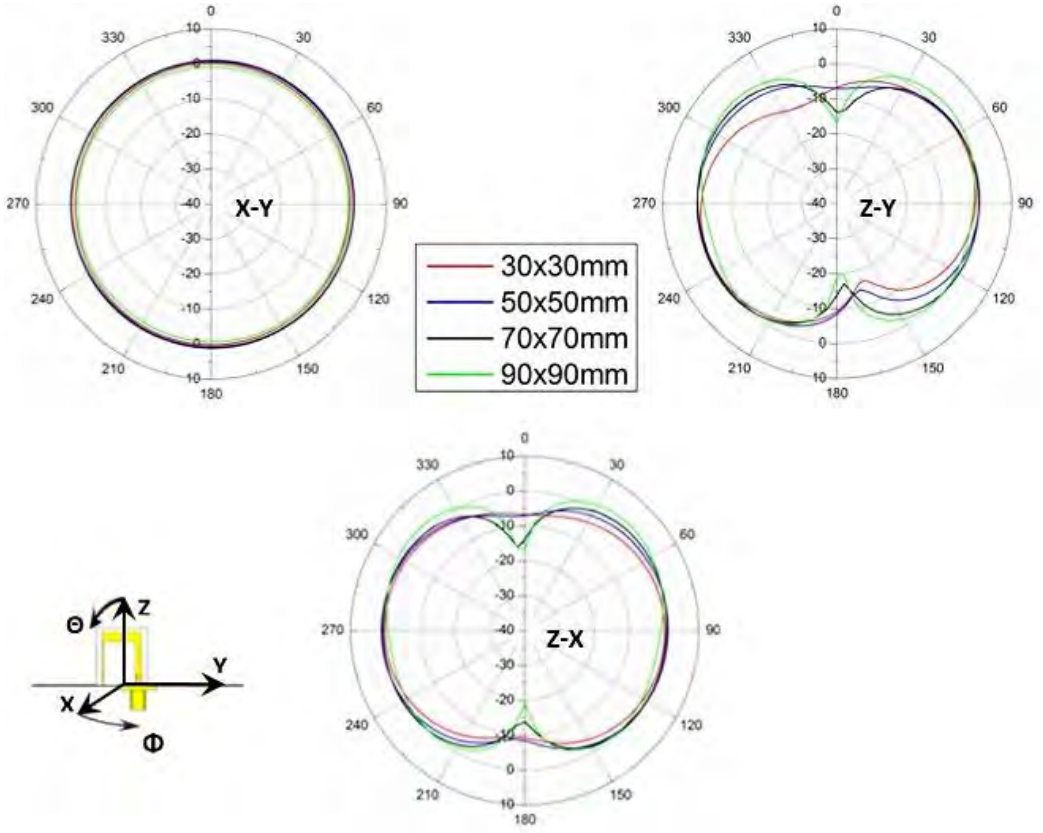


**Figure 3.11. Simulated radiation patterns for various ground plane sizes at 2.45 GHz.**

To investigate the installed performance of the proposed antenna, a simulation model is created (Fig. 3.13) with the antenna in a plastic enclosure made from Plexiglas ($\varepsilon r = 3.6$, $\tan\delta = 0.001$ and thickness = 3 mm) with outer dimensions 190 × 190 × 40 $mm^3$ (L × W × H). Two scenarios were evaluated, with the antenna located in the centre and in the corner of the plastic enclosure as shown in the Fig. 3.13.

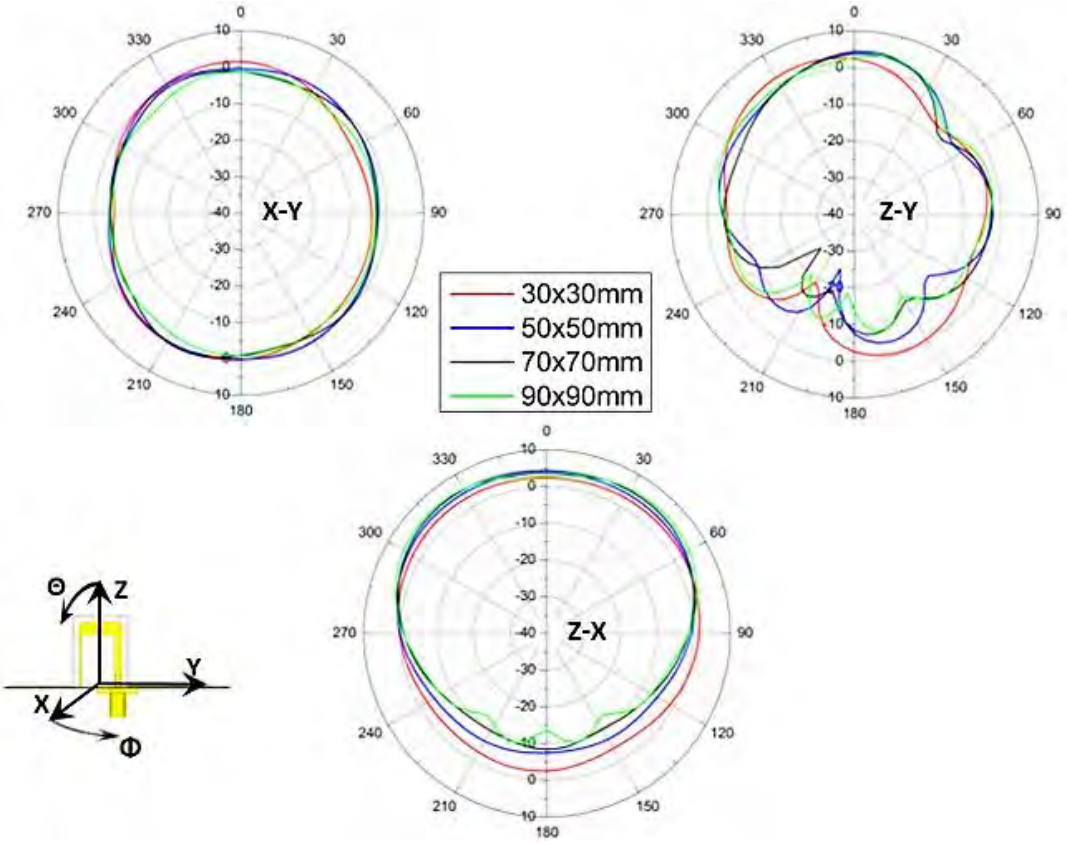


**Figure 3.12. Simulated radiation patterns for various ground plane sizes at 5.8 GHz.**

Fig. 3.14 show the simulated $S_{11}$ for the two different positions. From inspection of the results, the first resonant frequency shifts slightly downwards due to the wall permittivity loading and this becomes more acute when the monopole is closer to the wall surface (corner). For the case that the antenna is located in the centre of the enclosure the resonant frequency shifted downwards by 0.01 GHz and for the corner located case the frequency shifted downwards by 0.05 GHz.

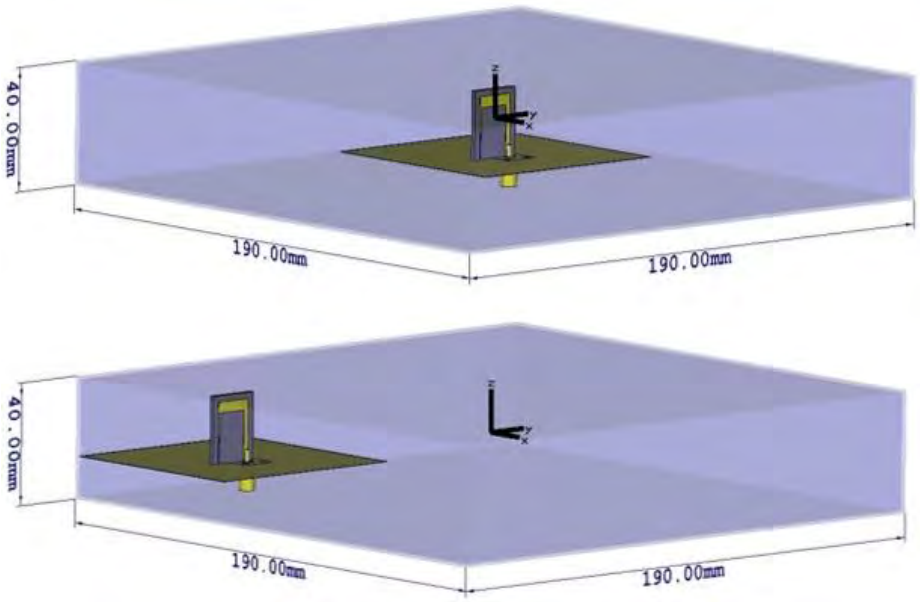


**Figure 3.13. The simulation model with the antenna located in the (a) centre of the plastic enclosure and the antenna located in the (b) corner of the plastic enclosure.**

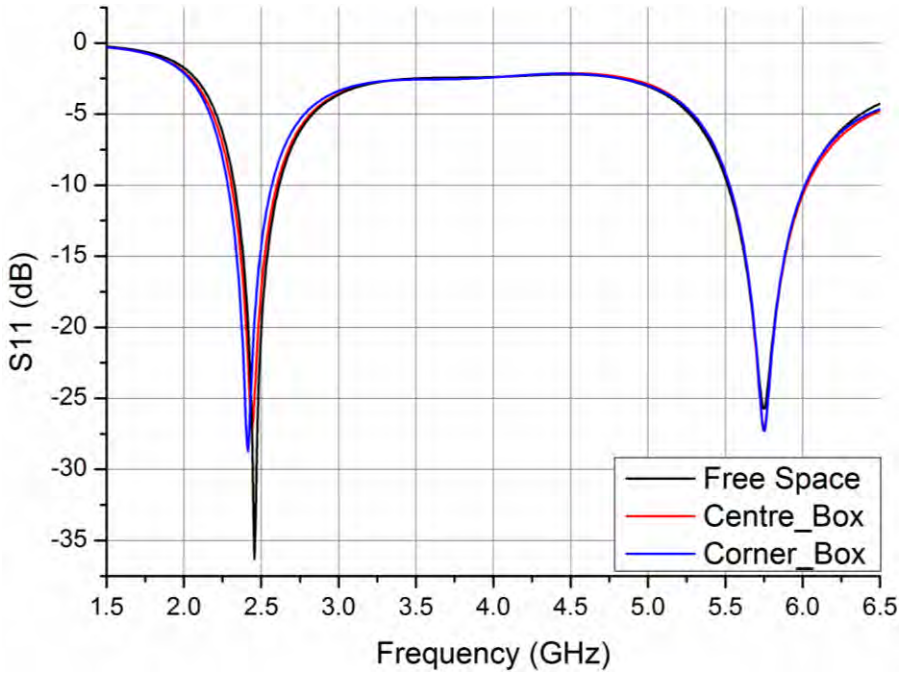


**Figure 3.14. Simulated $S_{11}$ for two different locations of the antenna into the plastic enclosure.**

## 3.4 Simulated and Measured Results

The simulated and measured $S_{11}$ for the folded monopole with the 70 × 70 $mm^2$ ground plane is shown in Fig. 3.15. The simulated and measured results are in good agreement. The lower band has a −10 dB impedance bandwidth of 300 MHz (2.34 − 2.64 GHz) for the simulated results and 280 MHz (2.32 − 2.6 GHz) for the measured results. For the upper band the simulated results provide 530 MHz (5.56 − 6.09 GHz) bandwidth, while the measured results provide 500 MHz (5.61 − 6.11 GHz) bandwidth. The fractional bandwidth for the first band is 11.4% and for the second 8.6%.

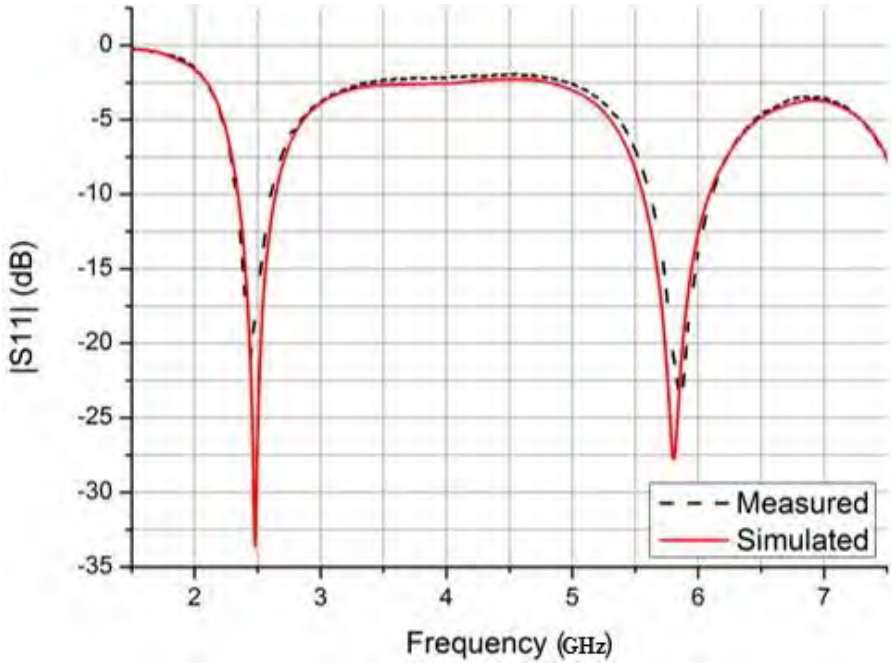


**Figure 3.15. Simulated and measured $S_{11}$ for the printed folded monopole antenna.**

The simulated and measured azimuth (y–x) and elevation (z–x) plane radiation pattern at both frequencies are illustrated in Figs. 3.17 and 3.18. All the measured gain patterns are illustrated against the simulated patterns in 10 dB/division scaled plots. For each radiation pattern the cross-polar and the co-polar components are presented together.

From the obtained results it is seen that at the lower frequency (Fig. 3.17) the omnidirectional pattern provides good polarization discrimination in the azimuth (y–x) plane. Cross-polar components in the higher frequency (Fig. 3.18) in both planes are due to the greater flow of current in the horizontal strip of the monopole. The measured peak realized gain is 2.0 dBi for the first resonance and 5.7 dBi for the second resonance.

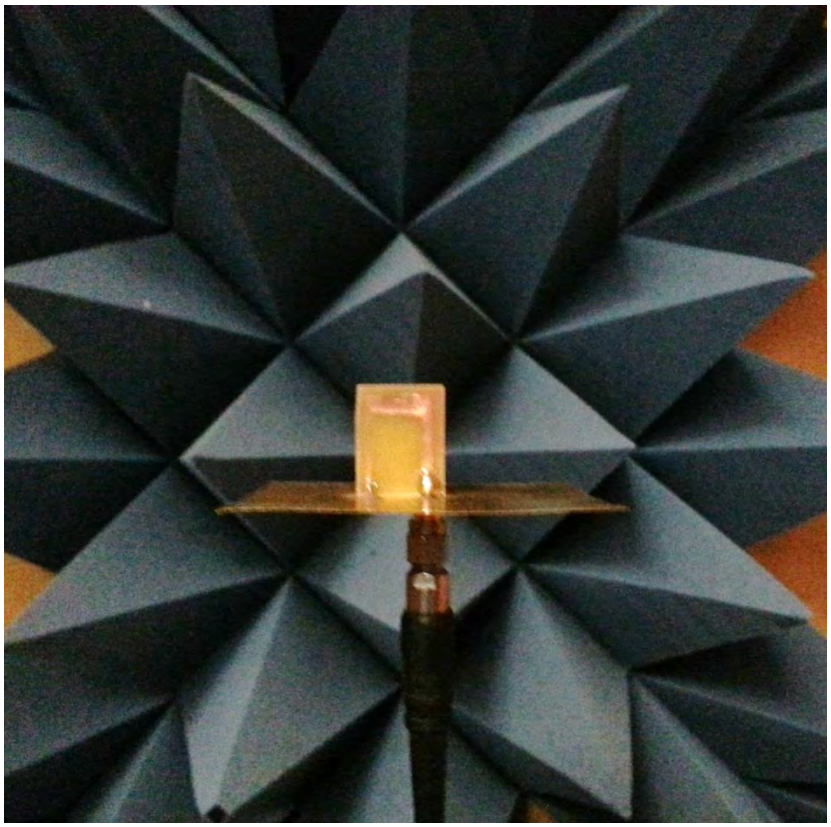

**Figure 3.16. The printed folded monopole antenna in the anechoic chamber.**

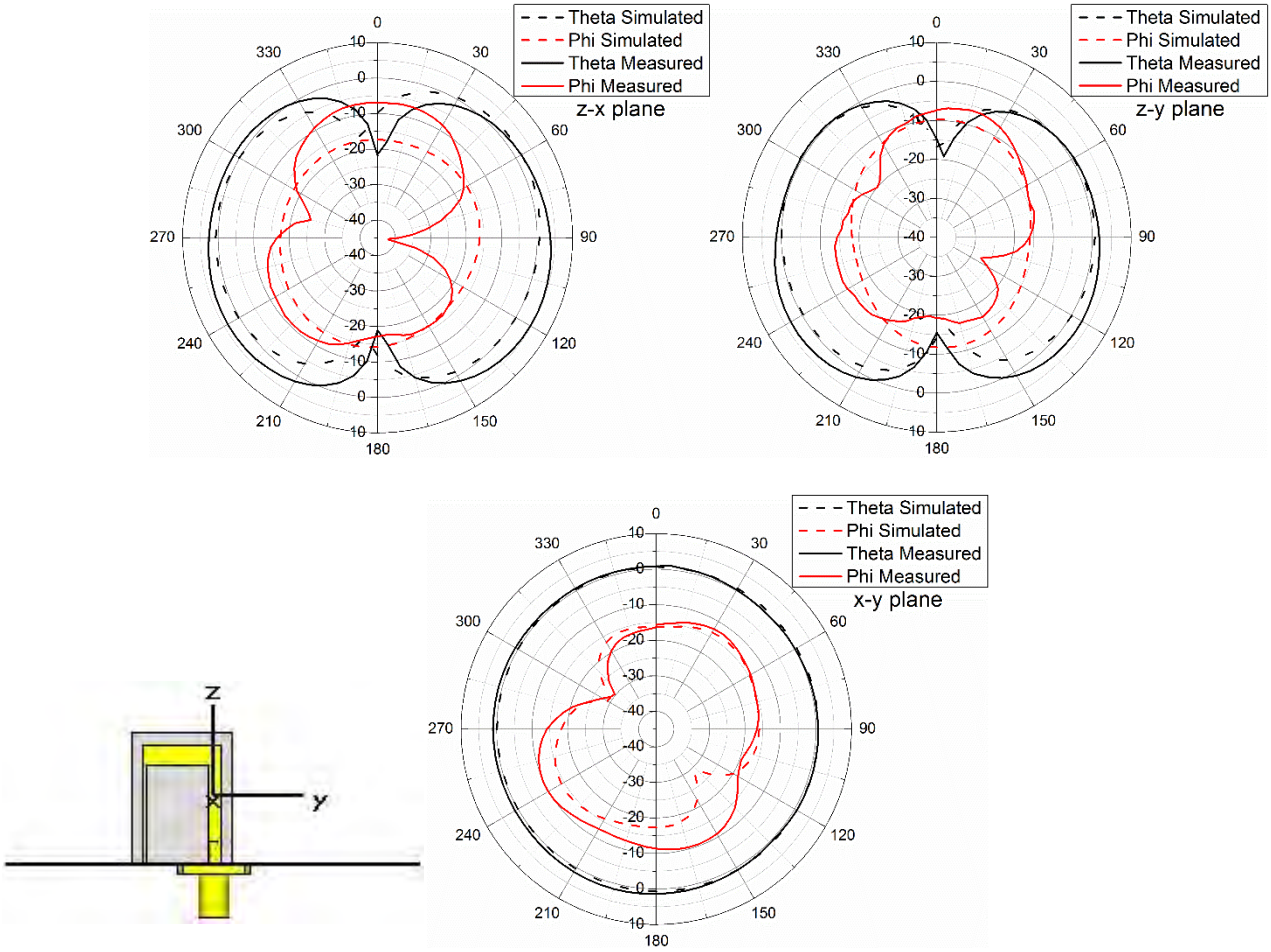


**Figure 3.17. Measured and simulated radiation patterns at 2.45 GHz.**

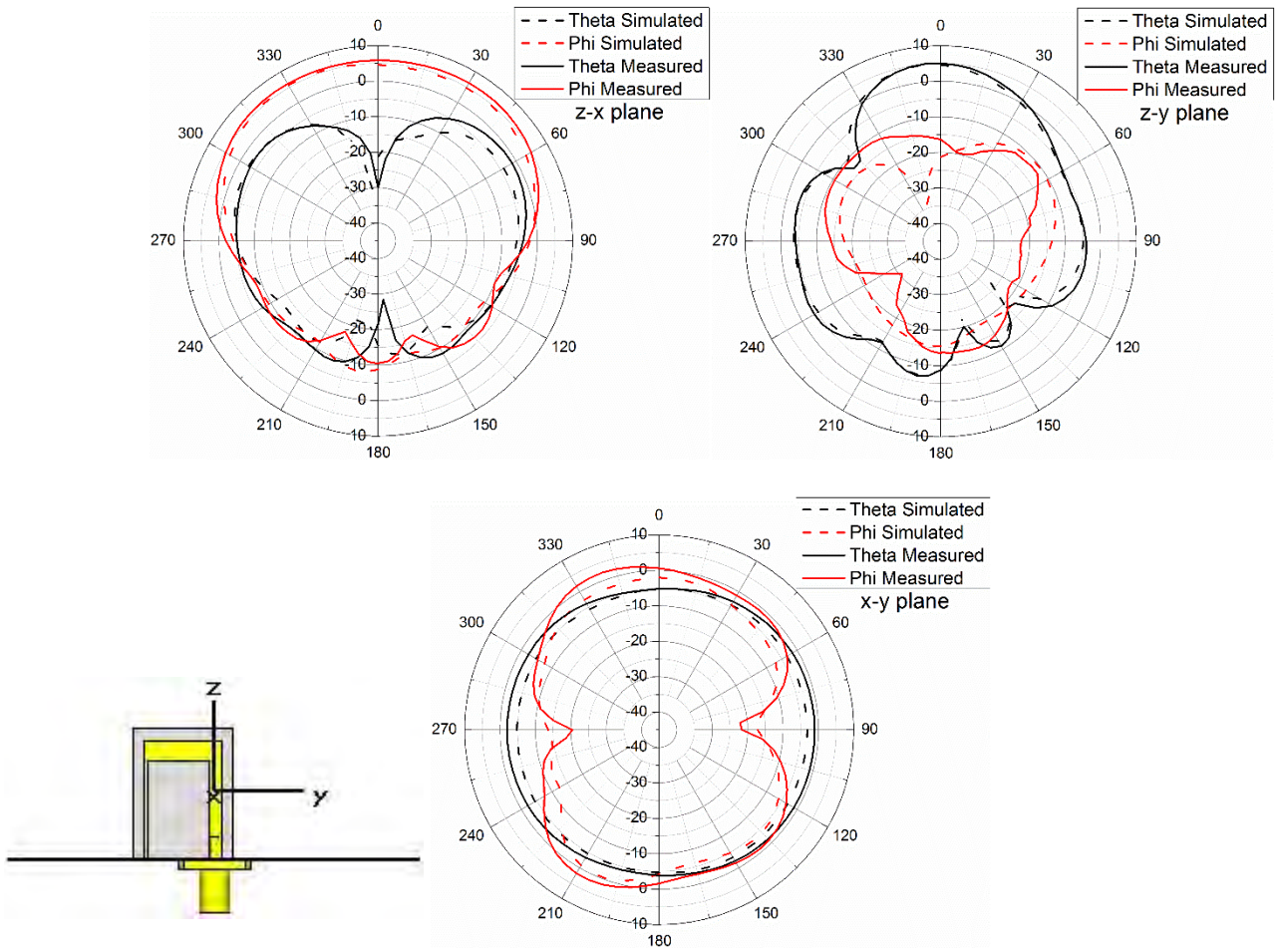


**Figure 3.18. Measured and simulated radiation patterns at 5.8 GHz.**

## 3.5 CONCLUSIONS

This chapter presented the study of the performance of a printed folded monopole antenna in the WLAN frequency range which is placed on a conventional rectangular ground plane. A parametric investigation of key geometrical parameters of the monopole as well as the effect of each parameter to the general radiation performance of the

monopole is reported. The folded monopole is studied also in terms of the ground plane size. The obtained results showed that the ground plane as an integral part of the antenna effectively controls the first resonant frequency (impedance matching and frequency shifting), improving also the total efficiency over the operating frequency range. The effect of the ground plane on radiation pattern as its size increased is turned to be a more dipole-like at the E–plane for the first resonance. For the second resonance when the ground plane size is increased the antenna becomes more directive at $\theta = 0°$ direction and less directive at $\theta = 180°$. The proposed antenna provides good omnidirectional radiation characteristic at both bands, is low profile, with additional benefit of a large frequency-ratio range which is easy to control.

# 4. Planar Inverted-F Antennas

Planar Inverted-F Antennas [32, 33, 34, 35, 36] are generally used in the portable devices market due to their low-cost and low profile architecture. They provide broad band and omnidirectional radiation properties.

This chapter describes the implementation of two Planar Inverted-F antennas (PIFAs) which can be used for machine-to-machine (M2M) applications in a broad frequency range. Performance metrics include impedance bandwidth and radiation patterns.

In the first section a dual-band Planar Inverted-F antenna covering the lower and the upper LTE band is described. The second section introduces a dual PIFA antenna which is more compact and covers the whole lower LTE band and partially the upper LTE band. A parametric investigation of key geometrical parameters of both antennas is given as well as the effect of the ground plane size on the general radiation performance.

## 4.1 Dual Band LTE PIFA for M2M Applications

A dual band PIFA antenna was designed for machine-to-machine (M2M) applications to enable broadband functionality at both LTE frequency bands 690 − 960 MHz and 1710 − 2690 MHz. It is required to meet standards specifications of −6 dB $S_{11}$ and 50%

total efficiency or greater across the proposed frequency range. The antenna size is suitable to integrate in terminal devices for mesh networking applications, automotive and vehicles and generally for indoor and outdoor assets.

### 4.1.1 ANTENNA DESIGN

The geometry and coordinate system of the antenna is shown in Fig. 4.1. A 178 mm × 247 mm ground plane consists of a single sided FR-4 substrate (Table 2.1). The front and the rear part of the PIFA antenna (Fig. 4.1(a), (b)) are printed on FR-4 layers (Table 2.1) with dimensions $l$ = 67 mm (≈ 0.18$\lambda_0$ with $\lambda_0$ = 481.15 mm at 623.5 MHz) mm × $h$ = 30 mm (≈ 0.08$\lambda_0$). The top part of the PIFA antenna consists of a thin brass layer (Table 2.1) with dimensions $l$ = 67 mm × $w$=33 mm (≈ 0.09$\lambda_0$). The PIFA is fed via a 50 Ω SMA connector through the ground plane to a feeding strip of width $f$ = 2.7 mm which is located $a$ = 20.5 mm from the left edge of the antenna. The fold-over metallization lengths for the front and back sections are $d$ = 23 mm and $b$ = 12 mm respectively. The shorting strip has width ($c$) of 7.4 mm and is printed on a thin FR-4 layer (thickness = 0.2 mm) it touches the inner part of the FR-4 rear side layer and connects to the top face of the antenna. The shorting strip is located 20 mm ($s$) away from the left edge of the antenna.

In Fig. 4.2 a general view of the manufactured dual band LTE PIFA prototype is demonstrated. Several fabrication details can be considered as typical for the considered antenna prototype. The soldering of the top plate with the two vertical FR-4 layers was

very crucial as well as the connection of the very thin shorting strip with the brass top plate and the ground plane was challenging and precise execution was needed.

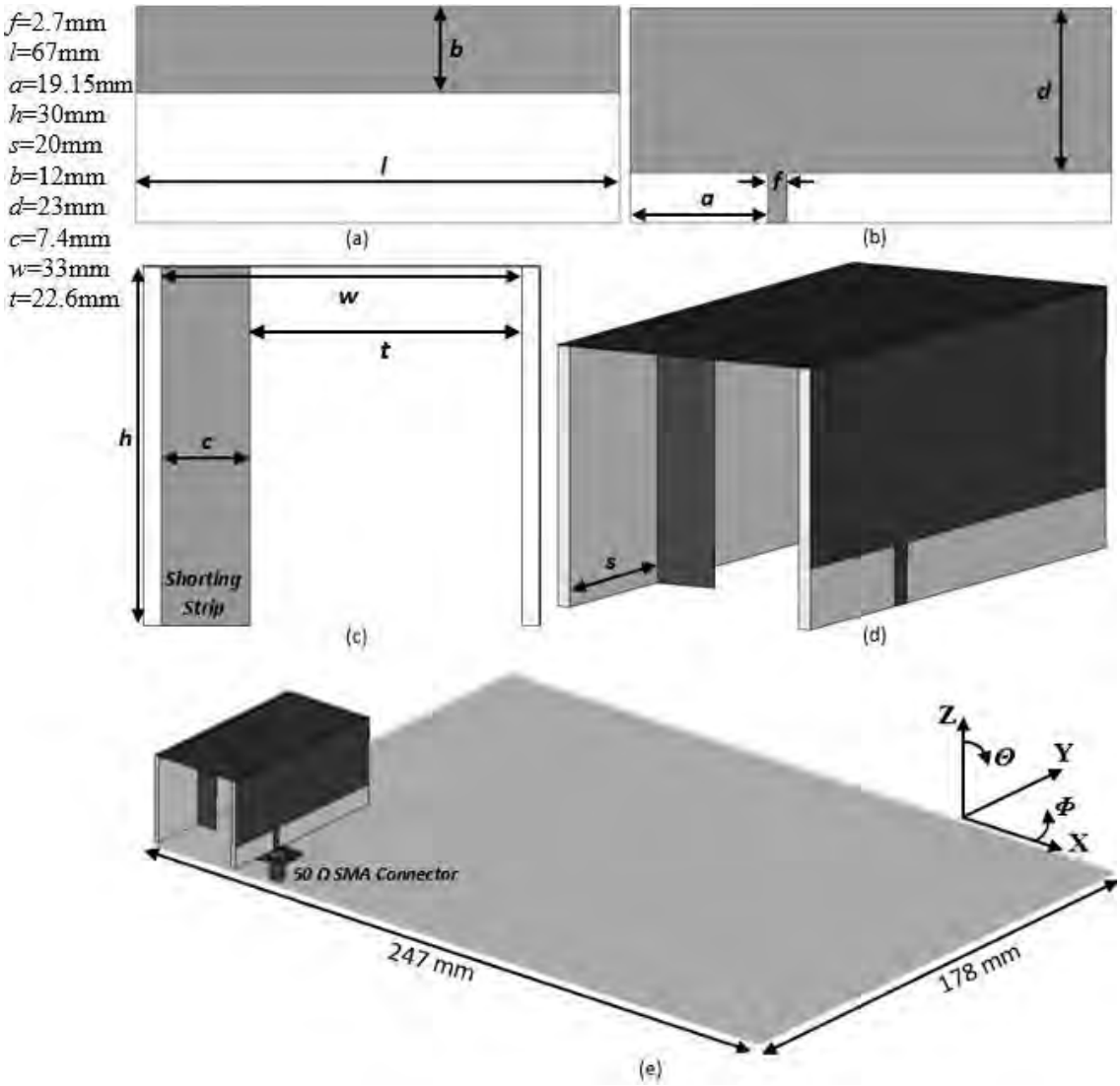


**Figure 4.1. Rear view (a), Front view (b), Left view (c), General view (d), CST simulation model and the coordinate system (e).**

**Figure 4.2. Manufactured dual band LTE PIFA prototype.**

### 4.1.2 PARAMETRIC STUDY

A parametric study of five key geometrical parameters of the antenna is made. The position of feeding strip (*a*) is optimised to obtain the desired resonance bands. From the $S_{11}$ (Fig. 4.2) it is seen that moving the feeding strip of the PIFA antenna from the left to the right side shifts the first resonance upwards and effectively controls the impedance matching of both bands. The optimised value of the parameter (*a*) for the proposed antenna is 19.15 mm.

The operating frequency of the antenna is strongly dependent on its height (*h*). The height (*h*) is varied from 25 mm to 40 mm in 5 mm increments. As the height increases (Fig. 4.3), the impedance matching at the first resonance improves. For the second and third resonance as the height increases, the impedance matching deteriorates. The optimized value of the height (*h*) for the proposed antenna is 30 mm, providing good matching for both LTE bands.

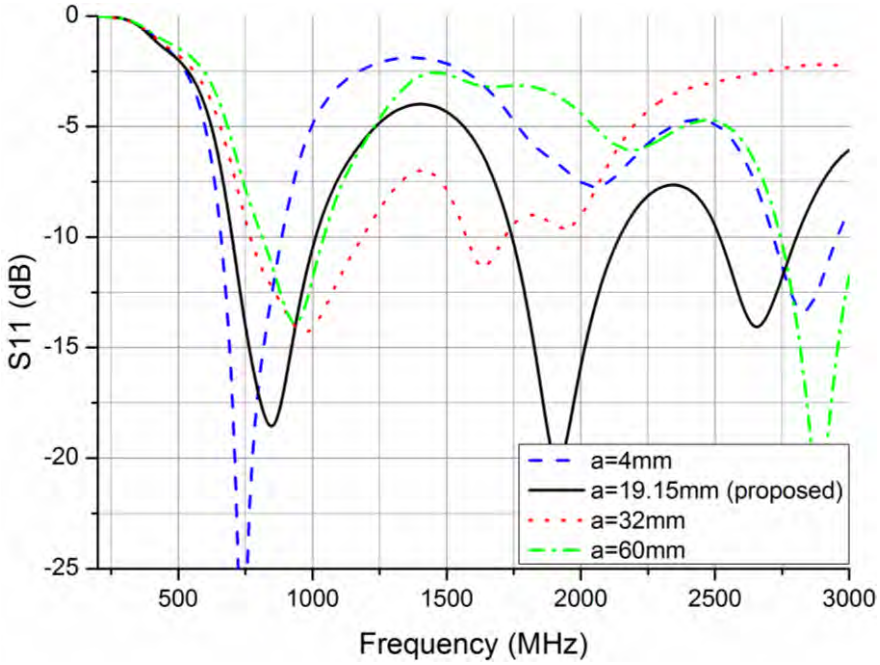


**Figure 4.3. The simulated $S_{11}$ dependence on the feeding strip position (*a*) of the PIFA.**

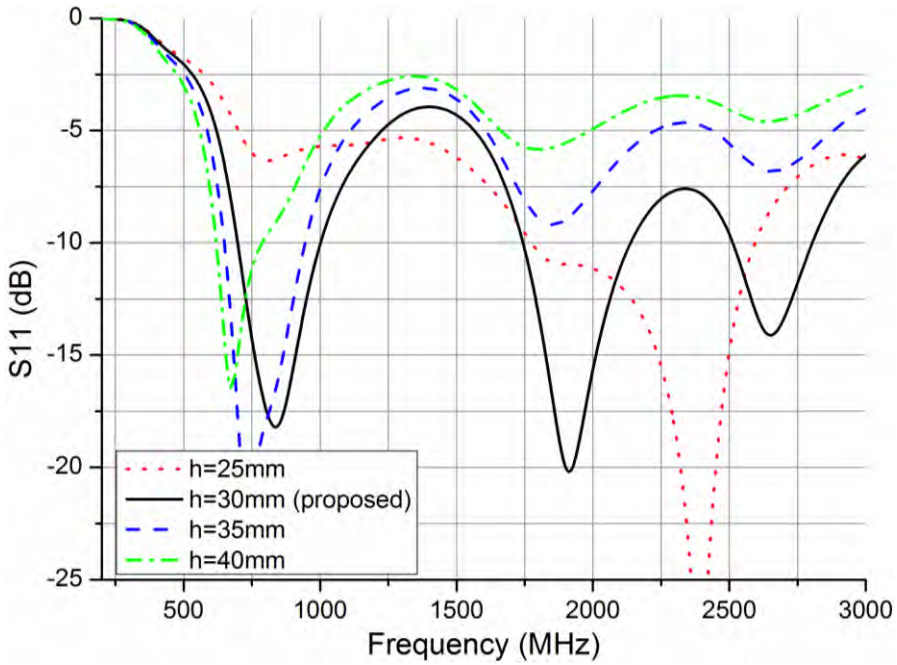


**Figure 4.4. The simulated $S_{11}$ dependence on the height (*h*) of the PIFA.**

The height (*b*) of the back folded section is investigated. In Fig. 4.4 simulated results for the parameter (*b*) are shown. As the value of the back folded section (*b*) increases from 5 mm to 27 mm, the second band shifts downwards with a little effect on the lower resonance. A proposed value for the PIFA length (*b*) was chosen to be 12 mm.

The height of the front folded section (*d*) is also investigated. From the obtained results (Fig. 4.5) it is clear that the impedance matching of the second resonance is improved as the parameter (*d*) is increased. However, the impedance matching of the first resonance is also strongly dependent on this parameter. The proposed value of the parameter (*d*) is 23 mm.

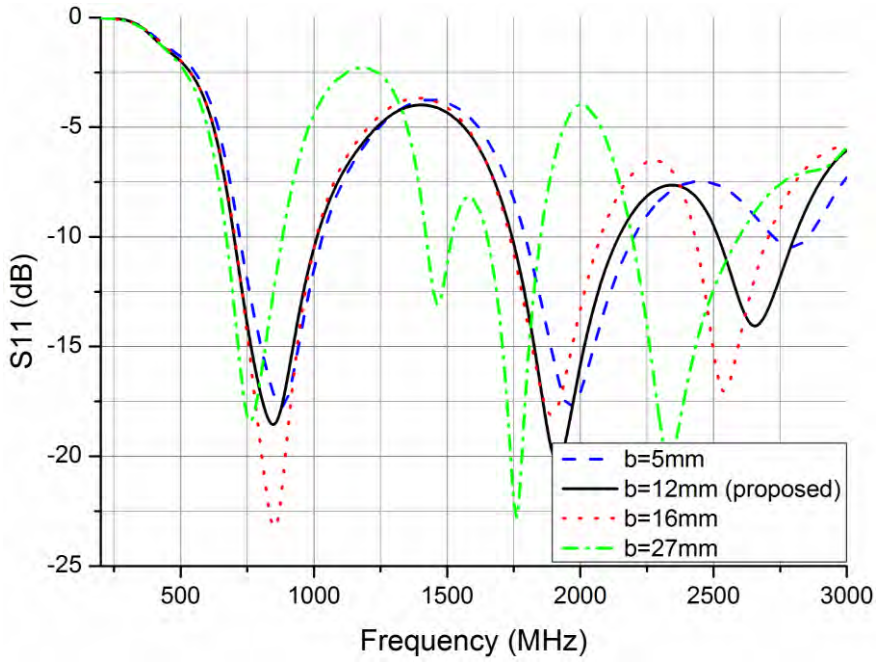


**Figure 4.5. The simulated $S_{11}$ dependence on the length of the rear folded section (*b*) of the PIFA.**

Another way to obtain the desirable frequency bands is to define the position (*s*) of the shorting strip. The positon of the shorting strip is varied from the left side (0 mm) of the antenna to the right side (67 mm). The obtained results clearly show that all resonant frequencies can be controlled (impedance matching and frequency shifting) by varying the parameter (*s*). By considering the results of Fig. 4.6 the best value of the length (*s*) is 20 mm.

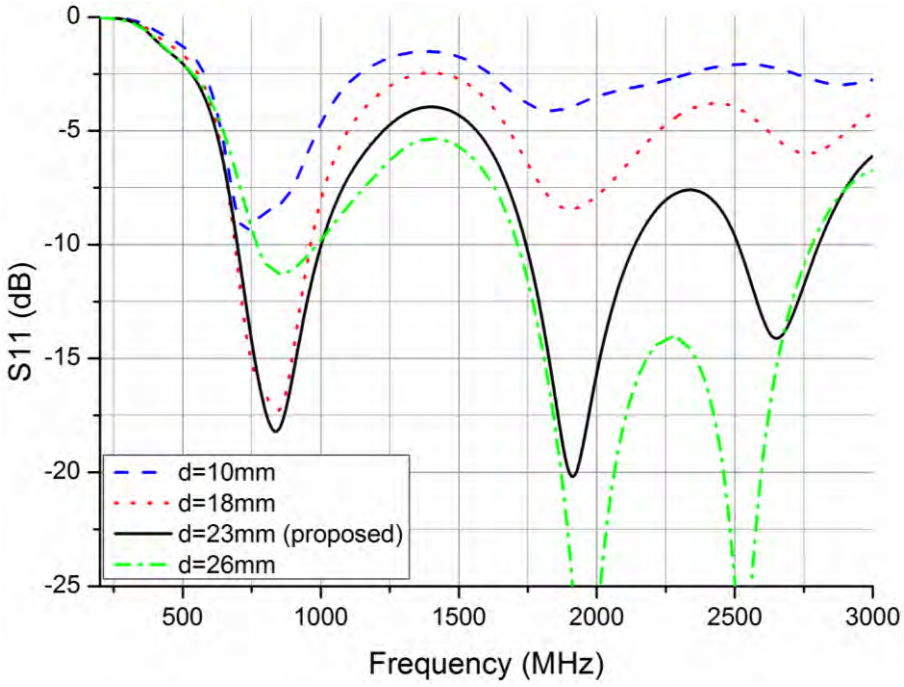


**Figure 4.6. The simulated $S_{11}$ dependence on the length of the front folded section (*d*).**

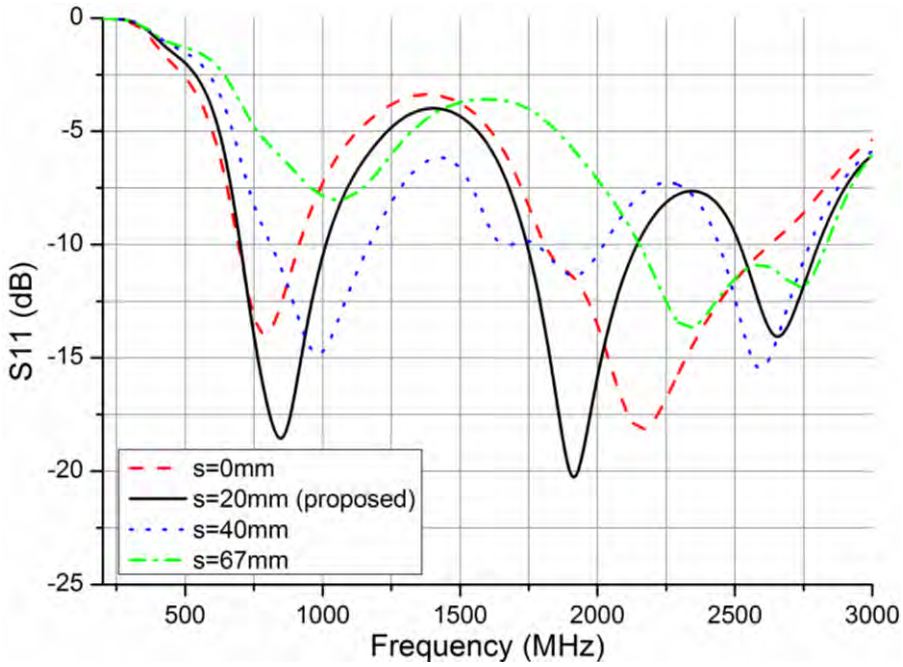


**Figure4.7. The simulated $S_{11}$ dependence on the shorting strip position (*s*) of the PIFA.**

### 4.1.3 Ground Plane Investigation

The position of the PIFA antenna on the ground plane (Fig. 4.7) as well as the ground plane size, has a significant influence on the antenna performance [72]. A parametric study of the PIFA position on the ground plane demonstrates that the optimum position is the bottom left corner of the ground plane. For the y-axis the antenna is moved from the bottom left corner (0 mm) of the ground plane to the top right corner (111 mm) with a step size of 37 mm. For the x-axis the antenna is moved from the bottom left corner (0 mm) to the bottom left corner (210 mm) with a step of 70 mm.

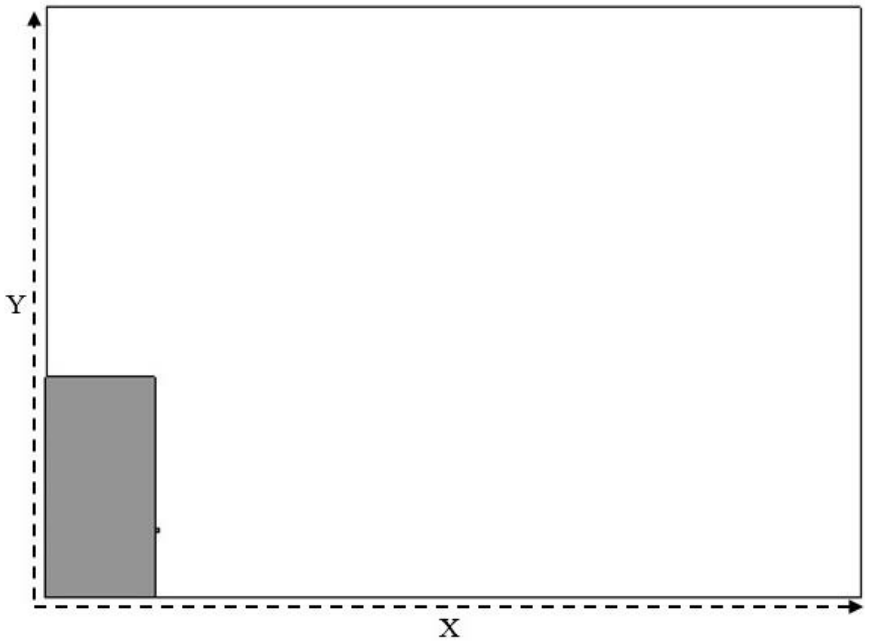


**Figure 4.8. The parameters X and Y which define the position of the PIFA antenna.**

Figs. 4.9 and 4.10 show that the position of the PIFA along the edge greatly influences the impedance matching and the bandwidth of the lower resonances of the antenna. The position of the PIFA also effects the radiation pattern and the gain (Fig. 4.11). This can be explained by the finite ground plane having distinct characteristic modes depending on its size and the frequency [73]. The surface current of the ground plane for three different positions of the PIFA at 825 MHz is simulated using CST MWS and is presented in Fig. 4.8. When the PIFA is positioned in the bottom right corner of the ground plane a strong current distribution across the right side of the ground plane and especially at the two corners is excited. The ground plane excitation modes is turned to be a more dipole-like. On the other hand, when the PIFA is positioned in the middle of the bottom side and the right side of the ground plane the current distribution is weak without significant

contribution to the antenna radiation performance. In that case, the ground plane excitation modes is more monopole-like.

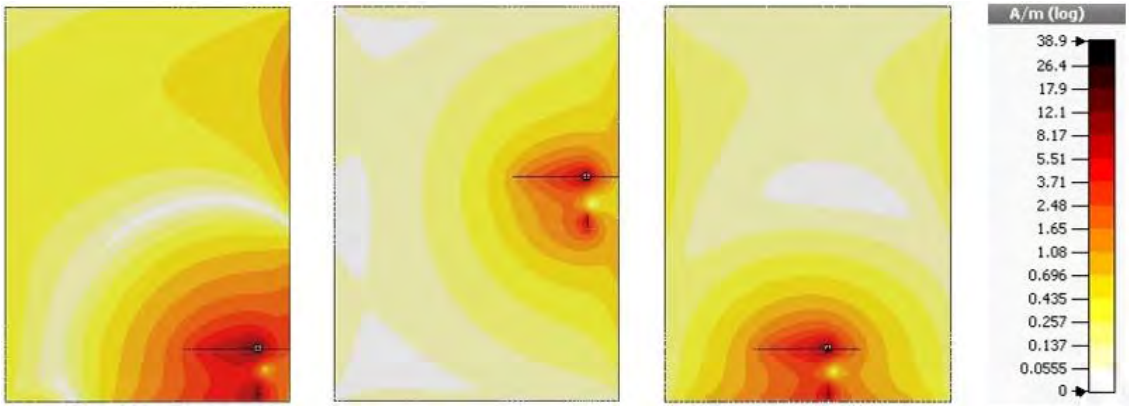


**Figure 4.9. Ground plane current distribution at 825 MHz for three different position of the PIFA.**

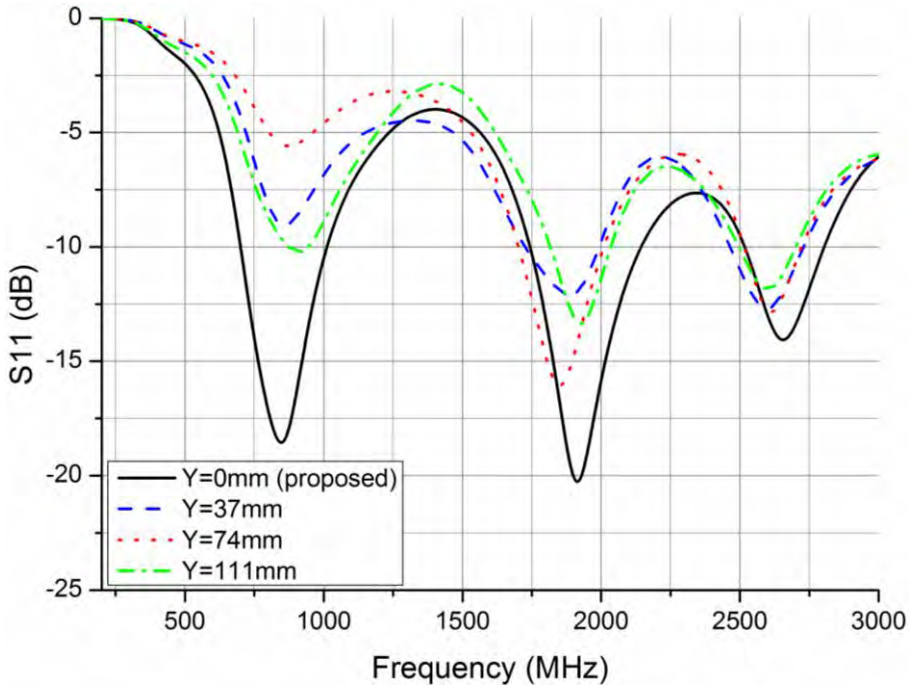


**Figure 4.10. Simulated $S_{11}$ when moving the antenna along y-axis.**

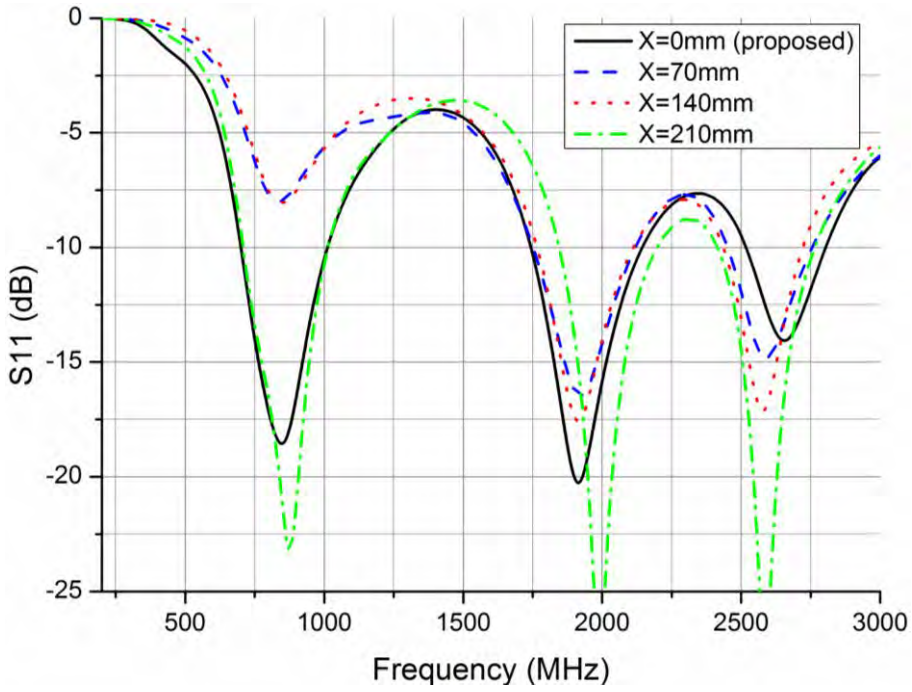


**Figure 4.11. Simulated $S_{11}$ when moving the antenna along x-axis.**

A parametric study of the ground plane size was made and simulations were carried out for ground plane sizes of 133 × 178 $mm^2$ to 237 × 346 $mm^2$. From the graph (Fig. 4.13) it is clearly visible that the antenna is not heavily dependent on the ground plane size due its electrical large size (< $0.84\lambda_0$ at 825 MHz) and does not significantly affect the three resonances.

Fig. 4.14 shows a plot of the simulated total efficiency (%) for various ground plane sizes. From the obtained results it is understood that the total efficiency of the antenna does not change significantly as the ground plane size varies.

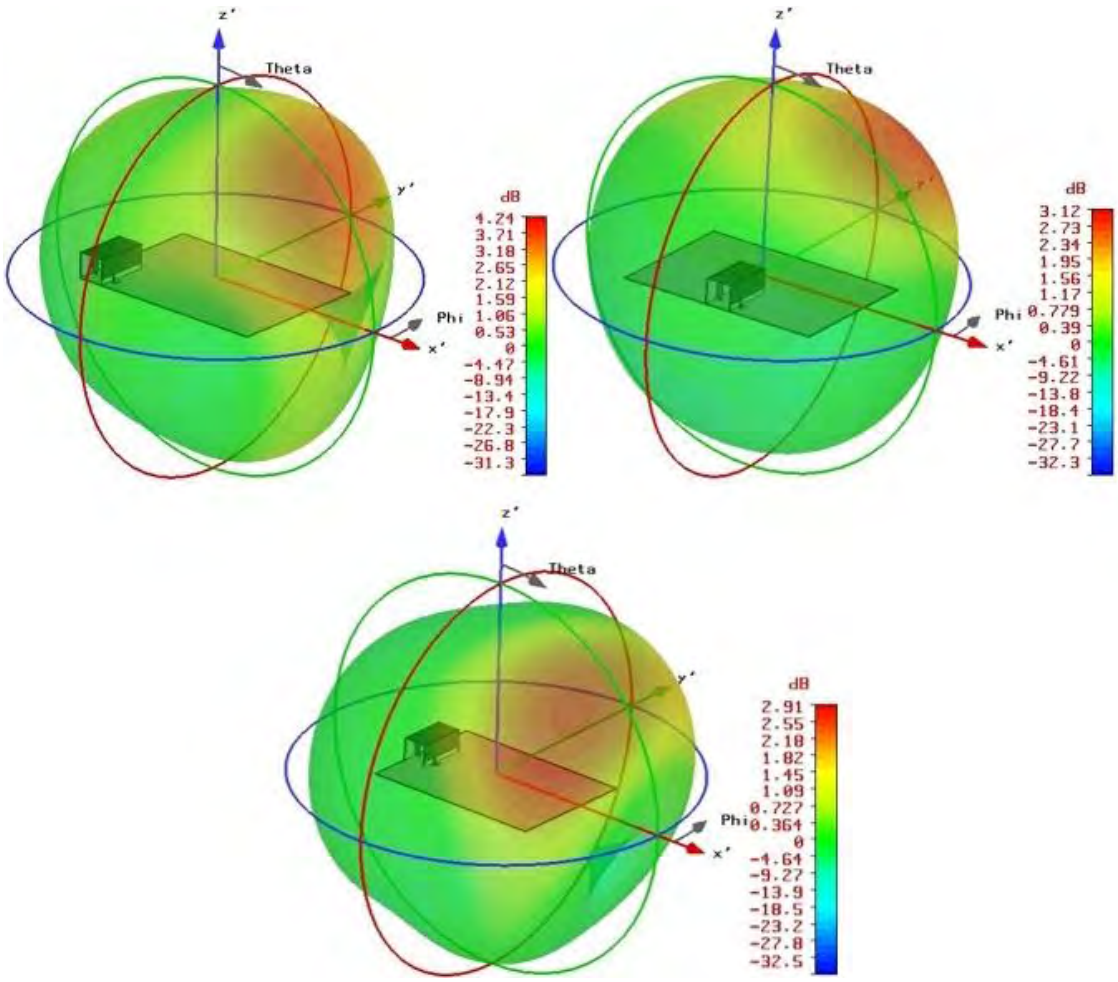


**Figure 4.12. Radiation patterns for different positions of the PIFA on the ground plane.**

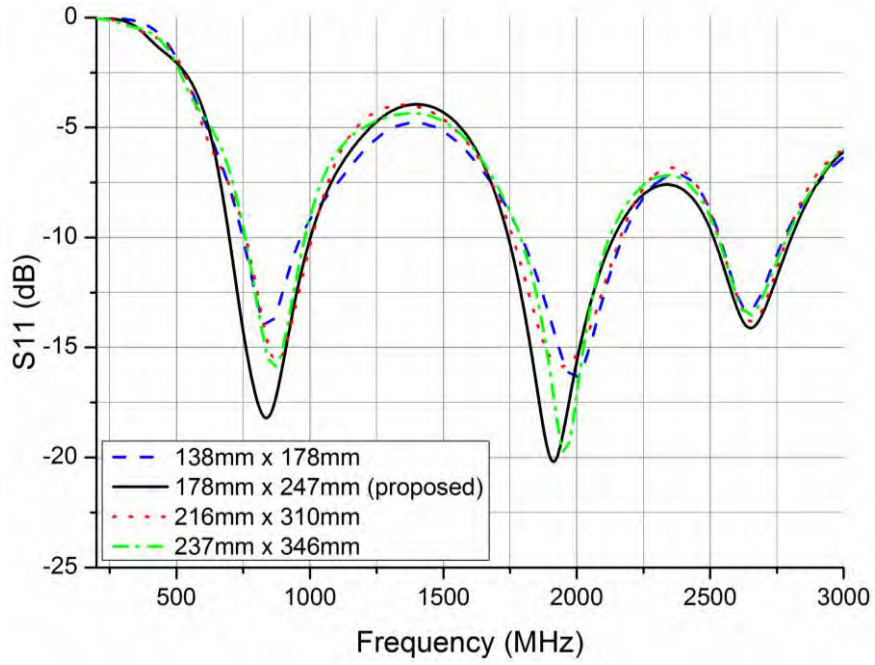


**Figure 4.13. The simulated $S_{11}$ dependence on the size of the ground plane.**

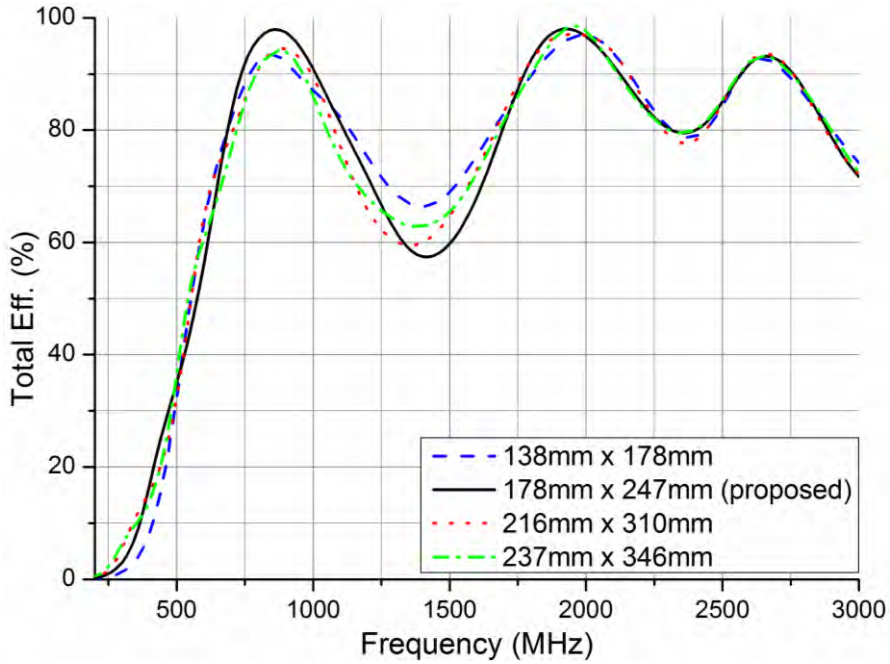


**Figure 4.14. Simulated Total Efficiency for various ground plane sizes.**

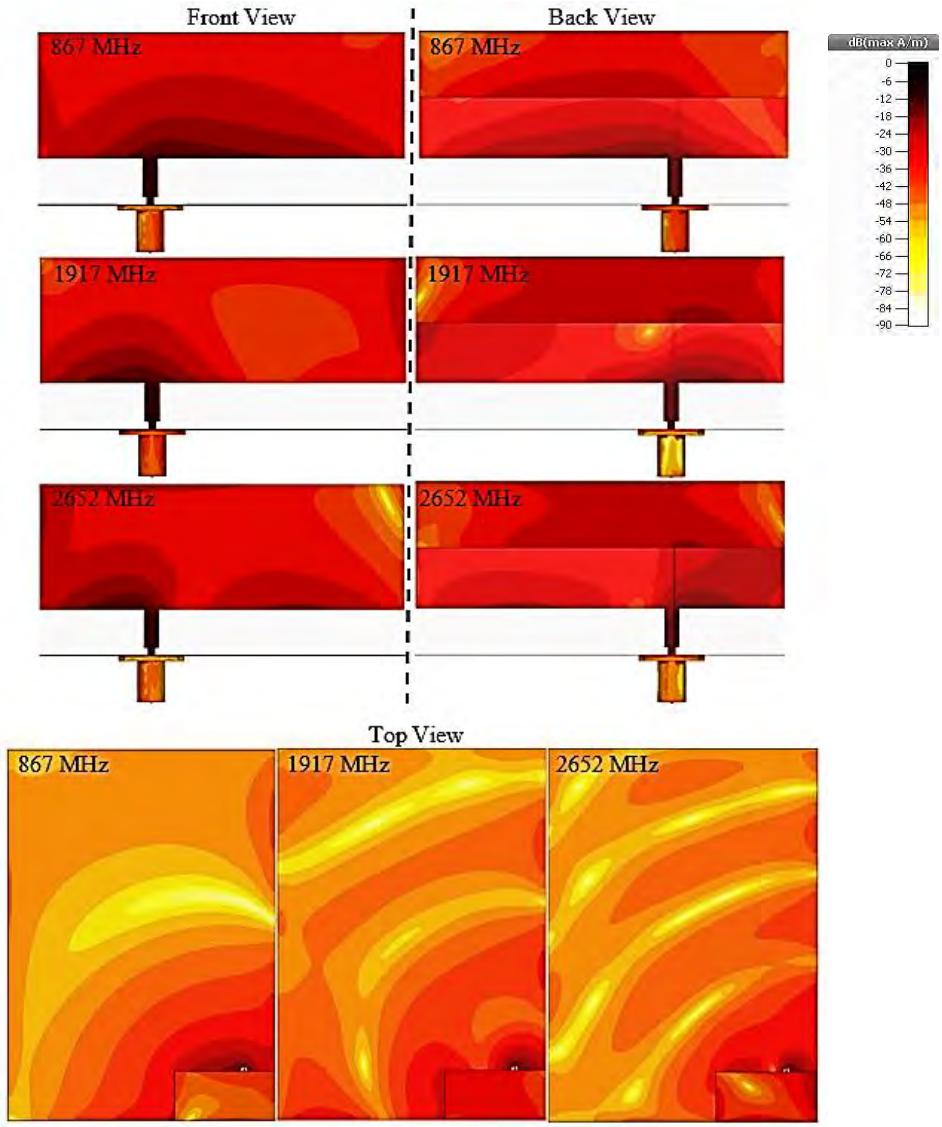


**Figure 4.15. Current Distribution at 867, 1917 and 2652 MHz.**

The surface current distribution at three frequencies is shown in Fig. 4.15. For the first resonant frequency it is evident that the main part of the antenna which resonates is the front folded part of PIFA and partially the back folded one. For the second and the third resonance the back folded part of PIFA contributes more to the radiation of the antenna.

From the top view it is particularly interesting be stated that the ground plane is an integral part of the antenna and contributes as a main part of the radiator at the three frequencies.

### 4.1.4 Simulated and Measured Results

The measured and simulated $S_{11}$ for the PIFA antenna placed on the 178 × 247 $mm^2$ ground plane are in good agreement as seen in Fig. 4.14. The $S_{11}$ was less than −10 dB over the range 688.5 − 1009.8 MHz, 1736.3 − 2121.5 MHz and 2459 − 2698 MHz giving fractional bandwidths of 40.6%, 20.87% and 9.31%, respectively. The frequency range for $S_{11}$ less than −6 dB is 623.5 − 1111.8 MHz and 1621.74 − 3007.04 MHz, (62% and 75%, respectively).

The simulated total efficiency at 825 MHz and 2200 MHz is 85% and 97% respectively. The maximum value is 98% at 1915.4 MHz (Fig. 4.15).

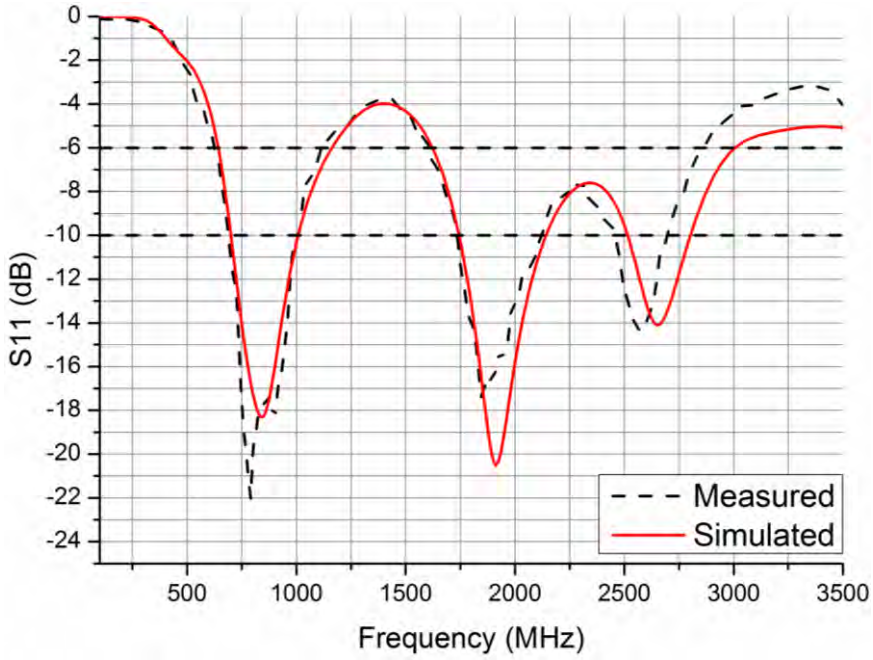


**Figure 4.15. Simulated and measured $S_{11}$ for the PIFA antenna.**

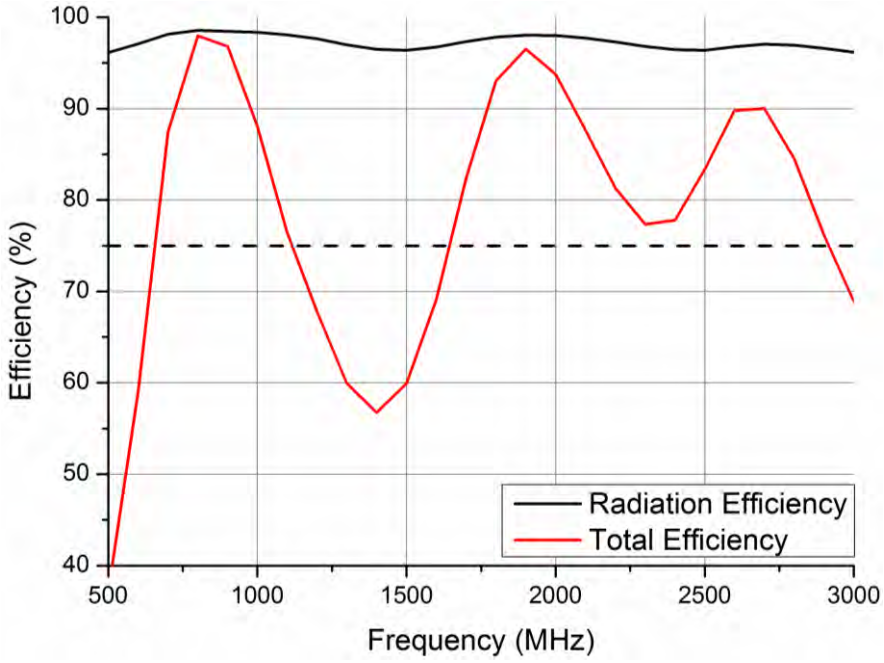


**Figure 4.16. The simulated total and radiation efficiency.**

In Figs. 4.16 and 4.17 the simulated and measured radiation patterns for (x–y) azimuth and (z–y), (z–x) elevation planes at 825 MHz and 2200 MHz are illustrated.

In the three planes at 825 MHz it is observed that the phi ($\varphi$) component provides good omnidirectional characteristics, which is also observed at the azimuth (x–y) plane of 2200 MHz for the theta ($\theta$) component. Moreover, at 825 MHz in the elevation (z–y) plane good discrimination between the two components is provided.

The measured maximum gain for the lower and upper band is 4.5 dBi and 6.4 dBi, respectively. The measured gain, averaged over the principle plane cuts (x–y, z–y and z–x) was −1.1, −1.2 and −2.1 dBi for 825 MHz and −1.4, −1.7 and −1.6 dBi for 2200 MHz.

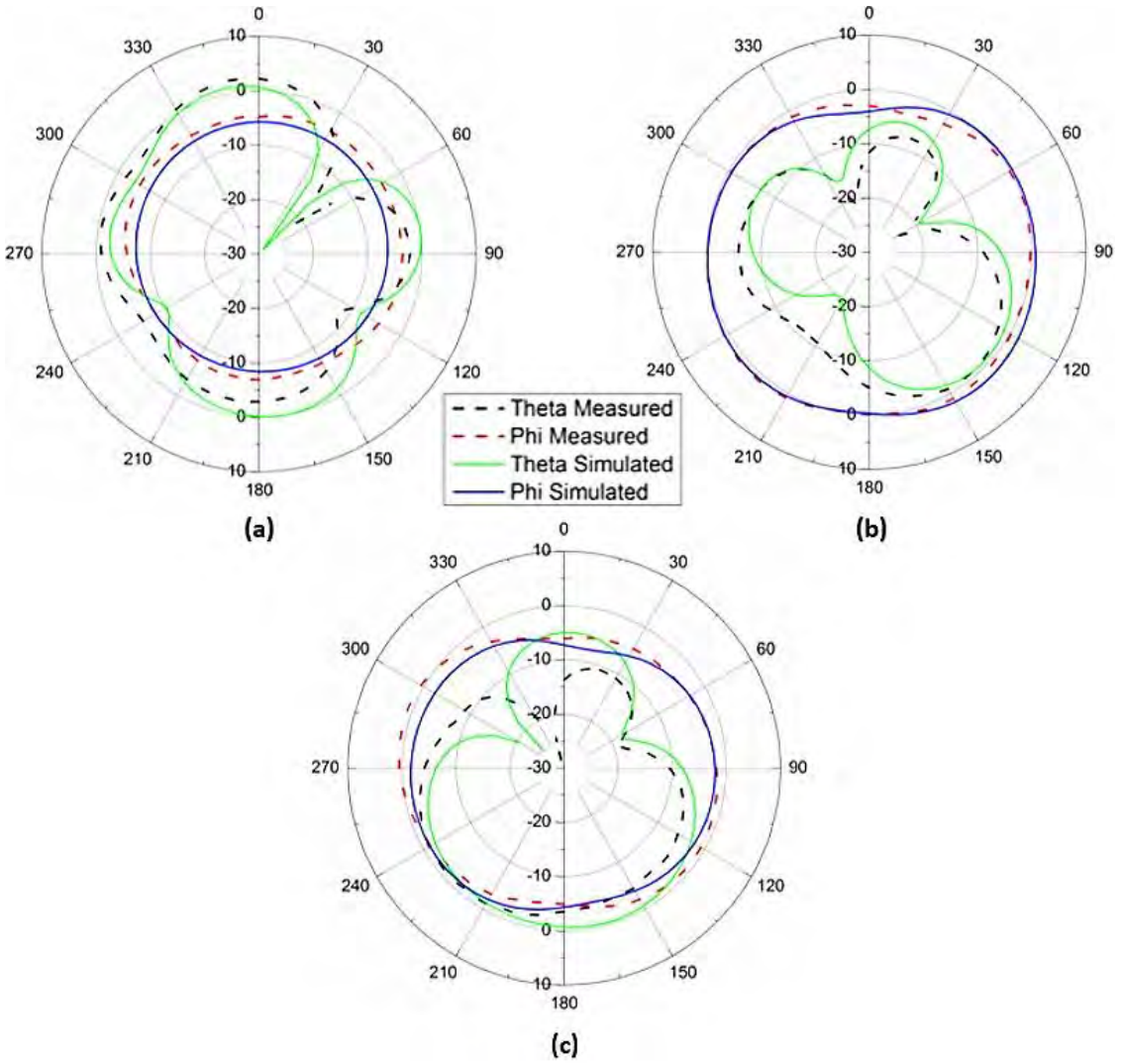


**Figure 4.17. Measured and simulated (a) azimuth (x-y), (b) elevations (z-y) and (c) (z-x) plane patterns at 825 MHz.**

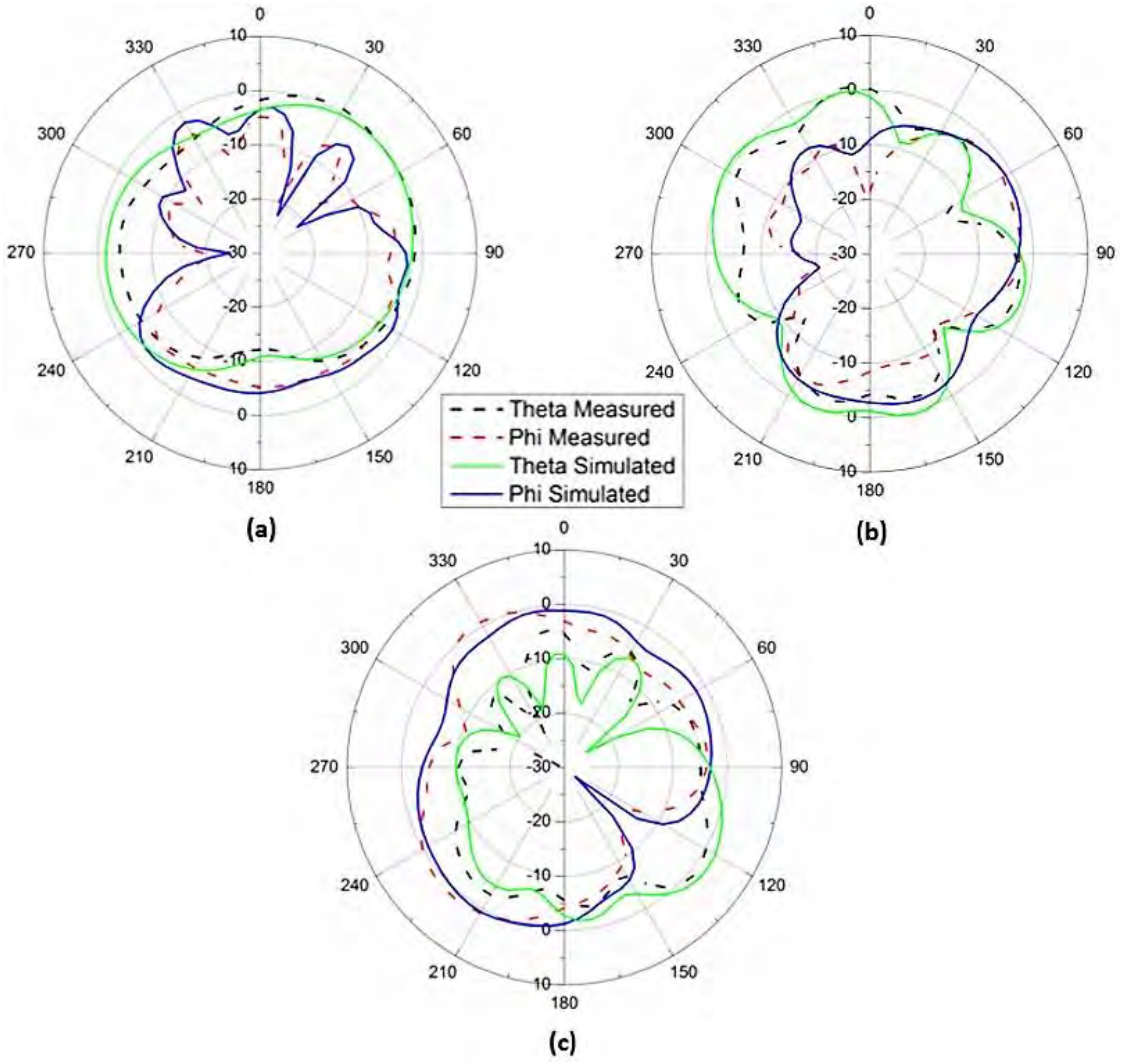


**Figure 4.18. Measured and simulated (a) azimuth (x-y), (b) elevations (z-y) and (c) (z-x) plane patterns at 2200 MHz.**

## 4.2 DUAL LTE PIFA FOR M2M APPLICATIONS

A Dual Planar Inverted-F-Antenna [32, 33, 34, 35, 36] placed on a 130 mm × 70 mm ground plane which is a typical M2M device PCB size. The antenna was designed with smaller size compared to the antenna of the first section and covers the lower LTE band (690 – 960 MHz) and partially the upper LTE band (1670 – 2067 MHz). The antenna is suitable for machine-to-machine (M2M) applications.

### 4.2.1 ANTENNA DESIGN

As a first step of the dual LTE PIFA antenna implementation is a single PIFA which resonates and provide one resonance. A long arm PIFA antenna resonates at lower frequency $f_1$ as well as a short arm PIFA resonates at higher frequency $f_2$ as it shown in Figure 4.19. A novel forked feed is introduced to combine the two PIFAs in the same geometry sharing the same feed, providing the dual band operation.

The antenna structure and coordinate system is depicted in Fig. 4.20. The radiating element is located on a FR-4 (Table 2.1) rectangular ground plane with dimensions 13 × 70 × 1.5 $mm^3$. The sides of the prototyped antenna are printed on thin FR-4 layers of thickness 0.2 mm with dimensions 70 mm (≈ $0.15\lambda_0$ with $\lambda_0$ = 455.9 mm at 658 MHz) ×19 mm (≈ $0.041\lambda_0$). The top part of the antenna consists of two thin copper layers (thickness = 0.15 mm). The top left (59.61 mm × 11 mm) and the top right (9.92 mm × 11 mm) part have a fold-over segments of length $a$ = 9.7 mm and $b$ = 18.3 mm respectively. The antenna comprises two PIFAs sharing the same feed. A small gap (0.2 mm) separating the two PIFAs (Fig. 4.21). The shorting strip of each PIFA has a

width of 0.2 mm. The antenna is fed via a 50 Ω SMA connector through the ground plane to a 5.1 mm wide feeding strip, forked at the top with a small gap (0.2 mm) to separate the two feeds.

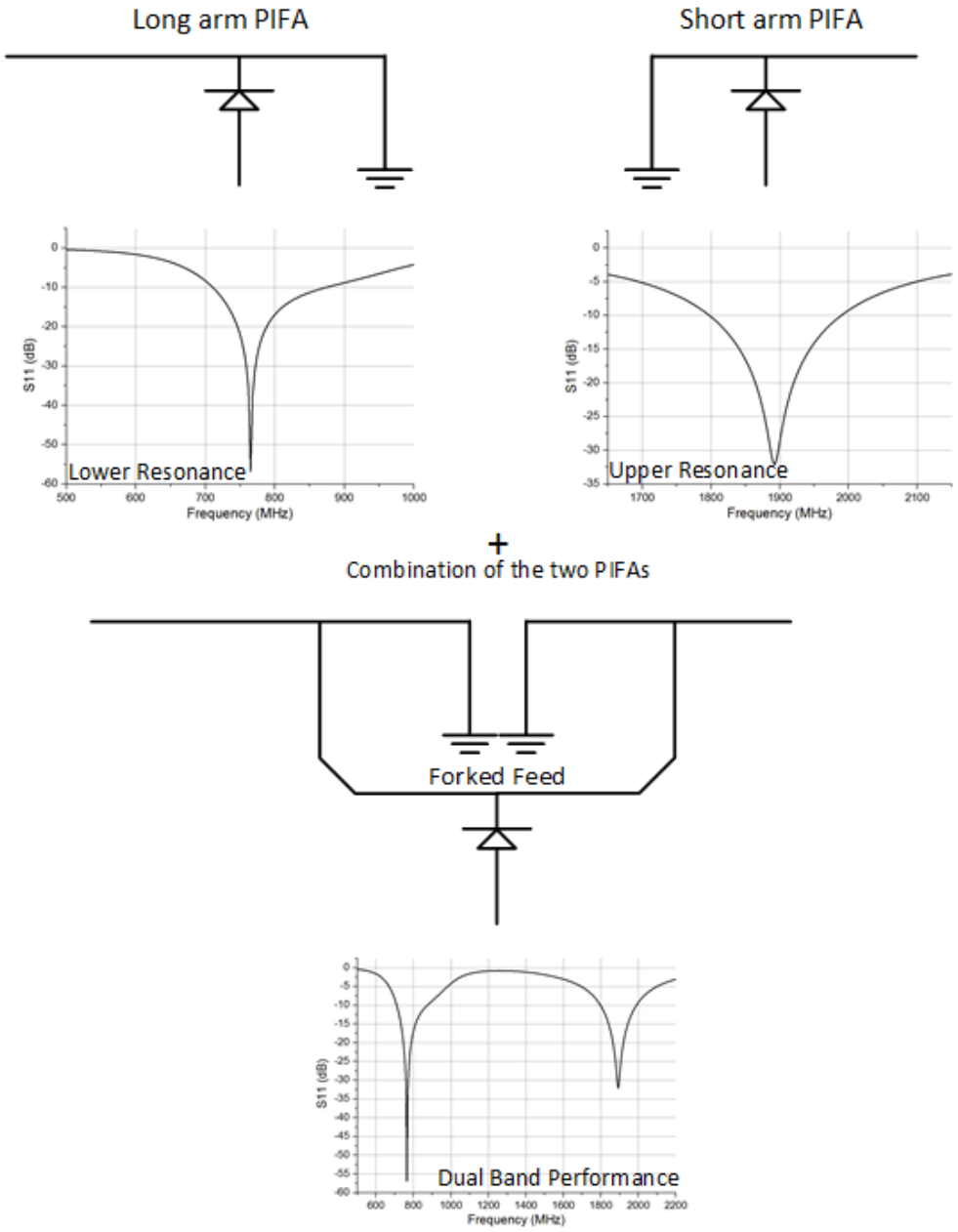


**Figure 4.19. Schematic illustration of dual LTE PIFA design evolution.**

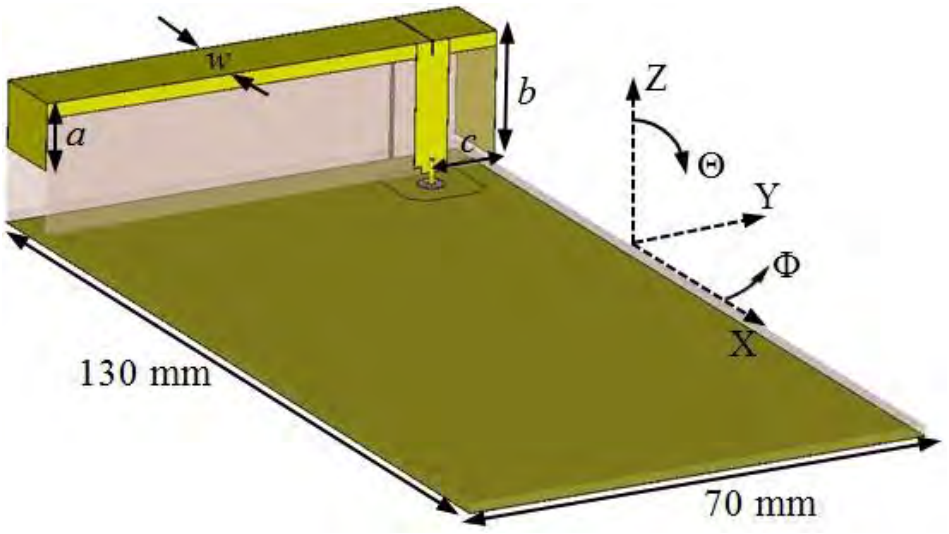


**Figure 4.20. Antenna Model and the coordinate system.**

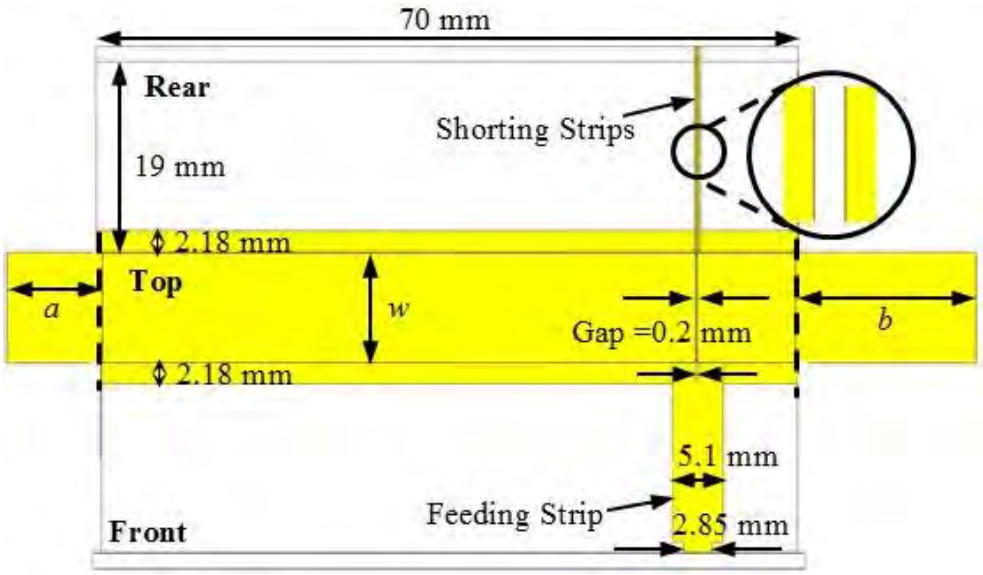


**Figure 4.21. Antenna geometry and parameters.**

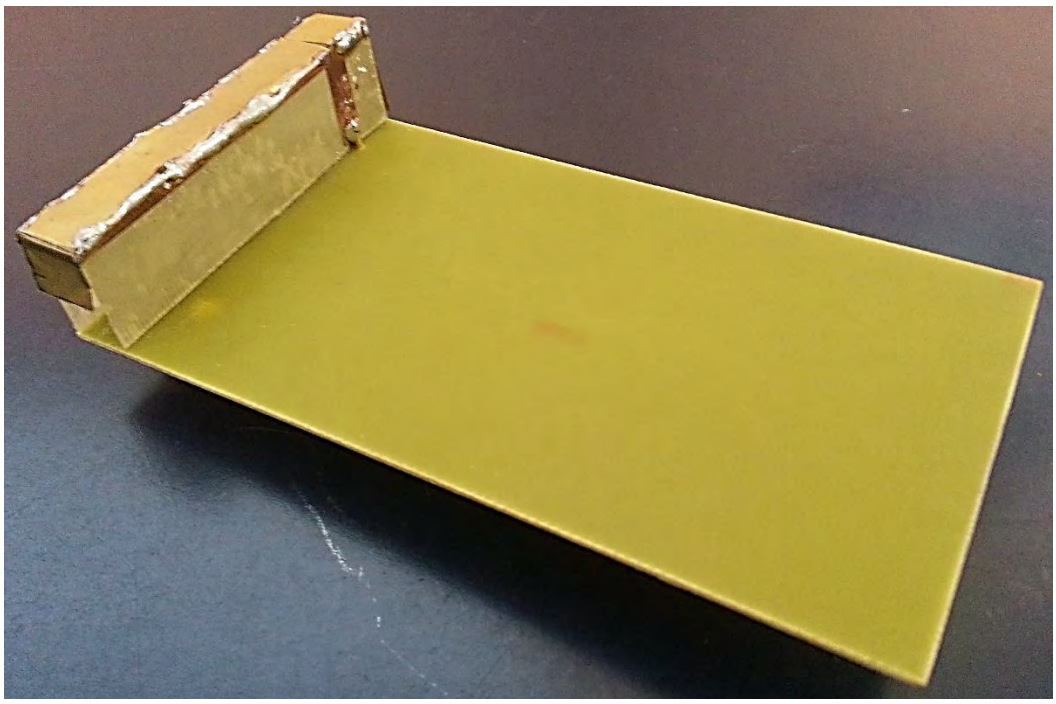

**Figure 4.22. Dual PIFA LTE Antenna prototype.**

## 4.2.2 PARAMETRIC STUDY

The dependence of the lower resonance on the height (*a*) of the left folded part was investigated for four different values. It is apparent that the matching and first resonant frequency is heavily dependent on this parameter as well as some effects on the second resonance. The optimum value of this parameter (*a*) is 9.7 mm.

The upper resonance is strongly dependent on the height (*b*) of the right folded section. The height (*b*) is varied from 16 mm to 19 mm. From the obtained result (Fig. 4.24) it is evident that the second resonant frequency can be controlled (impedance matching and frequency shifting) by varying the parameter *b*. The proposed value of the folded length (*b*) is 18.3 mm.

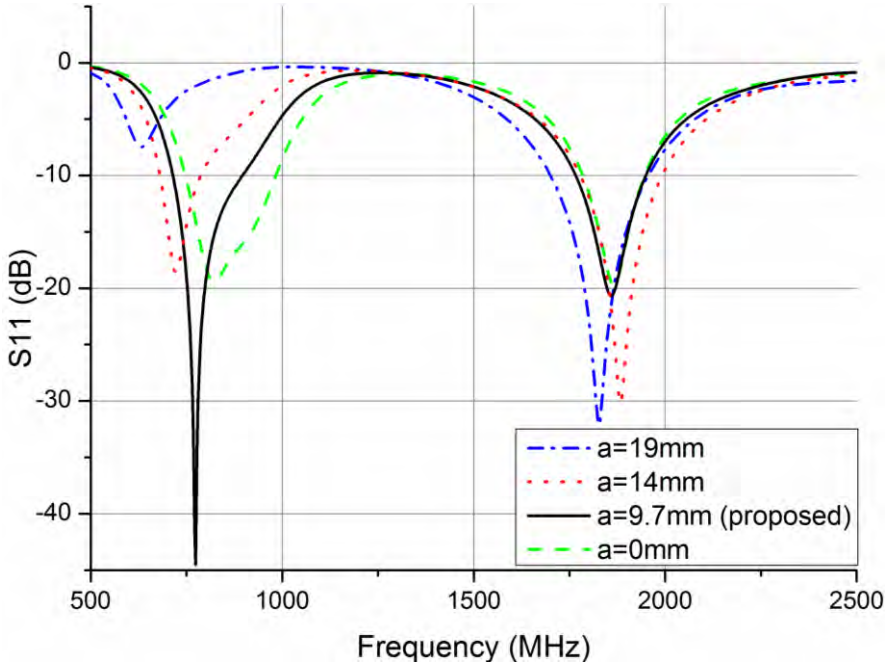


**Figure 4.23. Simulated $S_{11}$ variation for different values of (*a*).**

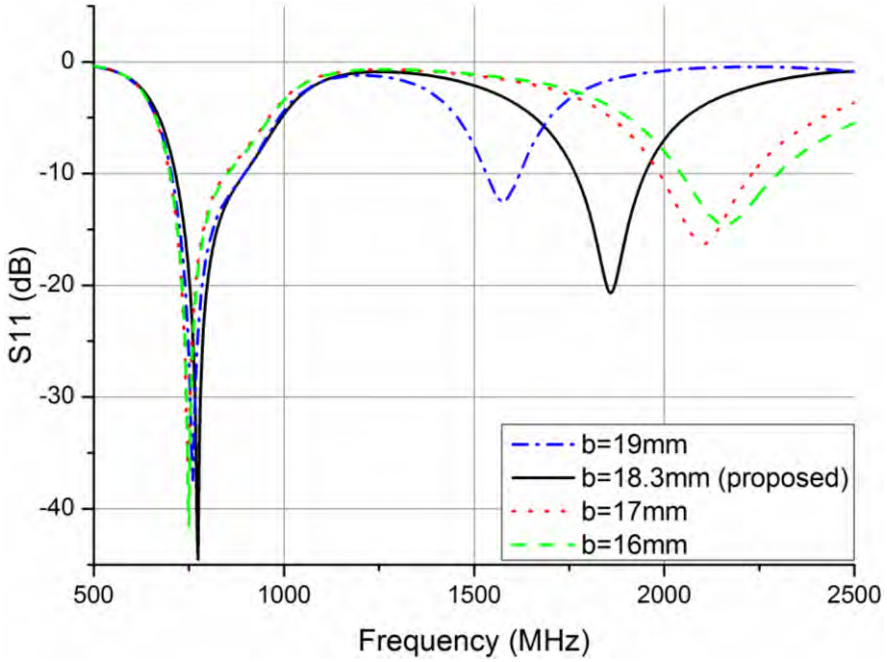


**Figure 4.24. Simulated $S_{11}$ variation for different values of (*b*).**

The position (*c*) of the feed and the shorting point can determine the electrical length of both PIFAs. As the feed and shorting point moved from the right side (5.97 mm) of the antenna to the centre (35 mm) both resonances are shifted. The frequency ratio $F_r = f_u/f_l$ between the upper and the lower resonance continuously increases from 1.43 to 2.99 as the value of (*c*) changes from 35 mm to 5.97 mm. The proposed value of the parameter (*c*) is 9.97 mm.

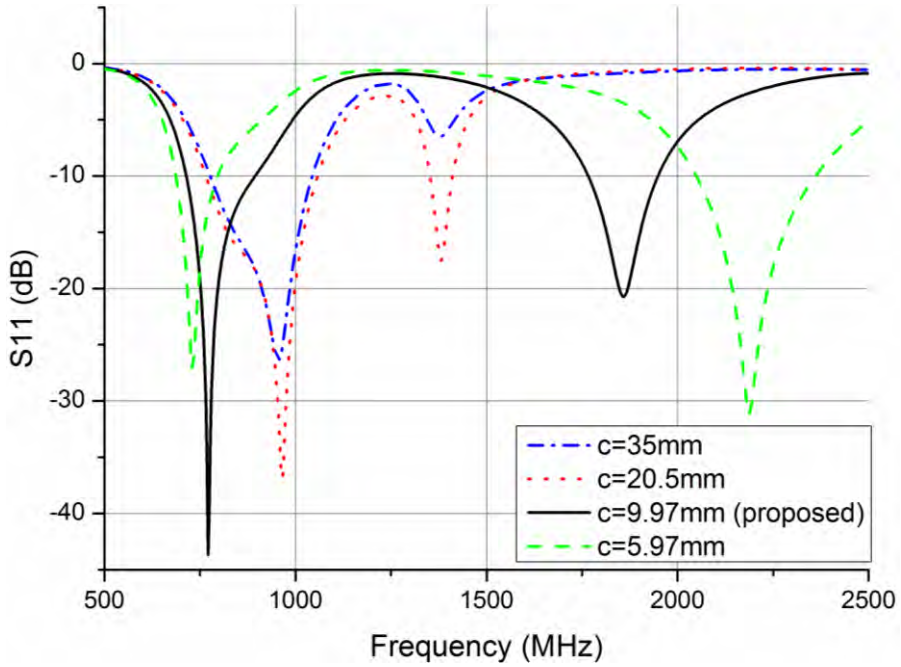


**Figure 4.25. Simulated $S_{11}$ variations for different values of (*c*).**

Finally, the last key parameter which is studied for this antenna is the width (*w*) of the top part of the two PIFAs. From the obtained results it is clear that the second resonance is effectively controlled and shifted downwards as the parameter (*w*) increased from 5 mm

to 14 mm. The width (*w*) has a strong impact and improves the impedance matching of the first resonant frequency. The proposed value of (*w*) is 11 mm.

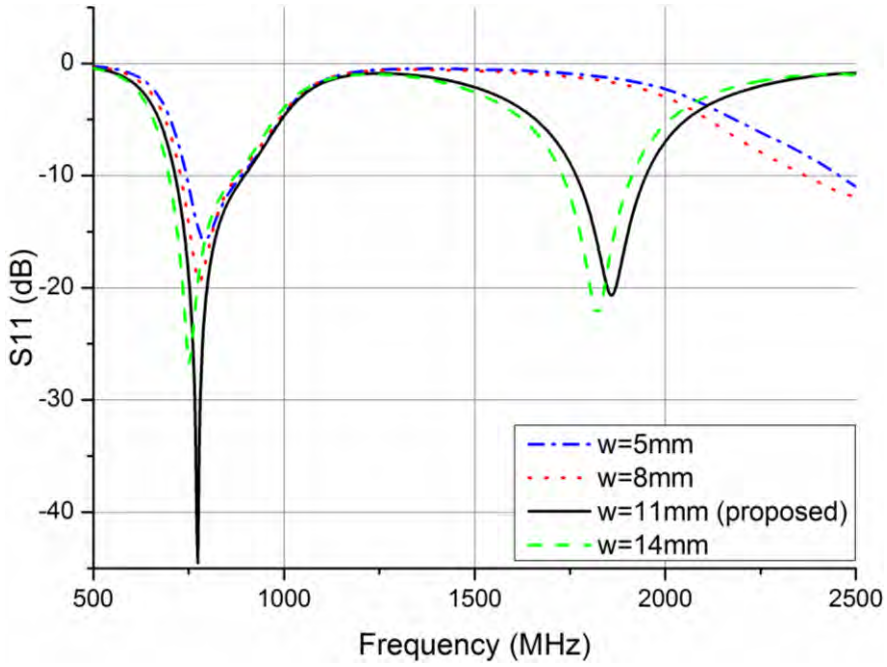


**Figure 4.26. Simulated $S_{11}$ variations for different values of (*w*).**

The current distribution at both frequencies is shown in Fig. 4.27. For the first resonant frequency (Fig. 4.27(a)) the main part of the antenna which resonates is the longest arm PIFA. The electrical length of the longest PIFA is almost 90 mm which is almost a quarter wavelength at 760 MHz ($\lambda_0/4$ = 98.6 mm). For the second resonance (Fig. 4.27(b)) the main current distribution comes from the shorter arm PIFA of the antenna. The length of the shortest PIFA is almost 46 mm which is slightly over a quarter wavelength at 1860 MHz ($\lambda_0/4 \approx 40.3$ mm).

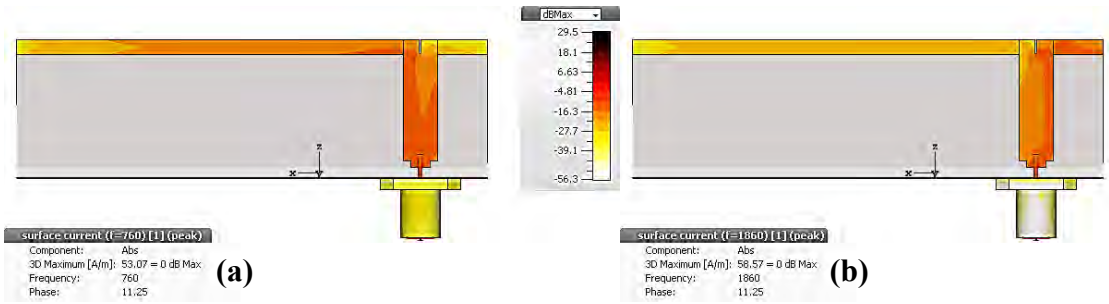


**Figure 4.27. The current distribution at (a) 760 MHz and (b) 1860 MHz.**

## 4.2.3 Simulated And Measured Results

In Fig. 4.28 the measured and simulated $S_{11}$ show good agreement. The antenna operates at 760 MHz with a −10 dB and −6 dB impedance bandwidth of 208 MHz (682 – 890 MHz) and 306 MHz (658 – 964 MHz) respectively for the lower band and at 1860 MHz with a −10 dB and −6 dB impedance bandwidth of 220 MHz (1750 – 1970 MHz) and 396 MHz (1671 – 2067 MHz) respectively for the upper band. The simulated results provide a −10 dB and −6 dB impedance bandwidth of 162 MHz (711 – 873 MHz) and 281 MHz (680 – 961 MHz) at the centre frequency of 765 MHz for the first band and a −10 dB and −6 dB impedance bandwidth of 192 MHz (1797 – 1989 MHz) and 341 MHz (1725 – 2066 MHz) at the centre frequency of 1893 MHz for the second band.

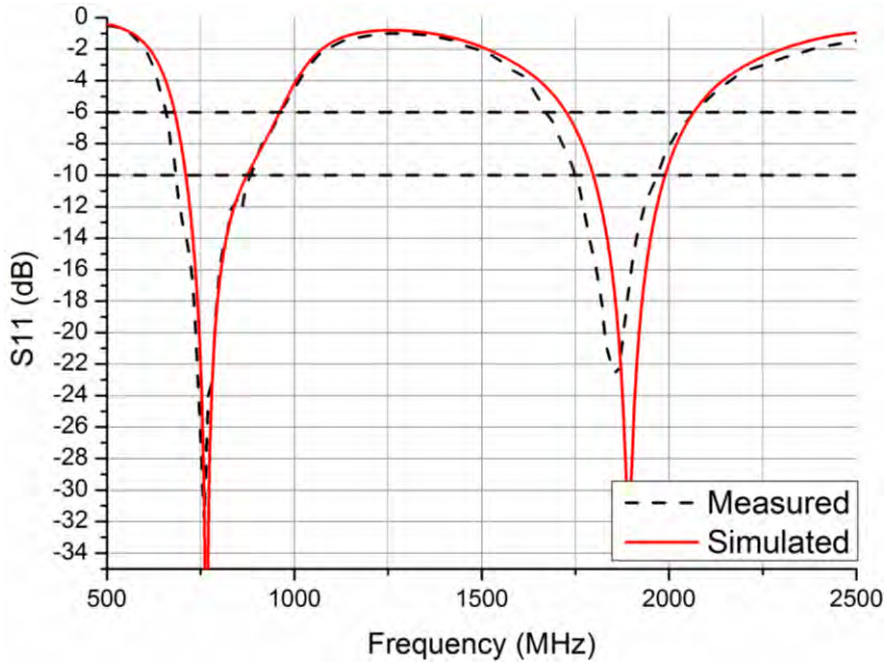


**Figure 4.28. Simulated and measured $S_{11}$ for the PIFA antenna.**

In Fig. 4.30 the measured and the simulated total efficiency and realized gain are given. There is a reasonable agreement between the simulated and measured results. The total efficiency and the realized gain of the antenna were measured by Microwave Vision Group (MVG) in StarLab 0.6 – 18 GHz and are listed in Table 4.1. This chamber uses the nearfield measurement technique to calculate the equivalent far-field data of the AUT. The antenna under test is positioned in the centre of a circular 'arch' which contains 15 separate measurement probes spaced equally apart as can be seen in Fig. 4.29. The antenna is rotated horizontally through 360° and the combination of this rotation and the array of probes allows a full 3D scan of the antenna to be carried out, allowing full 3D radiation patterns to be measured, plotted and analysed. Efficiency, gain and directivity

information can be transformed and calculated from the far-field radiation pattern data [74].

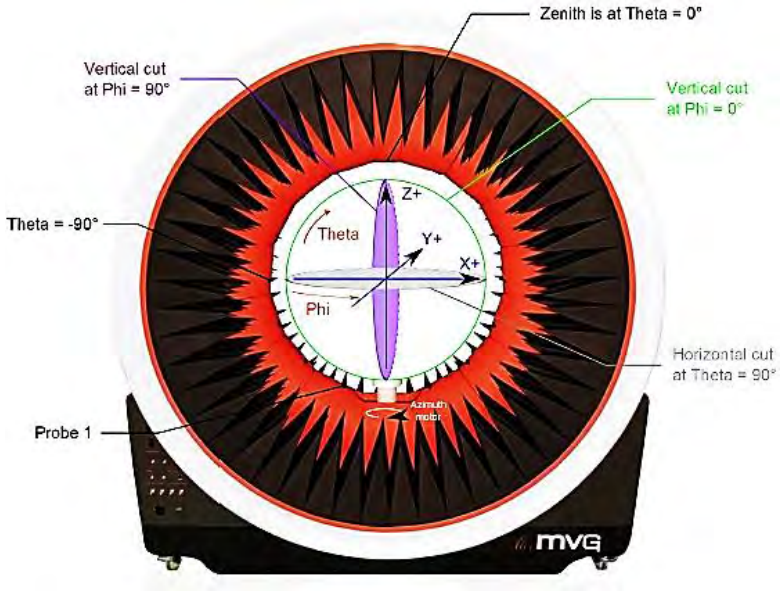


**Figure 4.29. StarLab spherical coordinate system [74].**

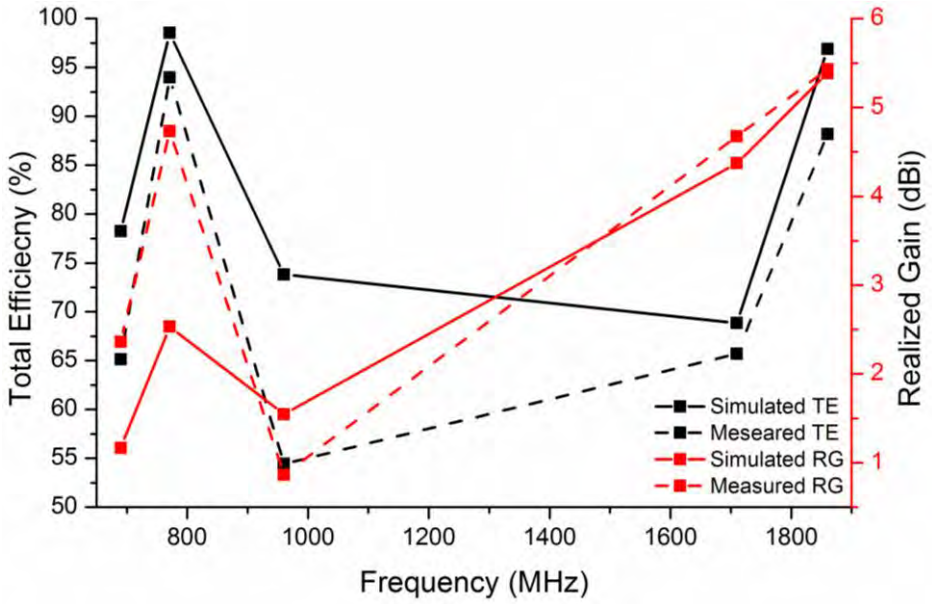


**Figure 4.30. Measured and simulated total efficiency and realized gain.**

**Table 4.1. Measured and Simulated Total Efficiency and Realized Gain.**

| *Frequency (MHz)* | Total Efficiency (%) | | Realized Gain (dBi) | |
|---|---|---|---|---|
| | Simulated | Measured | Simulated | Measured |
| **690** | 78.2 | 64.8 | 1.2 | 1.9 |
| **760** | 98.5 | 83.6 | 2.5 | 3.6 |
| **960** | 73.8 | 58 | 1.5 | 0.8 |
| **1710** | 68.8 | 65.2 | 4.4 | 3.5 |
| **1860** | 96.9 | 79.8 | 5.4 | 4.1 |

The radiation patterns of the three plane cuts (x–y, z–x and z–y) for 760 MHz and 1860 MHz are shown in Figs. 4.32 and 4.33 respectively. All the measured patterns are illustrated against the simulated patterns in 10 dB/division scaled plots.

It is observed that the theta ($\theta$) component provides good omnidirectional characteristics in the (x–y) plane for both frequencies, which is also observed in the (z–y) plane for 760 MHz for the phi ($\varphi$) component.

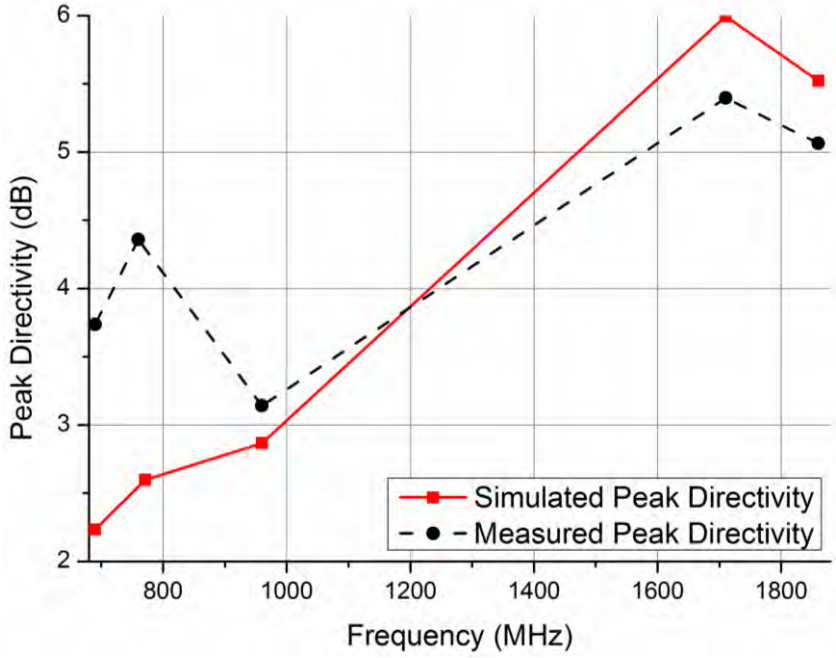


**Figure 4.31. Measured and Simulated Peak Directivity.**

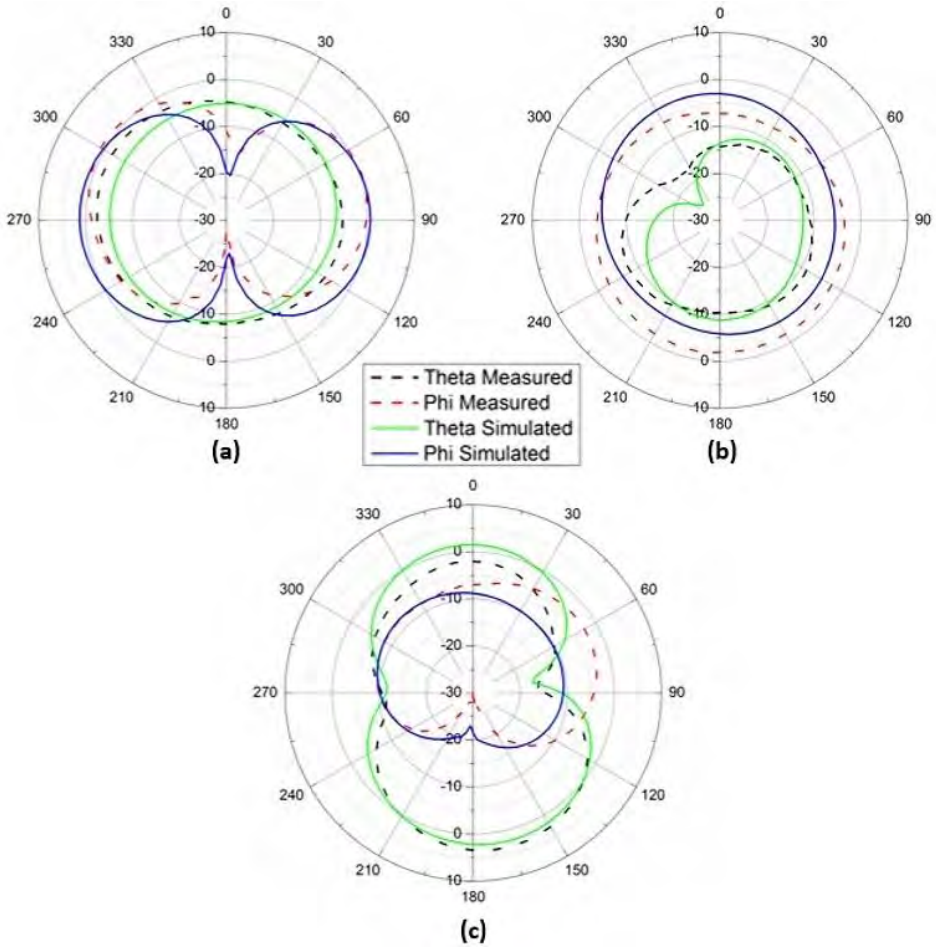


**Figure 4.32. Measured and simulated (a) azimuth (x-y), (b) elevations (z-y) and (c) (z-x) plane patterns at 760 MHz.**

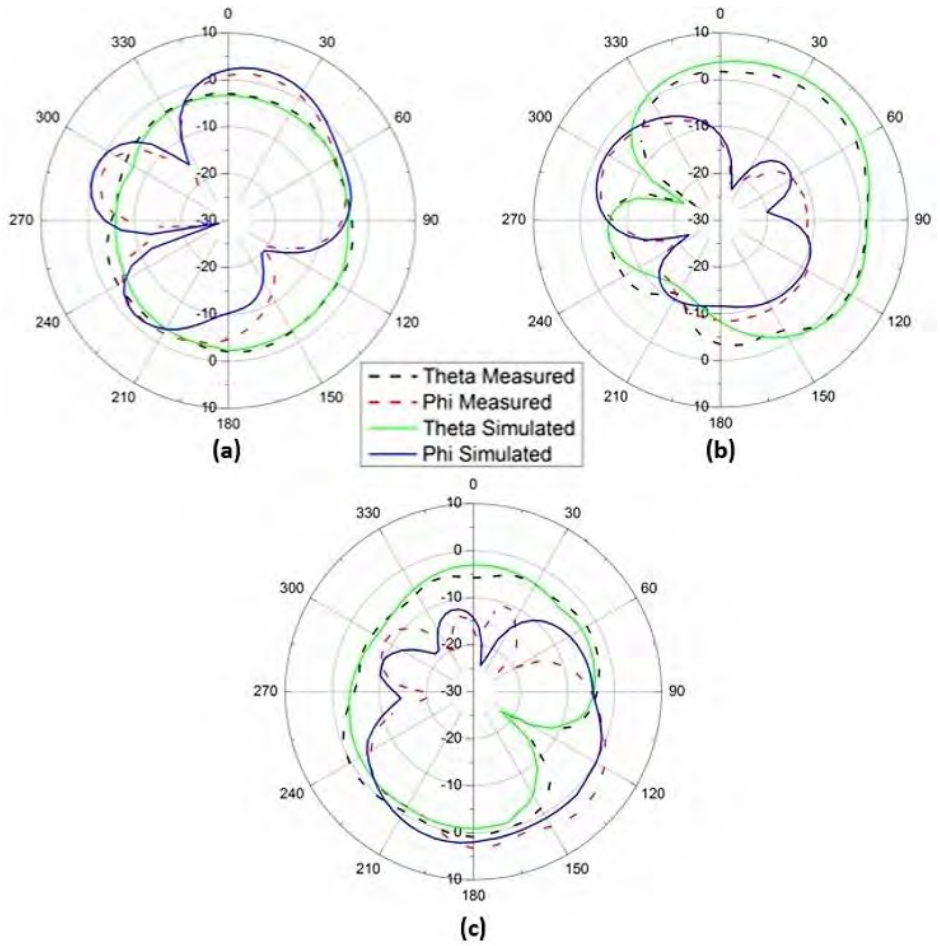


**Figure 4.33. Measured and simulated (a) azimuth (x-y), (b) elevations (z-y) and (c) (z-x) plane patterns at 1860 MHz.**

## 4.3 CONCLUSIONS

This chapter presented the study of the performance of two Planar Inverted-F antennas on rectangular ground planes in the LTE frequency range respectively. A parametric investigation of key geometrical parameters of the two antennas are reported.

The first PIFA antenna is studied in terms of the ground plane size and positioning. The obtained results show that the position of the PIFA on the ground plane effectively controls both resonant frequencies (impedance matching and frequency shifting). The $S_{11}$ shows stronger dependence on the ground plane size than the radiation properties and the total efficiency does not change significantly.

The second PIFA antenna which is smaller and mounted on a typical device size ground plane covers the lower LTE band and partially the upper. The proposed antenna has been optimised with good omnidirectional radiation characteristic at both bands, high efficiency and gain, is low profile, with additional benefit of a large frequency-ratio range $f_u/f_l = 2.44$ which is easy to control.

# 5. Meander Line Monopole Antenna

Meander line monopole antennas [21 22, 23, 24] are mainly used in compact and portable smart devices. With this state of the art technology, antenna designers are able to integrate compact meander line structures in small envelopes achieving broadband performance, providing also high gain and efficiency for its compact size.

This chapter proposes a geometry based on a folded meander line structure which is suitable for automated meter reading (AMR) systems [75]. The Electronic Communication Committee (ECC) allocates narrowband channels in the 410 – 470 MHz range [76]. CDMA and more recently eLTE operate in this band with channel bandwidths in the region of ~1 − 5 MHz [77, 78]. Performance metrics include impedance bandwidth, radiation patterns and total efficiency.

In this section a tuneable folded meander-line monopole antenna covering the lower UHF band (412 – 475 MHz) is studied. The antenna configuration is optimized for impedance matching. The effect of the ground plane size on the general radiation properties is analysed. Finally, the installed performance of the proposed antenna is investigated with the antenna embedded in a plastic housing and placed on a concrete wall.

## 5.1 MEANDERED ANTENNA FOR M2M APPLICATIONS

The antenna is designed for integration into a compact smart meter device for cellular communications technologies [79] which provides a tuneable functionality over the frequency range of 412 – 475 MHz. According to specifications for 450 MHz meter reading system applications [80], there is a requirement for an omnidirectional antenna and a $S_{11}$ of better than −6 dB over the proposed frequency range with narrow channel bandwidths and maximum EIRP of +27 dBm. Designing a small-size, high-efficiency, broadband antenna, is a considerable challenge for the antenna designer.

## 5.2 ANTENNA CONFIGURATION

The initial implementation idea which leads to the final meander line design is a folded monopole antenna as it shown in Fig. 5.1. The position of the feeding and the shorting strips is changed to the back side of the FR4 substrate allows more available space to confine the electrical length (meander line) into a compact physical size and to move to lower frequencies (Fig. 5.2).

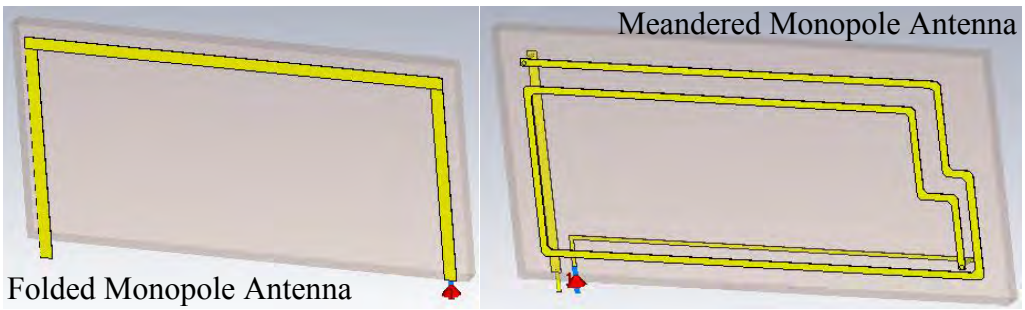


**Figure 5.1. Illustration of the antenna designed steps.**

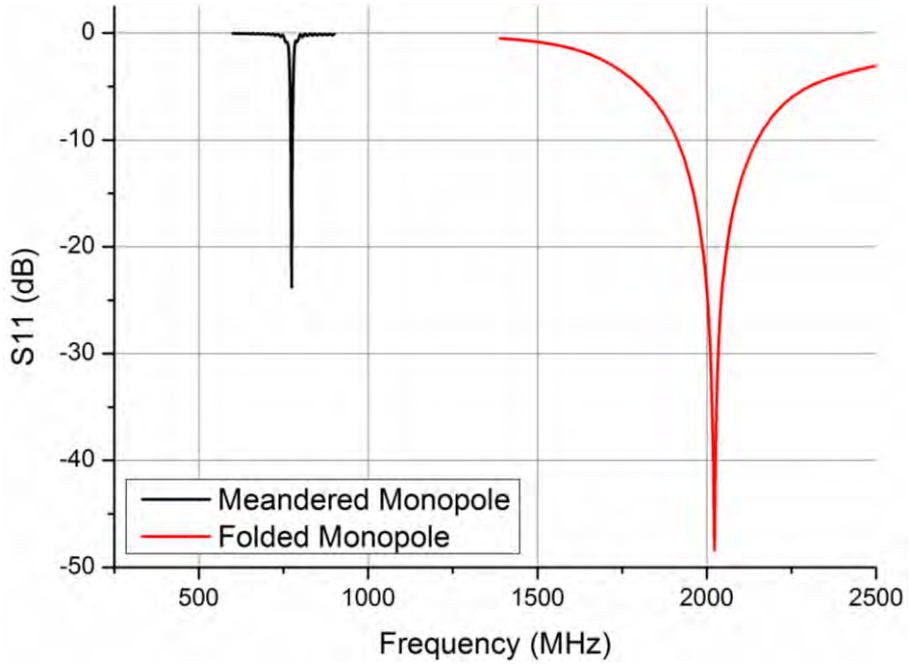


**Figure 5.2. Simulated $S_{11}$ for the two different antenna models.**

The antenna geometry, shown in Fig. 5.3, is printed on double-sided FR-4 substrate (Table 2.1). The antenna of height $h$ = 15 mm ≈ 0.02$\lambda_0$ ($\lambda_0$ = 724.5 mm at 414 MHz) and length $l$ = 42.3 mm ≈ 0.058$\lambda_0$ is located on the corner of a 130 mm × 70 mm ground plane which represents a typical device PCB. The feeding and shorting strips (width = 0.5 mm and 0.7 mm respectively) are located on the rear side of the substrate and connected to the meander line (width = 0.5 mm) on the front side using a via and a slider connector.

The separation between the horizontal strips $a_1$, $a_2$ and $a_3$ is 0.85 mm. The gap between the vertical strips $b_1$, $b_2$ and $b_3$ is 0.83 mm. The lower horizontal strips $c_1$ and $c_2$ have a separation of 0.5 mm and between $c_2$ and $c_3$ the separation is 0.68 mm. The gap between the two vertical strips $d_1$ and $d_2$ is 0.8 mm. The separation between the strips is optimised to obtain the best impedance matching for the desired frequency.

The moveable U-shaped aluminium via-slider is mounted through a slot in the substrate, connecting the two sides of the PCB. The start and end positions of the via-slider are at 0 mm ≤ $P$ ≤ 33.5 mm (Fig. 5.3). The monopole antenna is fed using a 50 Ω microstrip line (width = 1.3 mm) with a SMA connector below the ground plane.

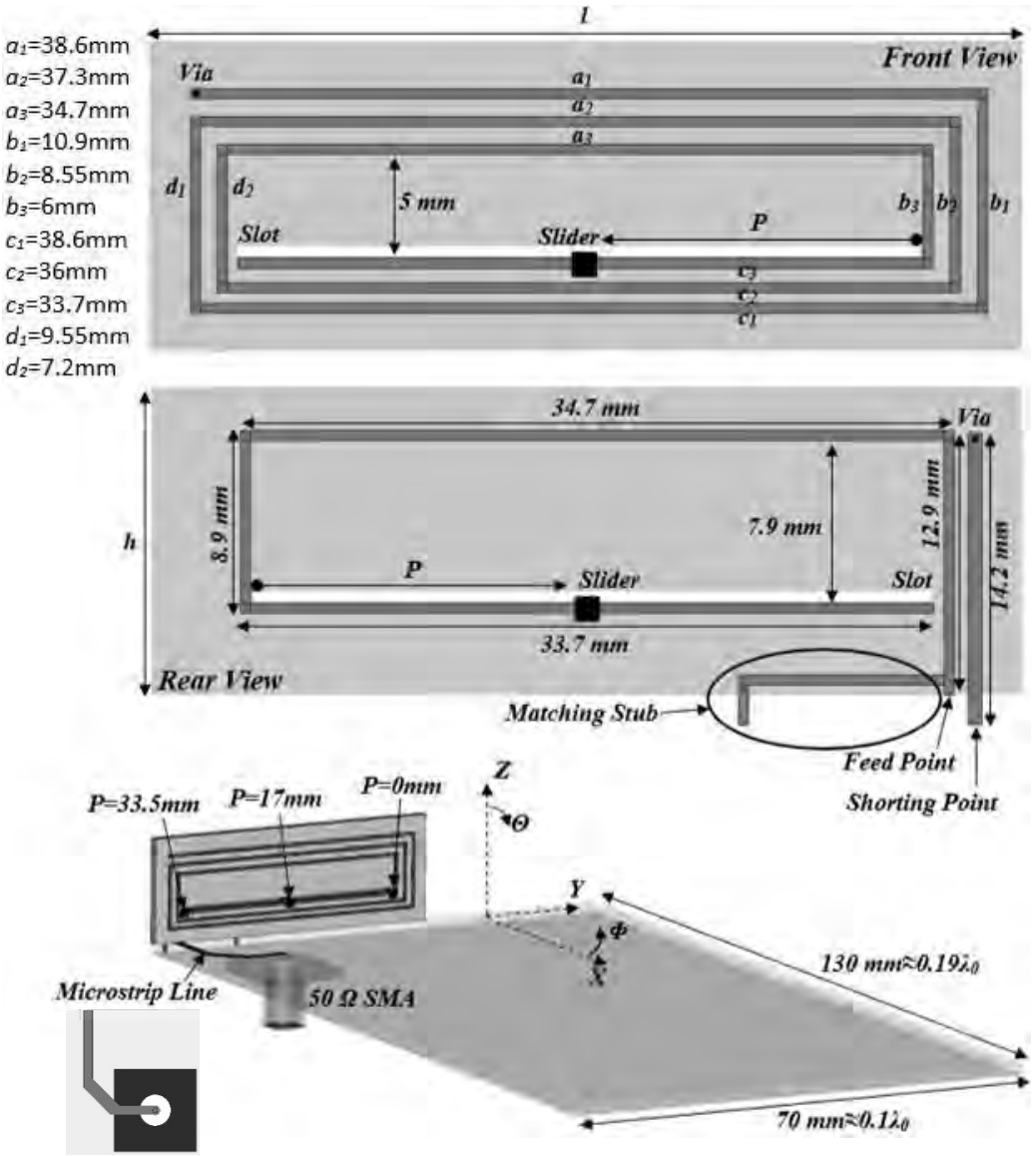


**Figure 5.3. Antenna geometry and the coordinate system.**

## 5.3 MATCHING STUB

To improve the impedance matching of the antenna, a matching stub is added and shorted to the ground plane as shown in Fig 5.4 (a) and also shifts downwards the resonant frequency by introducing additional capacitance and reducing the real impedance towards 50 Ω (Fig. 5.4 (b)). The matching stub consists of two strips (width = 0.5 mm) with horizontal and vertical length 10 mm and 2.5 mm, respectively.

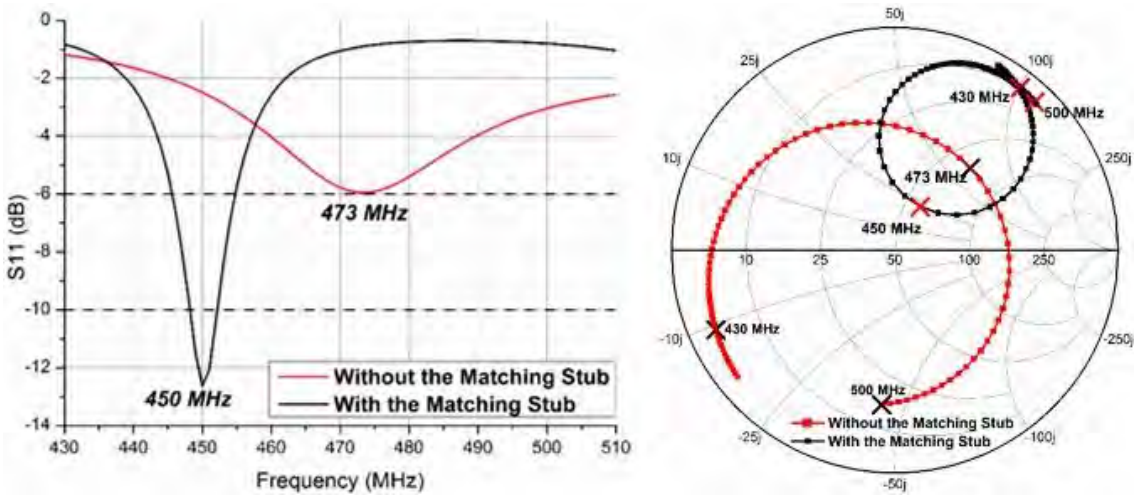


**Figure 5.4. (a) Improved impedance matching and control of frequency, (b) Smith chart.**

## 5.4 Ground Plane Size

The ground plane size was found not to have significant influence on the antenna performance. A parametric study of the ground plane size was made and simulations were carried out for ground plane sizes of 40 × 100 $mm^2$ to 170 × 230 $mm^2$. Fig. 5.5 shows a plot of the $S_{11}$ for different ground plane sizes. From the graph it is clear that the ground plane size does not significantly affect the resonant frequency and the impedance matching of the antenna. For the given ground plane sizes the resonant frequency does not change more than 4 MHz.

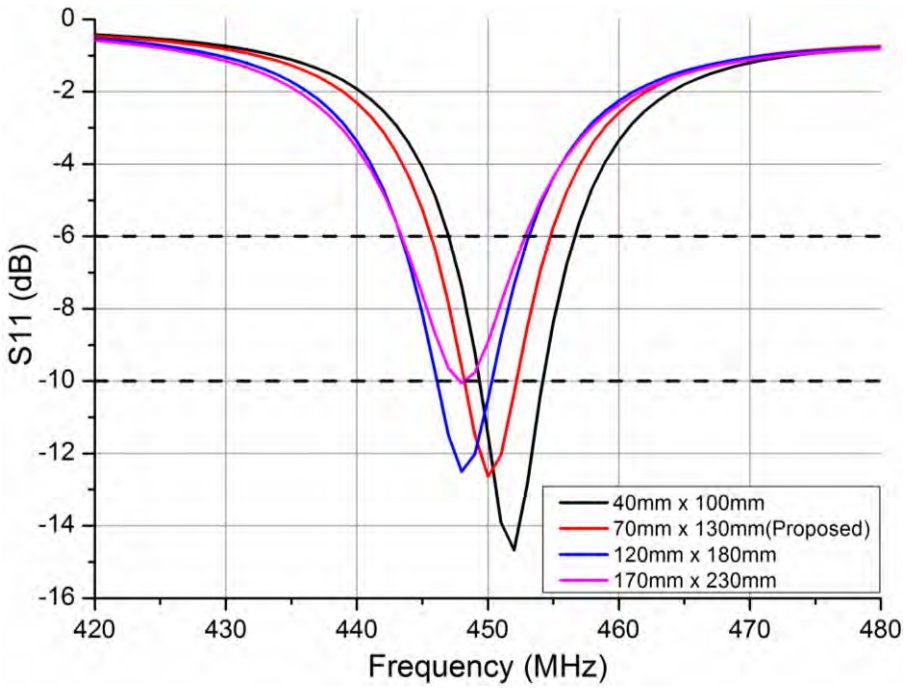


**Figure 5.5. Simulated $S_{11}$ dependence on the ground plane size.**

## 5.5 MEASURED AND SIMULATED RESULTS

In Fig. 5.6 the measured and simulated $S_{11}$ for 5 different tuning positions of the via-slider connector *P*, which controls the resonant frequency are shown. The measured −10 dB and −6 dB tuneable impedance bandwidth, is 412.4 – 474.8 MHz (BW = 62.4 MHz) and 71.6 MHz (409.5 – 481.1 MHz) respectively. The measured −6 dB and −10 dB bandwidths at 414 MHz ($\lambda_0$ ~ 724.5 mm) are ~8 MHz and ~3 MHz respectively.

The position of the via-slider for resonance at 450 MHz is *P* = 17 mm with a −10 dB impedance bandwidth of 7.2 MHz (446.5 – 453.7 MHz) and a −6 dB impedance bandwidth of 12.6 MHz (444.1 – 456.7 MHz).

The tuneability of the proposed antenna could be also achieved with diodes or varactors. However, the installation of diodes and varactors in a limited available space with the requirement of bias and DC suppliers is a constraint for implementation.

The meander-line monopole is the dominant part of the antenna which contributes and resonates at 450 MHz. The current distribution is shown in Fig. 5.7. The two open circuited lines after the slider connector are an integral part of the antenna reconfigurability and have been included in all simulations and measurements including total efficiency. If the open circuited strips are cut after tuning the antenna, this would cause a slight upward shift in frequency.

The total efficiency was simulated and measured and is illustrated in Fig. 5.8 for three different frequencies and indicates 21% total measured efficiency at 420 MHz, 24% at

450 MHz and 21.7% at 470 MHz. It is observed that there is a reasonable agreement between the simulated and measured results.

In an attempt to calculate the maximum theoretical total efficiency of the proposed antenna and to define how close is the measured values to the fundamental limitations, a mathematical explanation is described.

Harrington [7] defined the natural gain limit for a practical antenna: $G_{max}=(ka)^2+(ka)$. In [81] the maximum directivity of an antenna appointed with the following reasonable formula: $D_{max}=(ka)^2+3$. The relation between the antenna gain and directivity is expressed through the following formula:

$$G_{max} = \eta \times D_{max} = G_{max}/D_{max} = (ka)^2 + ka/(ka)^2 + 3 \quad (5.1)$$

Based on the previous expression, the maximum total efficiency is equal to:

$$\eta_T = (1 - |\Gamma|^2) \times \eta = (1 - |\Gamma|^2) \times [(ka)^2 + ka/(ka)^2 + 3], \quad (5.2)$$

where $k$ is the wave number in free space, $k = 2\pi/\lambda$ and $a$ is the radius of the minimum sphere that encloses the antenna. The theoretical and measured total efficiency values of the antenna are listed in Table 5.1. The radius $a$ of the proposed antenna's radiansphere was calculated at 74.2 mm which is $0.11\lambda_0$ of the respective wavelength $\lambda_0 \approx 667$ mm at 450 MHz. The wavenumber $k$ at 450 MHz is 0.0094 and $ka = 0.0094 \times 74.2 \approx 0.69$. The theoretical maximum total efficiency is calculated through the formula (5.2):

$$\eta_T=(1-|\Gamma|^2)\times [(ka)^2+ka/(ka)^2+3]=(1-|\Gamma|^2)\times 0.335=0.98\times 33.5=0.328\approx 32.8\%.$$

As can been seen from the acquired results in Table 5.1 the measured total efficiency is very close to the theoretical maximum values, which shows that the proposed antenna is quite efficient compared to its size and to the operating frequency range.

**Table 5.1. Comparison of theoretical and measured total efficiency.**

| ***Total Efficiency (%)*** | 420 MHz | 450 MHz | 470 MHz |
|---|---|---|---|
| Theoretical | 28 | 32.8 | 30 |
| Measured | 21 | 24 | 21.7 |

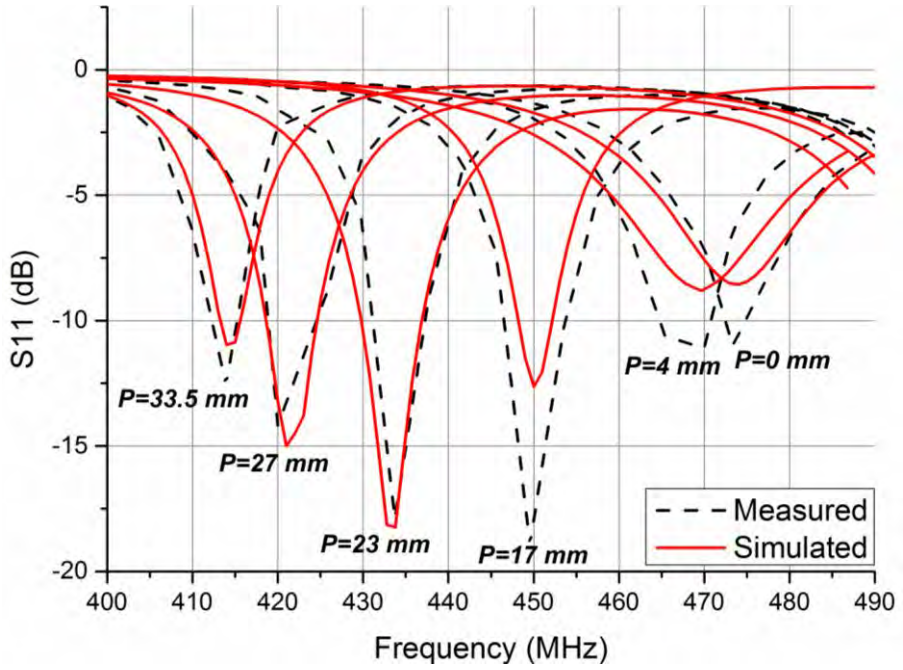


**Figure 5.6. Simulated and measured $S_{11}$.**

In Figs. 5.10 to 5.12 the measured and simulated azimuth (x–z) and elevation (x–y) and (y–z) plane radiation patterns at 450 MHz are illustrated. In Fig. 5.11 it is seen that the omnidirectional pattern provides good polarization discrimination in the elevation (x–y) plane. The maximum measured gain is −6.1 dBi. There is good agreement between the measured and the simulated results. The radiation patterns are stable across the tuneable band.

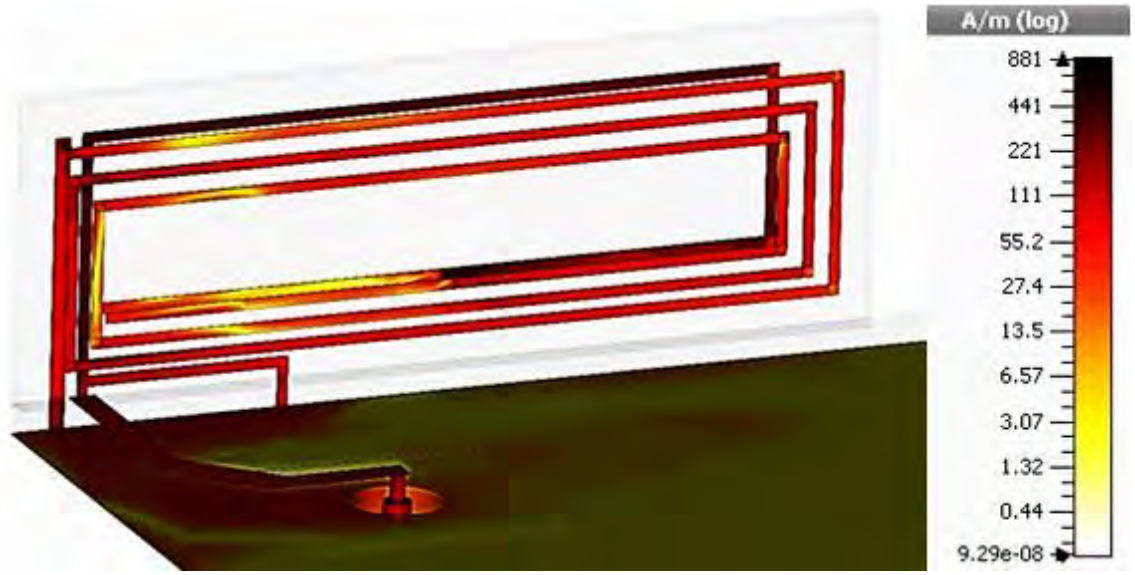


**Figure 5.7. Current distribution at 450 MHz.**

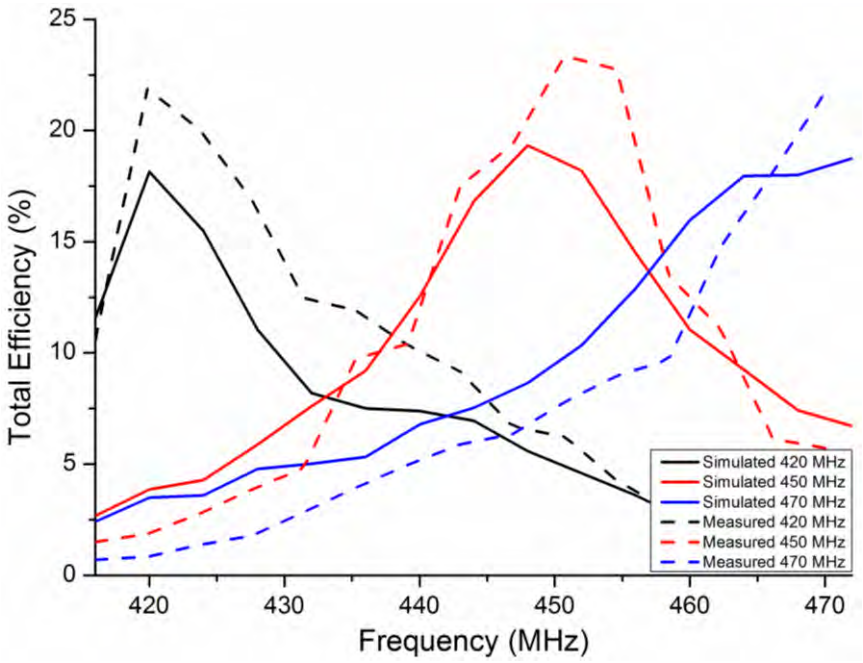


**Figure 5.8. Total measured and simulated efficiency of the antenna at 420, 450 and 470 MHz.**

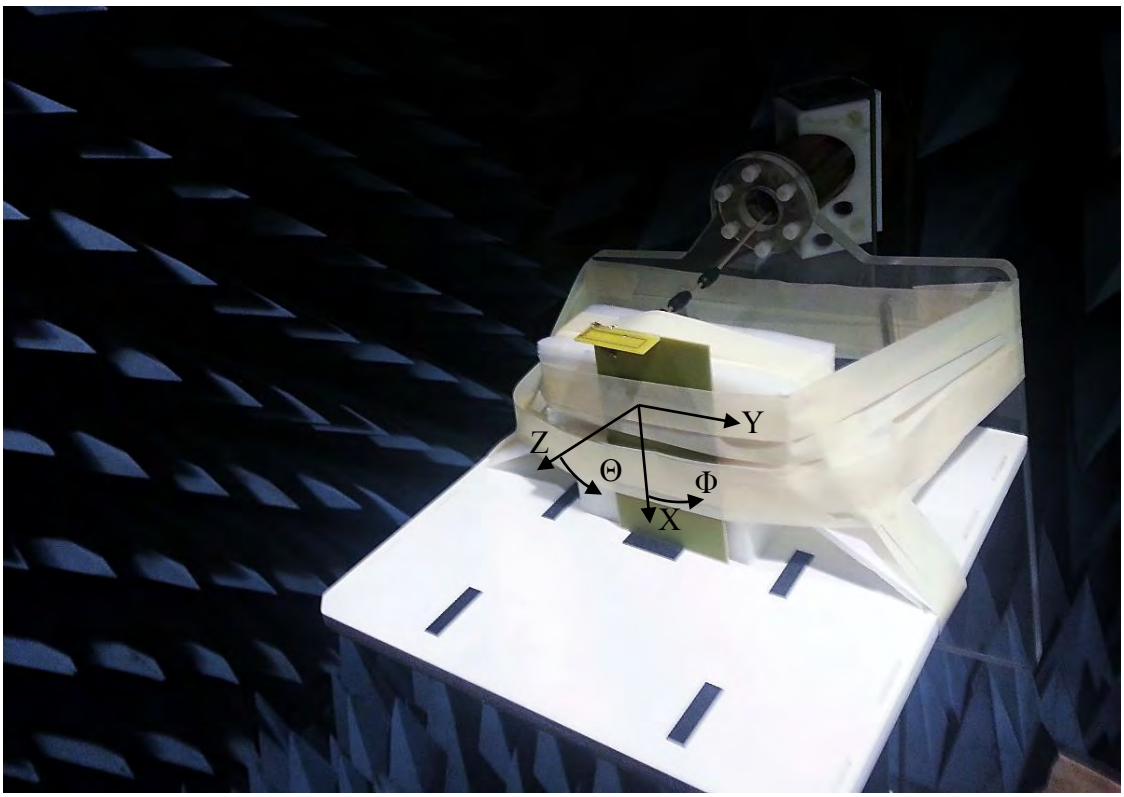


**Figure 5.9. The antenna inside the anechoic chamber.**

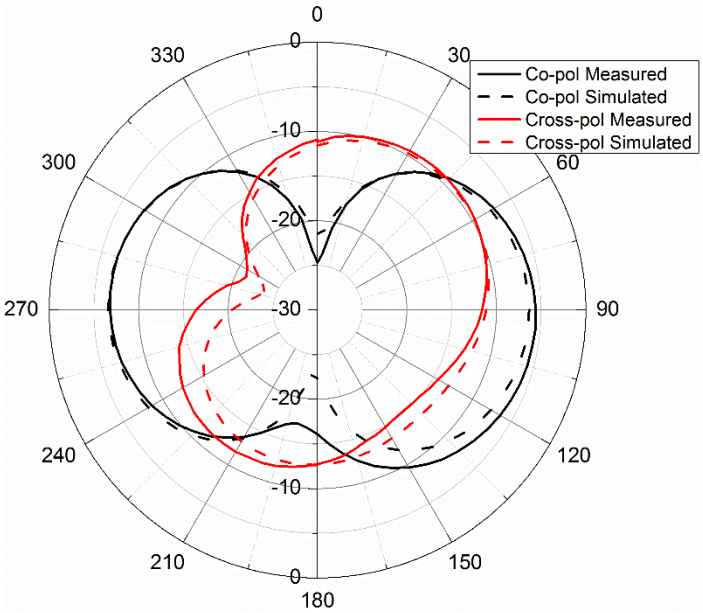


**Figure 5.10. Azimuth radiation patterns in the xz-plane at 450 MHz.**

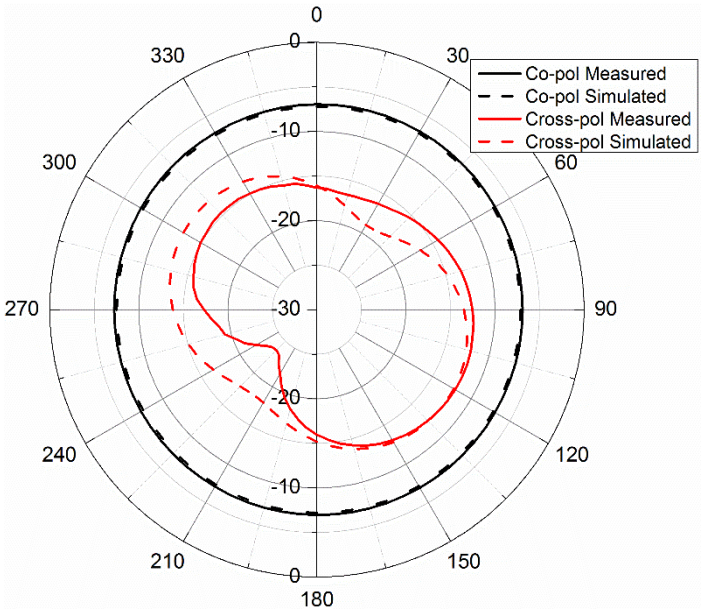


**Figure 5.11. Elevation radiation patterns in the xy-plane at 450 MHz.**

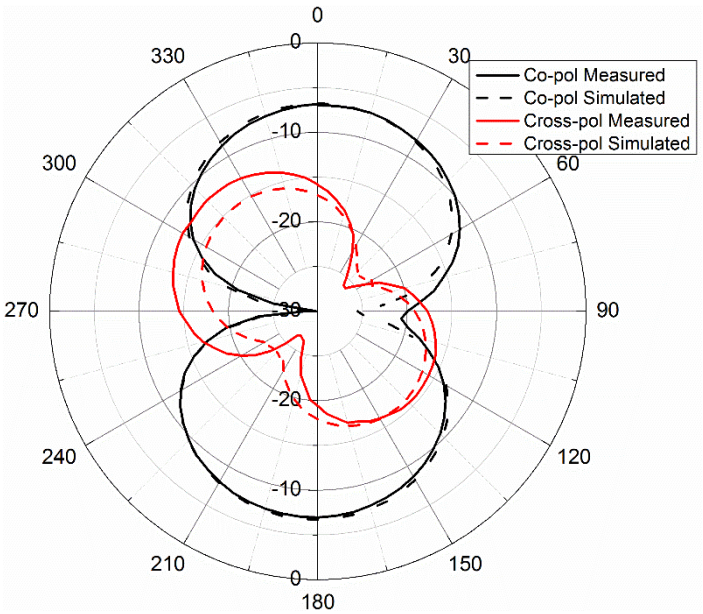


**Figure 5.12. Elevation radiation patterns in the yz-plane at 450 MHz.**

## 5.6 INSTALLED PERFORMANCE

To investigate the installed performance of the proposed antenna, a simulation model is created (Fig. 5.13) with the antenna in a Plexiglas housing ($\varepsilon_r = 3.6$, $\tan\delta = 0.001$ and thickness = 3 mm) with outer dimensions 81 × 266 × 172 $mm^3$ (H × L × W) and placed on a concrete wall ($\varepsilon_r = 5.8$ at 450 MHz, thickness = 200 mm). Two scenarios were evaluated, with the antenna ground plane oriented parallel and perpendicular to the wall surface as shown in the Fig. 5.13.

Figs. 5.14 and 5.15 show the measured and simulated $S_{11}$ for the two different orientations. From inspection of the results, the resonant frequency shifts downwards due to the wall permittivity loading and this becomes more acute when the monopole is closer to the wall surface (parallel case).

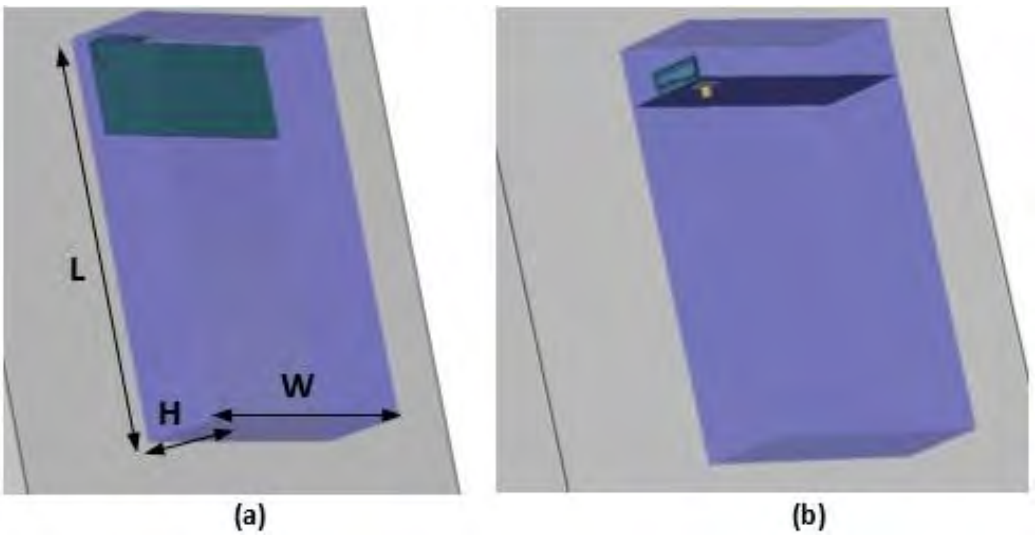


**Figure 5.13. The simulation model with ground plane (a) parallel to the wall and (b) perpendicular to the wall.**

The distance between the edge of the ground plane and the wall for the parallel and perpendicular case was respectively 13.1 mm and 3.5 mm. For the parallel case the resonant frequency shifted downwards by 8 MHz for simulation and by 9 MHz measured. For the perpendicular case the frequency shifted downwards by 7 MHz for simulation and by 7.5 MHz for the measured case.

To mitigate the wall proximity loading detuning effects, the slider was adjusted to tune the antenna back to 450 MHz. This also improved the total efficiency for both cases. The simulated total efficiency for the parallel case before retuning was 17.6% and after retuning was 22.9%. For the perpendicular case the simulated total efficiency before retuning was 14.5% and after was 19.7%. In both cases some energy is absorbed by the concrete wall. This absorption is greater for the perpendicular case where the total efficiency is 3.2 percentage points less than for the parallel case. For both cases the via-slider was re-adjusted to tune the resonant frequency to 450 MHz. The via-slider positions were $P = 21.3$ mm and $P = 20.3$ mm for the parallel and perpendicular cases respectively.

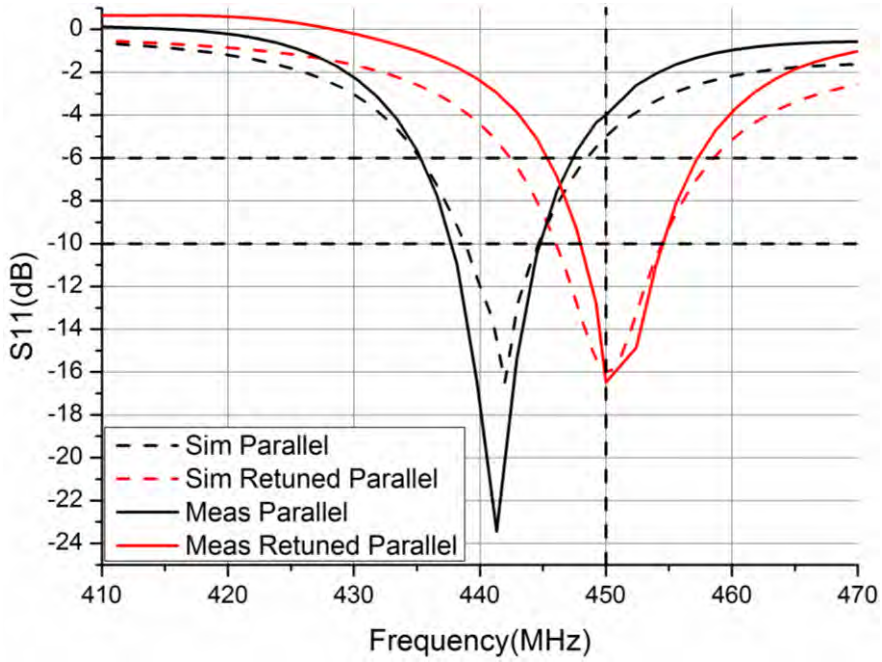


**Figure 5.14. Simulated and measured $S_{11}$ for the parallel case.**

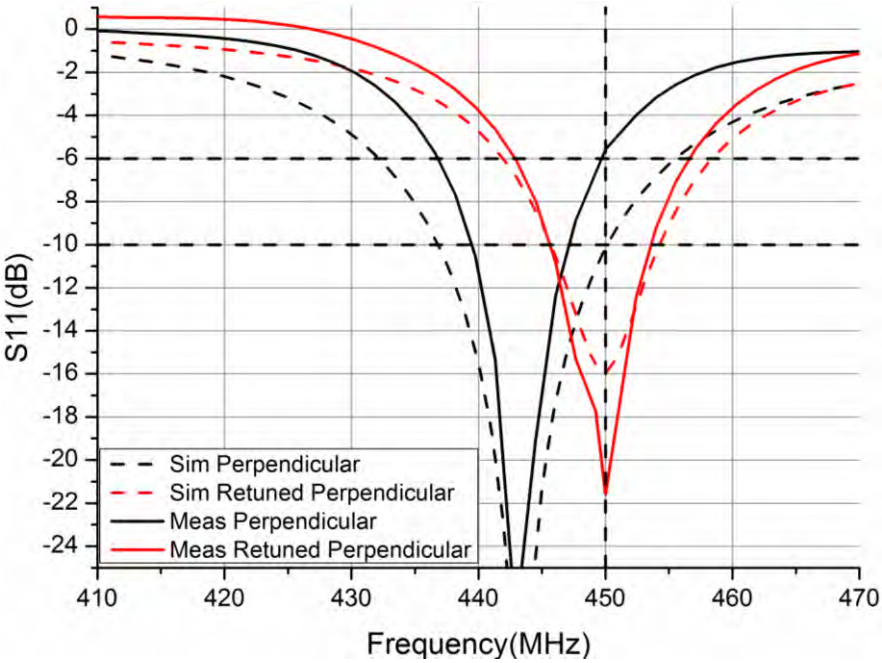


**Figure 5.15. Simulated and measured $S_{11}$ for the perpendicular case.**

## 5.7 CONCLUSIONS

In this chapter a study of a meander-line folded monopole antenna for emerging applications in smart metering at 450 MHz was presented. The proposed compact antenna was studied in terms of the ground plane size, the matching stub role and the via-slider connector with respect to the monopole performance. The results show that the $S_{11}$ characteristic is not heavily dependent on the ground plane size. The frequency is shifted downwards by 23 MHz with a significant impedance matching improvement by adding a matching stub into the antenna geometry. The electrical length of the monopole is increased and controlled by introducing a via-slider which connects the sides of the PCB. The rear feeding and grounding position allows more freedom of available space for the meander-line and confines the electrical length into a compact physical size. The antenna provides 21% to 24% measured total-efficiency across the tuneable bandwidth.

The packaged antenna performed well despite material loading and when installed on a concrete wall. The via-slider tuneable position can re-adjusted to tune the resonant frequency of the monopole to 450 MHz.

# 6. VHF & UHF Meandered Monopole Antenna

Intelligent metering systems for the measurement of water, gas, heat and electricity consumption enable modern smart cities. These smart metering applications require a long range link between the sensor grid nodes and the data aggregators, overcoming building penetration losses. The demand for harmonised frequency bands for several existing and new applications led the Electronic Communication Committee (ECC) [82] to reconsider the use of the 169 MHz and 433 MHz bands. The Wireless Metering Bus (WM-Bus) specification, introduced a narrow band channel of 75 kHz with a maximum EIRP of +27 dBm (+500 mW) [83] providing long range solutions.

The size of a smart metering device is typically around 150 × 150 $mm^2$ with a volume which must house the electronic components, battery and the integrated antenna. Meander line structures [21, 22, 23, 24] due to their low compact size are suitable for integration in small envelopes achieving broadband performance with omnidirectional characteristics.

In this chapter a dual-band folded meander line monopole antenna for Advanced Metering Infrastructure (AMI) [84] and Wireless-M-Bus applications operating in the

VHF and lower UHF bands is presented. Performance measures include impedance bandwidth, radiation patterns, total and radiation efficiency.

## 6.1 VHF & UHF MEANDERED MONOPOLE ANTENNA

A dual-band printed antenna is designed for integration in smart meter devices for Wireless M-Bus and M2M applications operating at 169 MHz and 433 MHz. The antenna configuration is optimized for impedance matching at both frequencies. A parametric investigation of key geometrical parameters is reported. The proposed antenna provides omnidirectional radiation characteristics and excellent measured total efficiency.

## 6.2 ANTENNA CONFIGURATION

The basic procedure steps for designing a novel dual-band miniaturized antenna based on a meander line topology is presented in Fig. 6.1. As the first step, a basic folded monopole (Fig. 6.1 (a)) is employed to design the antenna. The antenna resonates at around 1100 MHz with poor impedance matching (Fig. 6.2 blue line). The two horizontal strips (feeding and shorting) are meander (Fig. 6.1 (b)) in order to introduce more electrical length to the antenna geometry shifting the resonant frequency downward by 500 MHz (Fig. 6.2 red line). The final design step is defined with the shorting strip not be shorted anymore, but with an open end and positioning to the back side of the substrate (Fig. 6.1 (c)) providing better isolation from the feeding strip and increasing the electrical length of the antenna. The last antenna is dual band (Fig. 6.2 black line) with the lowest resonant be shifted downwards more than 300 MHz from the previous one.

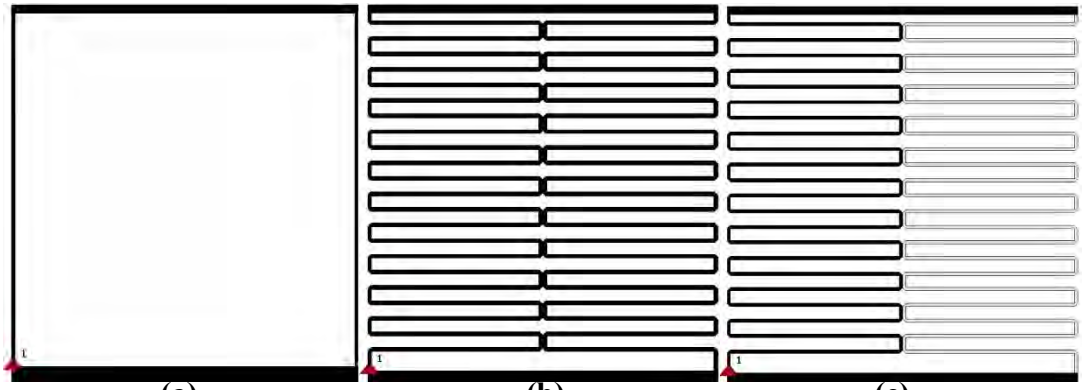


**Figure 6.1. Schematic illustration of the three basic design models.**

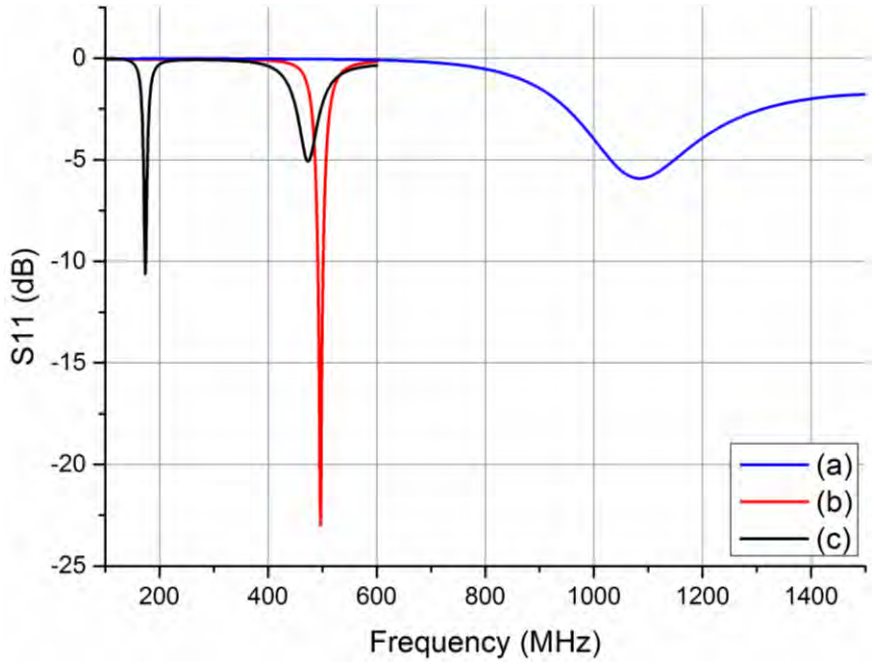


**Figure 6.2. Simulated $S_{11}$ for the three basic design models.**

The antenna (Fig. 6.3) is printed on double-sided FR4 substrate, (Tabled 2.1) with dimension of 150 mm × 150 mm ≈ ($0.085\lambda_0$, $\lambda_0$ = 1775.15 mm at 169 MHz) representing the meter motherboard. The meandered monopole of height $h$ = 40.23 mm ($\approx 0.02\lambda_0$) and length $l$ = 45.02 mm ($\approx 0.025\lambda_0$) is located on the corner of the ground plane. The antenna is fed with an SMA connector through a 50 Ω microstrip line (width = 2.94 mm) which is stepped to a short section (length = 0.85 mm and width = 0.35 mm) which connects to the antenna through via 1. The rear meander line (width = 0.35 mm) with uniform spacing runs up the substrate to via 2 which connects to an extended meander line section located at the front with an 4.25 mm open end which terminates 0.31 mm away from the ground plane level. The introduction of a shunt lumped inductor (L = 56 nH, 0.2 Ω) 20.15 mm away from via 1 improves the matching at both frequencies as shown in Fig. 6.4.

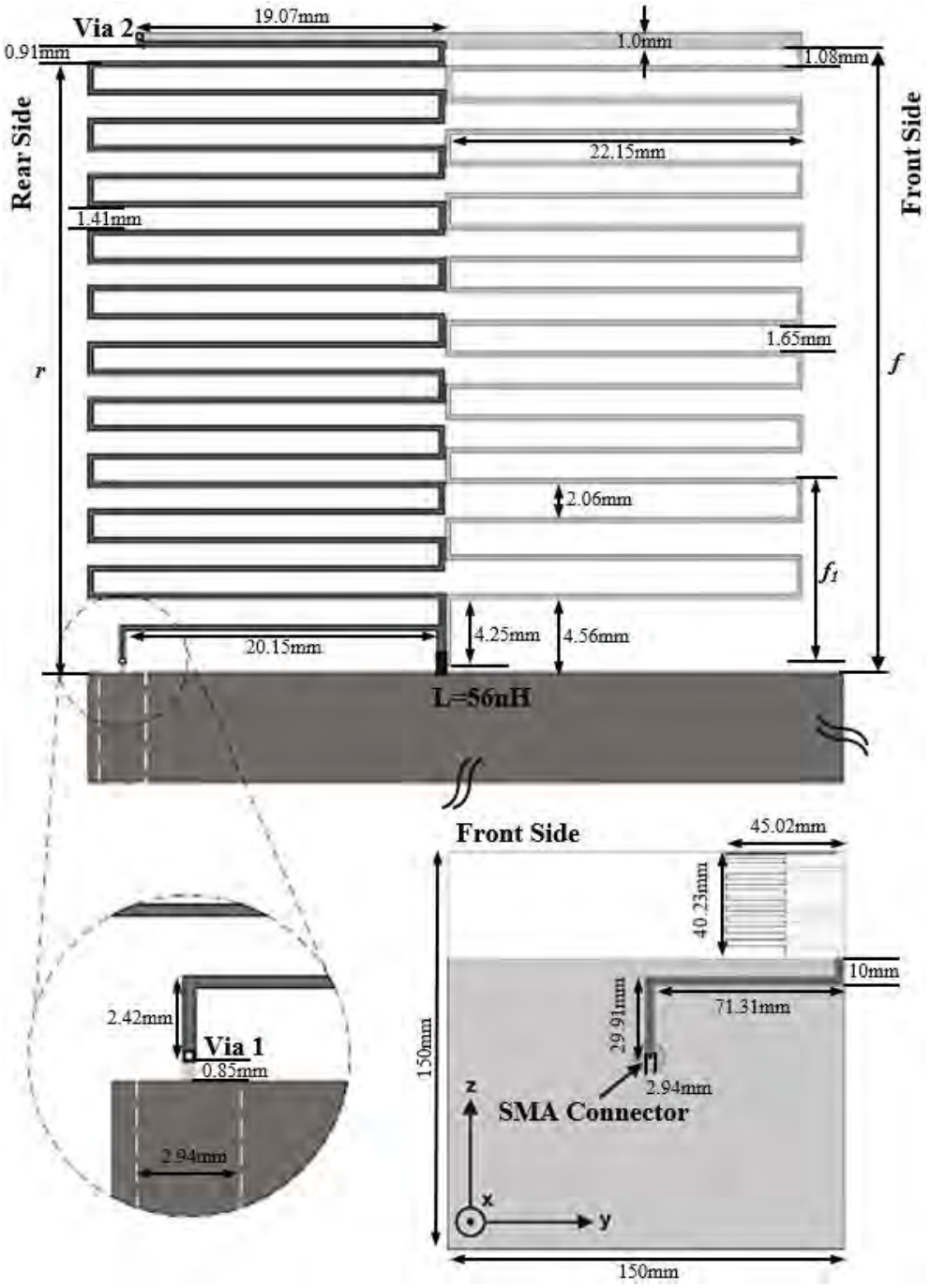


**Figure 6.3. Folded meander line monopole antenna and coordinate system.**

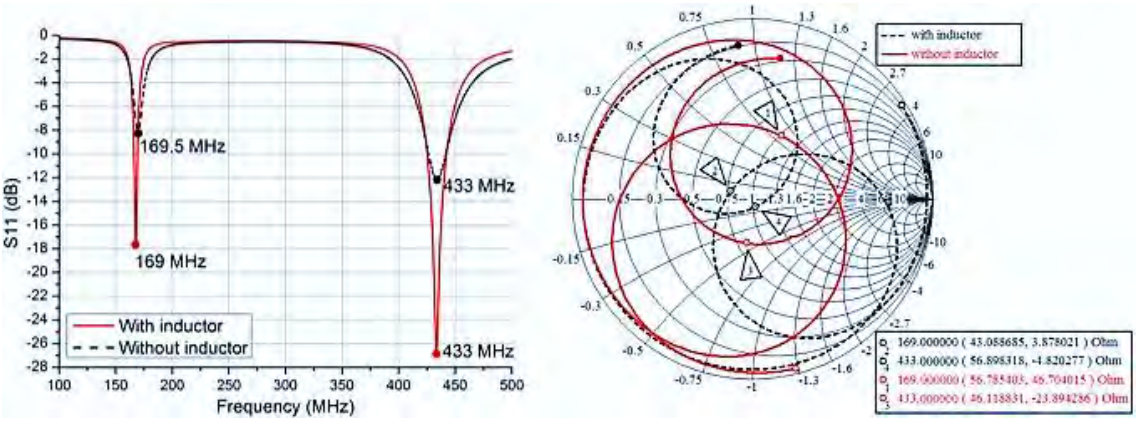


**Figure 6.4. Improved impedance matching and control of frequency.**

Practically, the presence of lumped elements (inductors/capacitors) introduce additional losses to antenna, but the main advantage of such designs is to improve impedance matching (Fig. 6.4), reducing the missmatch losses and thus, to increase the total efficiency of the antenna system. Looking at the $S_{11}$ results in Fig. 6.4 it becomes evident that the introduction of an inductor reduce the missmatch losses from 0.75 dB to 0.07 dB for the first resonance and from 0.28 dB to 0.01 dB for the second one.

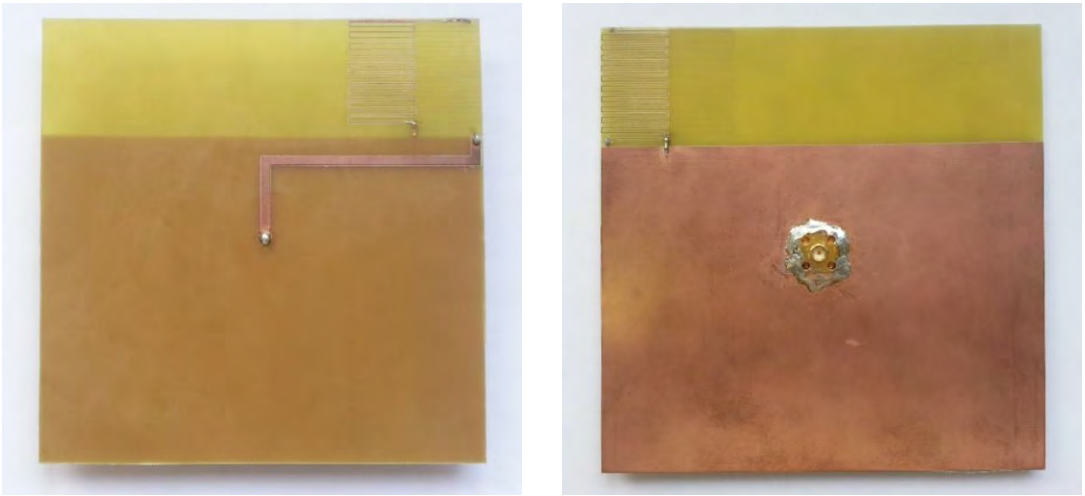

**(a)** **(b)**

**Figure 6.5. Manufactured meandered monopole prototype (a) Front View, (b) Rear View.**

## 6.3 PARAMETRIC INVESTIGATION

A parametric investigation of the variation of $S_{11}$ with respect to three geometric parameters of the meander line monopole shown in Fig. 6.1 is made.

The dual band operation of the monopole is strongly dependence on the height ($r$) of the rear meandered section, which was varied from 34 mm to 58 mm. The results indicate (Fig. 6.6) that as the height ($r$) is increased the first resonant frequency is shifted upwards while the second resonance is shifted downwards. From the current distribution Fig. 6.9(b) it can be seen that the rear meandered section mainly determinates the upper resonance. By selecting the value of $r$ = 38.3 mm both resonances can be tune to the desired values.

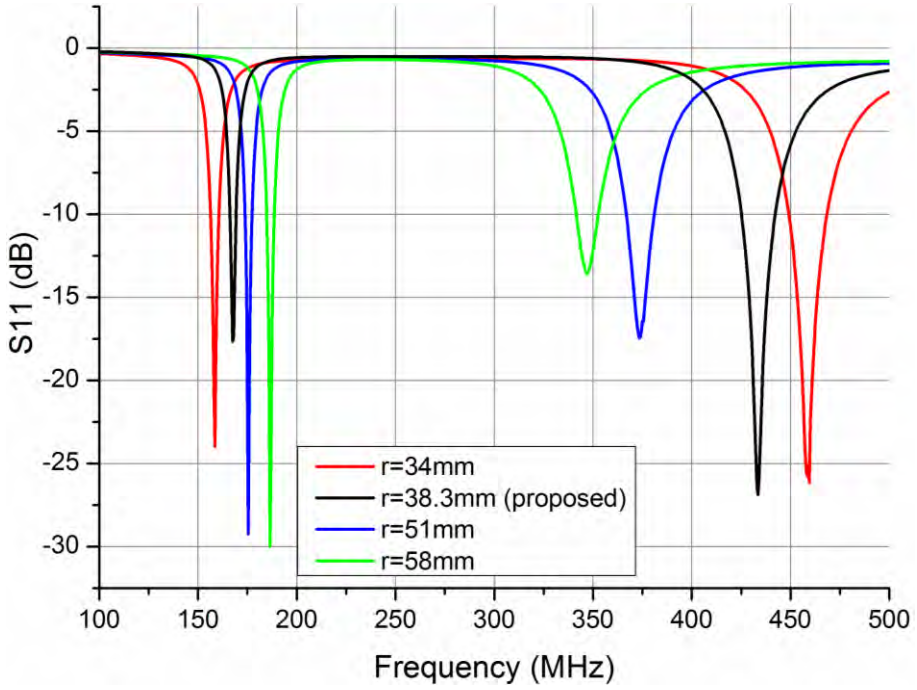


**Figure 6.6. The simulated $S_{11}$ dependence on the height *r* of the back meander line section.**

The height (*f*) of the front meander line section of the monopole was found to have a significant influence on the frequency-ratio range of the antenna. This height was varied from 30 mm to 48 mm. The simulations were made with uniform separation between the meander line strips. From the $S_{11}$ (Fig. 6.7) it is clearly visible that increasing the value (*f*) shifts the first resonance downwards with little effect on the upper resonance. The frequency-ratio between the upper and the lower resonance $F_r = f_u/f_l$ continuously increases from 1.61 to 3.11 as the value of (*f*) changes from 30 mm to 48 mm.

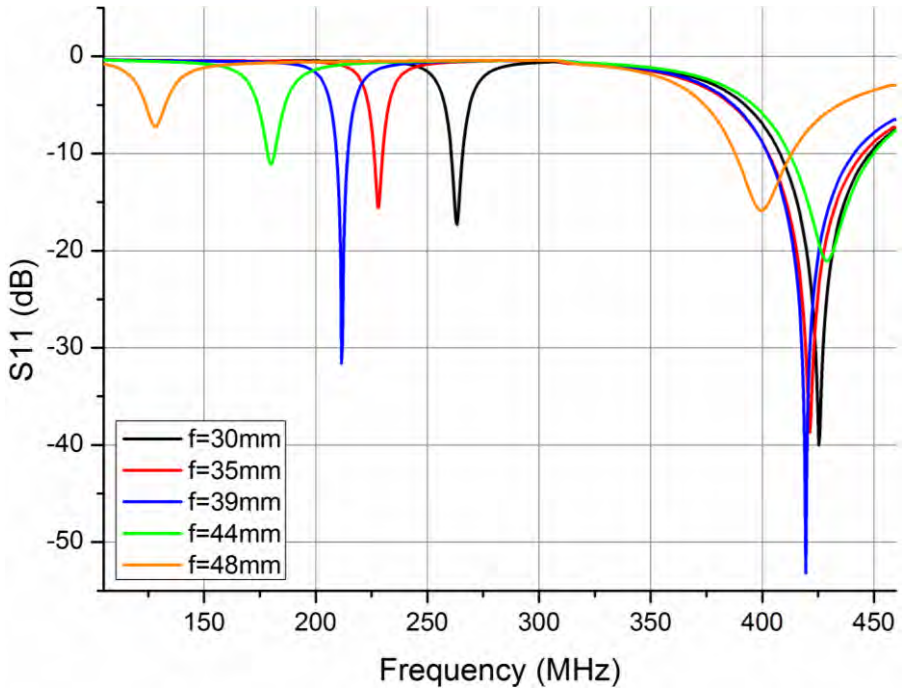


**Figure 6.7. The simulated $S_{11}$ dependence on the height *f* of the front meander line section.**

The dependence of the first resonance on the height ($f_1$) of the last two meander lines on the front of the monopole was investigated. The results are shown in Fig. 6.8. When the height ($f_1$) of the two last meander line strips is increased from 10 mm to 17.7 mm the

first resonance is shifted from 203 MHz to 144.5 MHz with little effect on the impedance matching. The second resonant frequency is not heavily dependent on from the height ($f_1$). This is confirmed by the current distribution (Fig. 6.9(b)) where the four last meander line strips do not carry a strong current. The proposed value is $f_1$ = 13.34 mm.

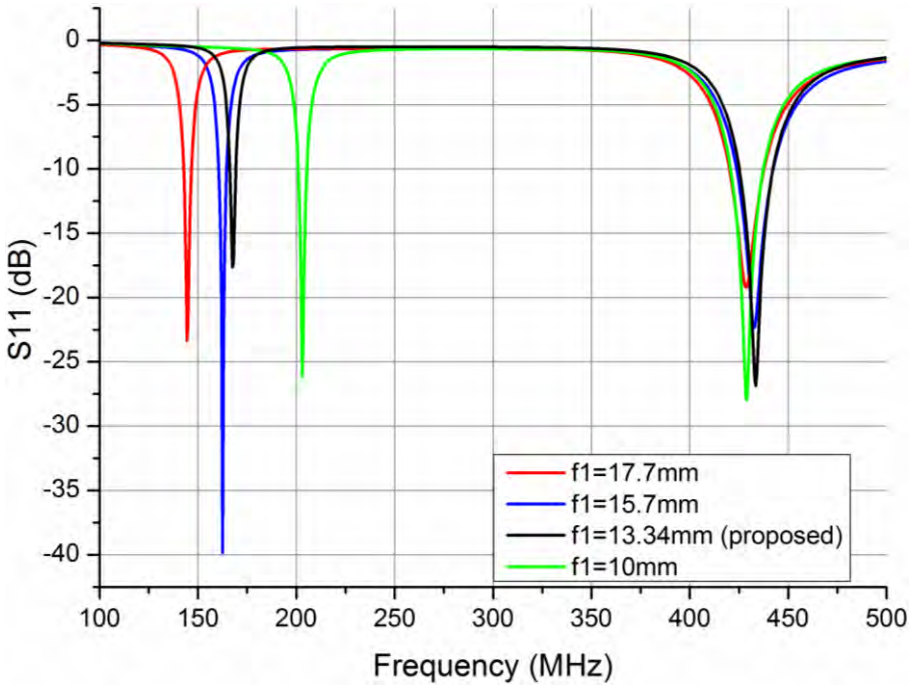


**Figure 6.8. The simulated $S_{11}$ dependence on the height $f_1$ of the last front four meander line strips.**

The performance of the antenna is based the fundamental frequency at which the structure resonates and radiates. That fundamental frequency is related to the antenna's resonant length which is caused by current paths (Fig. 6.9) within the structure. For the proposed antenna the lower rear side meandered section and the upper front side meandered sections determine the upper resonance (Fig. 6.9(b)) and the combined line sections provide the lower resonance (Fig. 6.9(a)). In both resonant frequencies the

ground plane excites strong currents at the horizontal and the vertical side which have same phase with the currents of the monopole. In the proposed antenna the ground plane is an integral part and reinforces and contributes to the radiation performance. It should be noted that in the upper resonance (Fig. 6.9 (b)) the current reversed the direction after a full wavelength along the rear side meandered section.

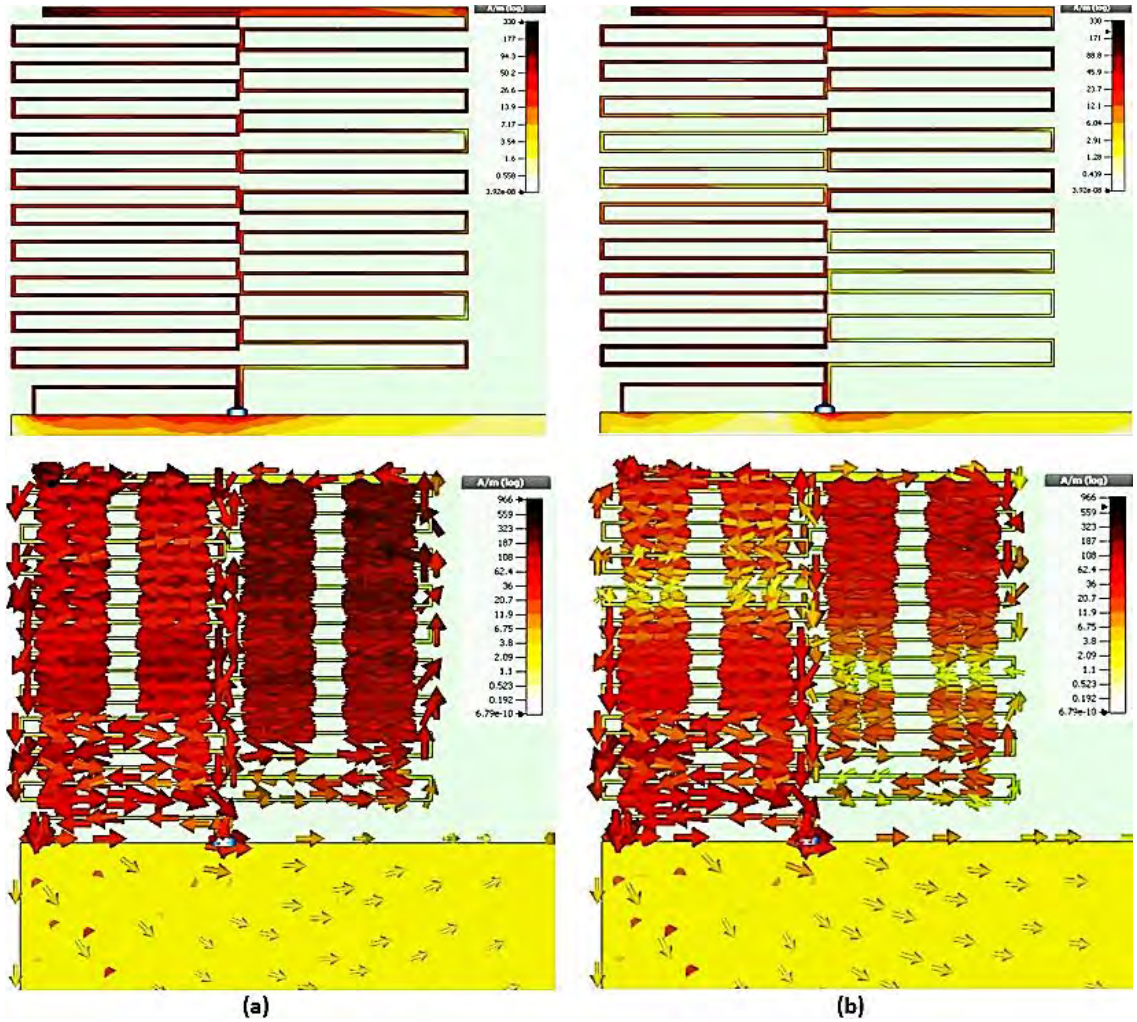


**Figure 6.9. The current distribution of the antenna in (a) 169 MHz and (b) 433 MHz.**

Placing meander line sections on opposite sides of the PCB provides isolation, miniaturization and greater freedom in controlling the frequency ratio. The frequency ratio $f_u/f_l$ of 2.56 is tuned and optimized by non-uniformity in the front meander line section as well as some coupling of the front and back meander lines.

## 6.4 Simulated and Measured Results

In Fig. 6.10 the measured and simulated $S_{11}$ is presented providing good agreement. The measured −6 dB and −10 dB impedance bandwidth was 5.8 MHz (165.7 − 171.5 MHz) and 3.3 MHz (167 − 170.3 MHz) respectively at 169 MHz and 53.9 MHz (417.5 − 471.4 MHz) and 26.4 MHz (424.7 − 451.1 MHz) at 433 MHz. The fractional bandwidths in −6 dB is 3.4% for the first resonance and 12.4% for the second, while the fractional bandwidths in −10 dB is 1.95% for the first resonant frequency and 6.1% for the second.

The simulated −6 dB and −10 dB impedance bandwidth was 5.7 MHz (164.9 − 170.6 MHz) and 3.1 MHz (166.2 − 169.3 MHz) at 169 MHz and 30.4 MHz (419.1 − 449.5 MHz) and 17.2 MHz (425.1 − 442.3 MHz) at 433 MHz.

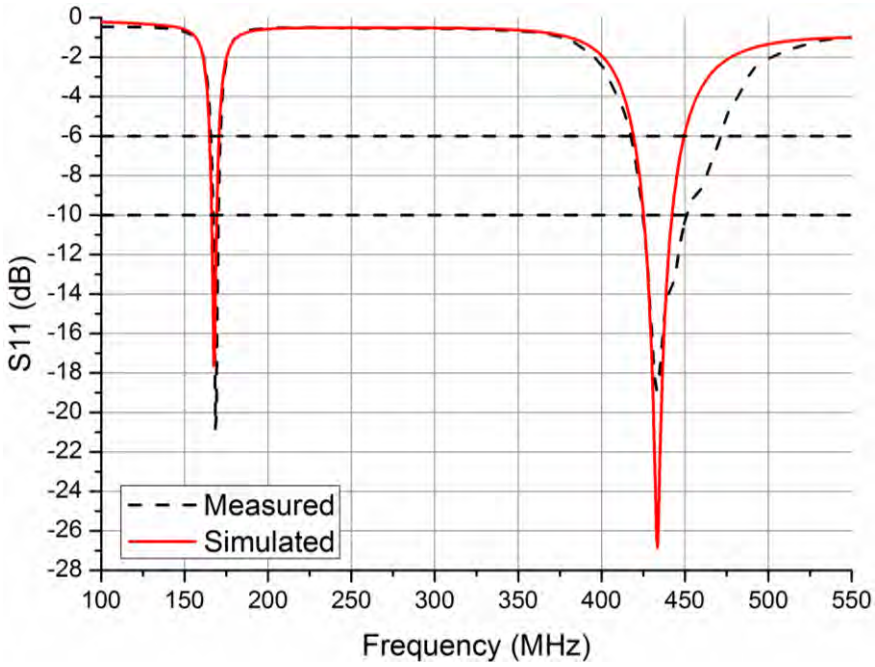


**Figure 6.10. Simulated and measured $S_{11}$.**

Efficiency measurements are performed using the Wheeler cap method [85] (Fig 6.11) using a metallic box of 610 × 610 × 360 $mm^3$. The measured radiation and total efficiency for the first resonance is 20.4%. For the second resonance the measured radiation and total efficiency is 50% and 49.4% respectively. These results are in good agreement with simulation which indicate a radiation and total efficiency of 18.3% and 17.8% at 169 MHz and 48.2% and 47.9% at 433 MHz respectively.

In Figs. 6.12 and 6.13 the measured and simulated azimuth (x–y) and elevation (x–z) plane radiation patterns at 433 MHz are illustrated. The maximum measured gain is 4.6 dBi. There is a good agreement between measurement and simulation. The maximum simulated realized gain at 169 MHz is −1.8 dBi. In AHFR Lab there is no suitable SGH available to test and measure the radiation patterns at 169 MHz.

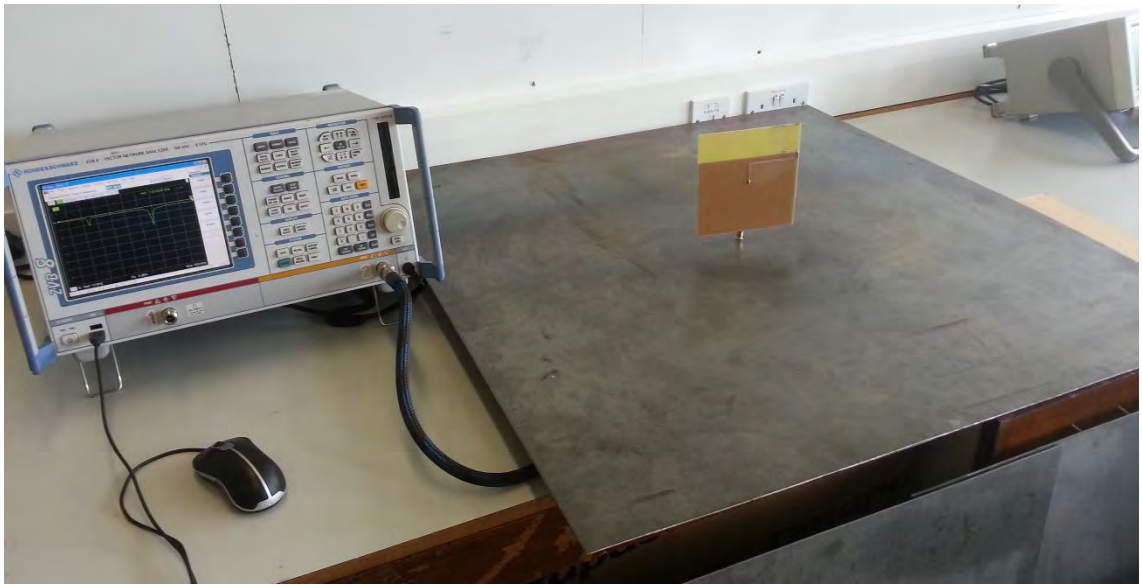

(a)


(b)

**Figure 6.11. Wheeler Cap measurement setup (a) without cap, (b) with cap.**

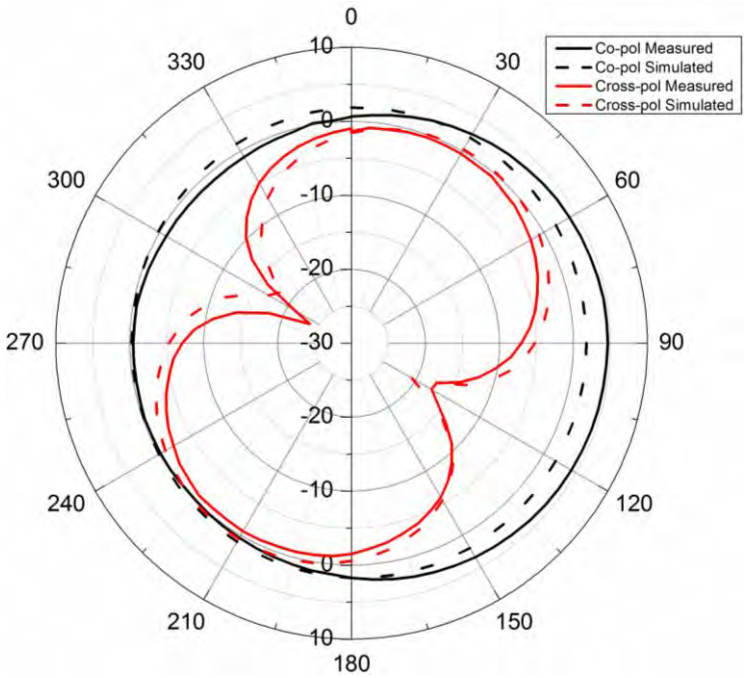


**Figure 6.12. Azimuth radiation patterns in the xy-plane at 433 MHz.**

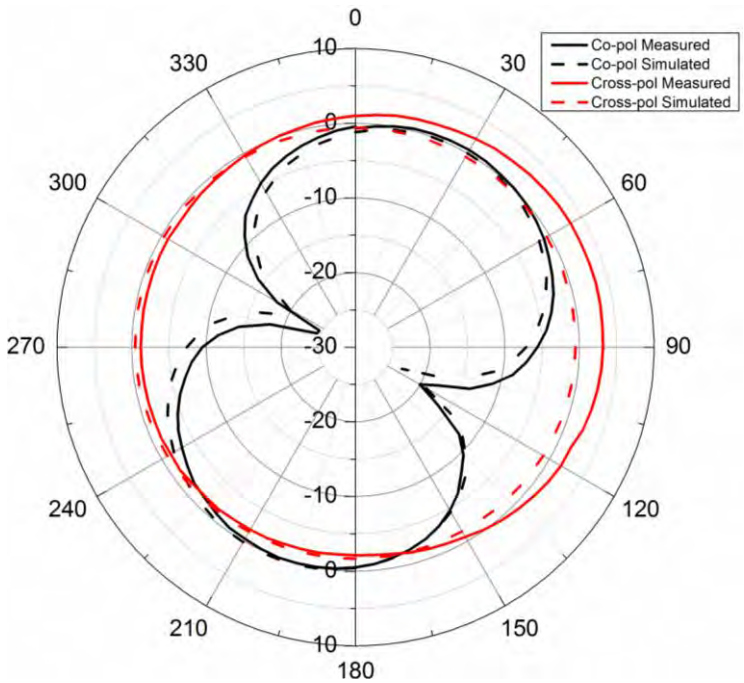


**Figure 6.13. Elevation radiation patterns in the xz-plane at 433 MHz.**

## 6.5 CONCLUSIONS

In this chapter a dual band folded meander line monopole antenna for emerging smart metering and M2M applications at 169 and 433 MHz is presented. Three key geometrical parameters of the proposed electrically small antenna were studied as well as the effect to the frequency ratio $F_r = f_u/f_l$ is reported. The introducing of a shunt lumped inductor was found to significantly improve the impedance matching of both resonant frequencies. The antenna provides good omnidirectional radiation characteristic at 433 MHz and more than 20% and 49% measured total efficiency at 169 MHz and 433 MHz respectively. The measured gain at 433 MHz is 4.6 dBi and the simulated gain at 169 MHz is −1.8 dBi. The antenna is low cost and easy fabricated with additional benefit of a large easy controlled frequency-ratio range.

# 7. Conclusions and Future Work

## 7.1 Conclusions

A number of small novel antenna designs have been researched, developed and are described in this thesis. Parametric studies were carried out on folded and meander line monopoles and planar inverted-F antennas. The proposed geometries are optimised and designed to provide sufficient bandwidth, good impedance matching, omnidirectional radiation characteristics with high gain and efficiency, maintaining compact size.

The main contributions of this dissertation are the following:

A folded and shorted printed monopole antenna has been proposed. A compact low profile structure has been designed based on these principles offering an easy controlled large frequency-ratio range and stable broad band omnidirectional radiation characteristics. Moreover, this approach provides a good polarization purity between horizontal and vertical polarized signals which is essential for maintaining the good link between the receiver and the transmitters.

Two Planar Inverted-F structures have been designed operating broad band, with high gain and efficiency. The effects of their key dimensional parameters have been

parametrically studied. Moreover, the antenna performance for different locations on the ground plane and for various dimensions of ground plane layout have been investigated accordingly. A size reduction of almost 50% was achieved when two PIFAs combined in one antenna share the same feed. The study has demonstrated a controllable large frequency-ratio range when the feeding and shorting point change position.

By seeking more compact solutions for low frequencies, two novel meander line folded monopole antennas were designed. Miniaturization has been provided by double sided PCB printed technique allowing integrating more electrical length into a compact physical size and isolating the two printed sides. Matching stub structures have been applied in order to improve the impedance matching. A via slider connector has been used to connect the two sides of the PCB, enabling tuneability of the impedance matching across a large frequency range and offering stable omnidiarectionality over the tuneable range. The strong dependence of the frequency-ratio range on the meander line separation was investigated in depth.

## 7.2 FUTURE WORK

During the development and test phase of this dissertation some research topics which are worth further investigation have been identified and are outlined here.

Further investigation could be made in topics related with installed performance of various antennas when they are integrated in actual devices. When an antenna is integrated in housing, the impedance bandwidth was slightly increased as well as the resonant frequency was shifted downwards [86]. The walls of the enclosure are effectively decreasing the gain and the efficiency of the installed antenna. Future work could focus on investigating the positioning of an antenna inside an enclosure in order to find the optimum position and orientation.

Another interesting topic for extensive investigation is the packaging impact to an integrated antenna in an actual device which contains numerous metal structures that could potentially interfere its performance. Metal structures near antennas can change input impedances and phase of received signals. Design guidelines to eliminate the electromagnetic interference (EMI) emitted from the RF components and circuits could be developed [87, 88]. To eliminate the electromagnetic emissions and keep EMI to a minimum it would be very important to arrange the layout of ground planes to minimize EMI [89, 90].

Further development could be done on ground planes which have been found to affect the general performance of antennas [91, 92, 93]. The position and the orientation of the antenna on the ground plane can dramatically affect the general performance [94]. Further research could be devoted to the extensive investigation of different ground plane shapes.

Two compact solutions suitable for integration into packaging were proposed in this thesis for smart metering applications. The double sided PCB printed meandered shape and the matching stub technique were the two techniques for miniaturization providing isolation between the meander line sections and improving the impedance matching across the operating frequency range. A further study on broad-banding meander line antennas should be made as well as an investigation on providing more than 2 bands [95, 96].

A compact VHF antenna is proposed suitable for integration into packaging. Test and measurements of the radiation patterns at 169 MHz were not carried out due to the non-availability of a large sized anechoic chamber and a suitable Standard Gain Horn antenna. Further research efforts should focus on the outdoor measurements [97, 98] where many factors, such as the directivity of the antenna under test, the frequency range and mechanical features of the antenna (size, weight and volume) should be considered to ensure the performance metrics are measured with sufficient accuracy.

# Bibliography

[1] C. A. Balanis, *Antenna Theory*, New Jersey: John Wiley & Sons, 2005.

[2] J.-H. Kim and H.-M. Lee, "Efficient Electrically Small Wide Band Planar Antenna for SAR Reduction," *in 20th International Zurich Symposium on Electromagnetic Compatibility*, Zurich, 2009, pp. 269-272.

[3] F. C. C. (FCC), "Wireless Devices and Health Concerns," 2014. [Online]. Available: http://transition.fcc.gov/cgb/consumerfacts/mobilephone.pdf.

[4] *Standard for Safety Levels with Respect to Human Exposure to Radio Frequency Electromagnetic Fields, 3 kHz to 300 GHz*, IEEE International Committee on Electromagnetic Safety IEEE Std C95.1-1991, April 19 2006.

[5] H. Wheeler, "Fundamental limitations of small Antennas," *IRE Proc*, vol. 35, no. 12, pp. 1479-1484, December 1947.

[6] H. Wheeler, "The Radiansphere Around a Small Antenna," *IEEE Proceedings of The I.R.E.*, vol. 47, no. 8, pp. 1325-1331, August 1959.

[7] L. Chu, "Physical limitations of omni-directional antennas," *J. Appl. Phys*., vol. 19, no. 12, pp. 1163-1175, May 1948.

[8] R. Harrington, "On the Gain and Beamwidth of Directional Antennas," *IEEE Transactions on Antennas and Propagation*, vol. 6, no. 3, pp. 219-225, July 1958.

[9] R. Fano, "Theoretical limitations on the broadband matching of arbitrary impedances," *J. Franklin Inst.*, vol. 249, no. 1, pp. 57-83, January 1950.

[10] W. Stutzman and G. Thiele, *Antenna Theory and Design*, New York: John Wiley & Sons, 1998.

[11] C. Lin, "Dual-Band Folded Monopole Antenna with Slotted Ground Plane for WLAN Applications," vol. 15, pp. 53-60, 2010.

[12] A. Loutridis, M. John, G. Ruvio and M. J. Ammann, "A 2.45/5.8 GHz folded monopole antenna for WLAN applications," *in Antennas and Propagation Conference (LAPC)*, 2012 Loughborough, UK, 2012.

[13] T. Ito, T. Oki, H. Morishita, "Current reduction on the ground plane using additional element for WiMAX/WLAN folded monopole antenna," *in IEEE International Workshop on Electromagnetics (iWEM)*, Sapporo, 2014.

[14] G. Augustin, B.P. Chacko, T.A. Denidni, "Uniplanar folded monopole antenna for mobile phone applications in LTE/GSM/UMTS/WiFi band," *in IEEE Antennas and Propagation Society International Symposium (APSURSI)*, Memphis, 2014.

[15] J. Volakis, C. Chen, J. Halloran and S. Koulouridis, "Miniature VHF/UHF conformal spirals with inductive and ferrite loading," *in IEEE Antennas and Propagation Society International Symposium*, Honolulu, 2007, pp. 5-8.

[16] A. Loutridis, K. Yang, M. John and M. J. Ammann, "Compact Printed Spiral FM Antenna," *in Progress in Electromagnetics Research Symposium, Prague (PIERS)*, Czech Republic, 2015, pp. 37.

[17] C. Borja and J. Romeu, "On the behaviour of Koch island fractal boundary microstrip patch antenna," *IEEE Antennas and Propagation Society*, vol. 51, no. 6, pp. 1281 - 1291, June 2003.

[18] J. Gonzalez-Arbesu, S. Blanch and J. Romeu, "Are space-filling curves efficient small antennas?" *IEEE Antennas and Propagation Society*, vol. 2, no. 1, pp. 147 - 150, 2003.

[19] S. R. Best, "On the Resonant Behaviour of the Small Koch Fractal Monopole Antenna," *Microwave and Optical Technology Letters*, vol. 35, Issue: 4, pp. 311-315. Nov. 2002.

[20] K. J. Vinoy, K. A. Jose, V. K. Varadan and V. V. Varadan, "Hilbert Curve Fractal Antenna: A Small Resonant Antenna for VHF / UHF Applications," Microwave and Optical Technology Letters, vol. 29, Issue: 4, pp. 215-219. May 2001.

[21] A. Loutridis, M. John and M. J. Ammann, "Printed Folded Meander Line Dual-Band Monopole for TV White Space and GSM," *in 8th European Conference on Antennas and Propagation (EuCAP)*, The Hague, Netherlands, 2014, pp. 2848-2852.

[22] C.-N. Hu, W. Chen, J.-W. Huang and J. Chiu, "Design of a multiband coupled-meander-line monopole antenna for M2M applications," *in International Conference on Applications of Electromagnetism and Student Innovation Competition Awards (AEM2C)*, Taipei, 2010, pp. 264-268.

[23] S. R. Best and J. D. Morrow, "Limitations of inductive circuit model representations of meander line antennas," *in Antennas and Propagation Society International Symposium*, Columbus, OH, USA, 2003, pp. 852-855.

[24] T. J. Warnagiris and T. J. Minardo, "Performance of a meandered line as an electrically small transmitting antenna," *Transactions on Antennas and Propagation*, vol. 46, no. 12, pp. 1797 - 1801, 1998.

[25] V. Gonzalez-Posadas, C. Martin-Pascual, J. Jiménez-Martín and D. Segovia-Vargas, "Lumped-Element Balun for UHF UWB Printed Balanced Antennas," *IEEE Antennas and Propagation Society*, vol. 56, no. 7, pp. 2102 - 2107, July 2008.

[26] Niamien, M. A. C., Sharaiha, A., Collardey, S. Mahdjoubi, K., "An electrically small frequency reconfigurable antenna for DVB-H," *in IEEE International Workshop on Antenna Technology (IWAT)*, Tucson, March 2012, pp. 245-248.

[27] M. -I. Lai, T. -Y. Wu, J. -C. Hsieh, C. -H. Wang, S. -K. Jeng, " Design of reconfigurable antennas based on an L-shaped slot and PIN diodes for compact wireless devices," *IET Microwaves Antennas 7 Propagation*, vol. 3, Issue: 1, pp. 47-54, Feb. 2009.

[28] A. Alhawari, A. Ismail and M. Mahdi, " Reconfigurable Loaded Planar Inverted-F Antenna Using Varactor Diodes," *IEEE Antennas and Wireless Propagation Letters,* vol. 10, pp. 466-468, May 2011.

[29] S. -H. Chang, W. -J. Liao, "A Broadband LTE/WWAN Antenna Design for Tablet PC," *in IEEE Transactions on Antennas and Propagation*, vol. 60, Issue: 9, pp. 4354-4359, Aug. 2012.

[30] R. Mittra and S. Dey, "Challenges in PCS antenna design," *in IEEE Antennas and Propagation Society International Symposium*, vol. 1, Orlando USA, 1999, pp. 544-547.

[31] A.K. Skrivervik, J. F. Zurcher, O. Staub, J.R. Mosig, "PCS antenna design: the challenge of miniaturization," *IEEE Antennas and Propagation Magazine*, vol. 43, Issue: 4, pp. 12-27, 2001.

[32] K. Noguchi, S. Betsudan, T. Katagi and M. Mizusawa, "A compact broad-band helical antenna with two-wire helix," *IEEE Transactions on Antennas and Propagation*, vol. 51, no. 9, pp. 2176 - 2181, Sep. 2003.

[33] Sooliam Ooi, Boon Ping Koh, "Single-fed Dual Band UHF-GPS Helical Antenna," *in IEEE International Workshop on Antenna Technology (IWAT)*, March 2006, pp 184-187.

[34] D. Kearney, M. John and M. J. Ammann, "Miniature Ceramic PIFA for UWB Band Group 3 & 6," *IEEE Antennas and Wireless Propagation Letters*, vol. 9, pp. 28-31, Jan. 2010.

[35] A. Loutridis, M. John, M. J. Ammann, "A Dual Band LTE PIFA Antenna for M2M Applications," *Microwave and Optical Technology Letters*, vol. 57, Issue: 7, pp. 1655-1658. July 2015.

[36] H.-K. Ryu, E. Kim and J.-M. Woo, "Miniaturisation of printed inverted-F antenna using chip coupler for Bluetooth applications," *Electronics Letters*, vol. 46, no. 13, pp. 883 - 885, June 2010.

[37] D. Nashaat, H. Elsadek and H. Ghali, "Single Feed Compact Quad-Band PIFA Antenna for Wireless Communication Applications," *IEEE Transactions on Antennas and Propagation*, vol. 53, no. 8, pp. 2631 - 2635, Aug. 2005.

[38] L. Wei-Yu, W. Chun-Yih, W. Kin-Lu and T. Ming-Fang, "Internal Small-Size PIFA for LTE/GSM/UMTS Operation in the Mobile Phone," *in IEEE Antennas and Propagation Society International Symposium (APSURSI)*, Toronto, 2010.

[39] S. Bokhari, J.-F. Zurcher, J. Mosig and F. Gardiol, "A small microstrip patch antenna with a convenient tuning option," *IEEE Transactions on Antennas and Propagation*, vol. 44, no. 11, pp. 1521 - 1528, Nov. 1996.

[40] K. Wong, J. Kuo and T. Chiou, "Compact microstrip antennas with slots loaded in the ground plane," *in 11th International Conference on Antennas and Propagation*, vol. 2, Manchester, 2001, pp. 623-626.

[41] R. F. Graf, *Modern Dictionary of Electronics*, Newnes, 1999, p. 29.

[42] *Standard Definitions of Terms for Antennas*, IEEE Antennas and Propagation Society Std 145-1993, Mar. 18 1993.

[43] L. Kibona, "Analysis of the Effects of Rectangular Ground Plane on Radiation Pattern of the Monopole Antenna," *International Journal of Scientific and Research Publications (IJSRP)*, vol. 3, 2013.

[44] R. C. Johnson and H. Jasik, *Antenna Engineering Handbook*, 2nd ed., New York: McGraw – Hill, 1984.

[45] Z.N. Chen, Ed., *Antennas for Portable Devices*, 1st ed. Wiley-VCH, 2007

[46] Z.N. Chen, M.Y.W. Chia, *Broadband Planar Antennas*, Wiley, 2006

[47] K.-L. Wong, *Planar Antennas For Wireless Communications*, New Jersey: Wiley, 2003.

[48] G. Ruvio and M. J. Ammann, "A Novel Wideband Semi-Planar Miniaturized Antenna," *IEEE Transactions on Antennas & Propagation*, vol. 55, no. 6, pp. 1760-1767, 2007.

[49] T. Endo, Y. Sunahara, S. Satoh and T. Katagi. "Resonant Frequency and Radiation Efficiency of Meander Line Antennas," *Electronics and Communications in Japan. Part 2*, vol. 83, no. 1, pp. 52-58, 2000.

[50] T. J. Warnagirism and T. J. Minardo. "Performance of a Meandered Line as an Electrically Small Transmitting Antenna," *IEEE Trans. Antennas Propagation* vol. 46, issue: 12, pp. 1797-1801, Dec. 1998.

[51] K. Fujimoto, A. Henderson, K. Hirasawa and J.R. James, *Small Antennas*, Research Studies Press, England; John Wiley and Sons, New York 1987.

[52] W. L. Stutzman and G. A. Thiele, *Antenna Theory and Design*, John Wiley & Sons, 2012.

[53] *Standard Definitions of Terms for Antennas*, IEEE Antennas and Propagation Society Std 145-1983, June. 22 1983.

[54] J. S. McLean, "A Re-Examination of the Fundamental Limits on the Radiation Q of Electrically Small Antennas," *IEEE Transactions on Antennas and Propagation*, vol. 44, no. 5, pp. 672-676, May 1996.

[55] R. E. Colin and S. Rothschild, "Evaluation of Antenna Q," *IEEE Transactions on Antennas and Propagation*, vol. 12, issue: 1, pp. 23-27, 1964.

[56] R. L. Fante, "Quality factor of general ideal antenna," *IEEE Transactions on Antennas and Propagation*, vol. 17, issue: 2, pp. 151-155, 1696.

[57] J. M. Gonzalez, J. Romeu, E. Cabot and J. R, "Exploring the limits of Fractal Electrodynamics for the future telecommunication technologies," IST-2001-33055, 2003.

[58] D. Pozar, B. Kaufman, "Comparison of Three Methods for the Measurement of Printed Antenna Efficiency," *IEEE Trans. Antennas Propagation*, vol. 36, No. 1, pp. 136-139, January 1988.

[59] R.H. Johnston, J.G. McRory, "An improved small antenna radiation-efficiency measurement method," *IEEE Antennas and Propagation Magazine*, vol. 40, issue: 5, pp. 40-48, Oct. 1998

[60] W. E. McKinzie III, "A Modified Wheeler Cap Method for Measuring Antenna Efficiency," *in IEEE Antennas and Propagation Society International Symposium*, vol. 1, Montreal, Quebec, Canada, 1997, pp. 542-545.

[61] C.L. Holloway, H.A. Shah, R.J. Pirkl, W.F. Young, D.A. Hill, J. Ladbury, "Reverberation Chamber Techniques for Determining the Radiation and Total Efficiency of Antennas," *IEEE Trans. Antennas Propagation*, vol. 60, issue: 4, pp. 1758-1770, January 2012.

[62] G. Le Fur, C. Lemoine, P. Besnier, A. Sharaiha, "Performances of UWB Wheeler Cap and Reverberation Chamber to Carry Out Efficiency Measurements of Narrowband Antennas," *IEEE Antennas and Wireless Propagation Letters*, vol. 8, pp. 332-335, September 2008.

[63] CST GmbH – Computer Simulation Technology. 2014. [Online]. Available: https://www.cst.com/.

[64] T. Weiland, "A discretization method for the solution of Maxwell's equations for six-component fields," *Electronics and Communication (AEÜ)*, vol. 31, p. 116–120, 1997.

[65] M. Clemens and T. Weiland, "Discrete electromagnetism with the finite," *Progress In Electromagnetics Research (PIER)*, vol. 32, p. 65–87, 2001.

[66] M. J. Ammann, "A comparison of some low cost laminates for antennas operating in the 2.45 GHz ISM band," *in IEE Colloquium on Low Cost Antenna Technology*, London, 1998.

[67] M. Hiebel, *Fundamentals of Vector Network Analysis*, Munchen: Rohde&Schwarz GmbH & Co., 2014.

[68] Rohde&Schwarz, "R&S Vector Network Analyzers ZVA 8 / ZVA 24 / ZVA 40 Operating Manual," Rohde&Schwarz, 2005.

[69] E.A.C. NV, "ECCOSORB VHP-NRL very high Performance Broadband Pyramidal Absorber," EMERSON & CUMING Anechoic Chambers, 2010.

[Online]. Available: http://www.ecanechoicchambers.com/TB/EB-100%20-%20VHP-NRL.pdf.

[70] "Schwarzbeck Mess Elektronik," Schwarzbeck Mess Elektronik, 2014. [Online]. Available: http://www.schwarzbeck.com/.

[71] *Standard Test Procedures for Antennas*, IEEE Std. No. 149-1979, 1979.

[72] A. T. Arkko, "Effect of ground plane size on the free-space performance of a mobile handset PIFA antenna," *in Proc. 12th IEE International Conference on Antennas and Propagation*, vol. 1, Exeter, UK, Mar. 2003, pp. 316–319.

[73] R. F. Harrington, J. R. Mautz, "Theory of characteristic modes for conducting bodies," *IEEE Transactions on. Antennas and Propagation*, vol. 19, no. 5, pp. 622–628, Sept. 1971.

[74] MVG StarLab 650 MHz – 18 GHz, 2014. [Online]. Available: http://www.mvg-world.com/system/files/starlab_2014.pdf

[75] C. Brasek, "Urban utilities warm up to the idea of wireless automatic meter reading," *IEE Computing & Control Engineering Journal*, vol. 15, issue: 6, pp. 10-14, Jan. 2004.

[76] E. C. C. Report 39, "The technical impact of introducing CDMA-PAMR on 12.5 / 25 kHz PMR/PAMR technologies in the 410-430 and 450-470 MHz bands."

[77] R. E. Badra, "Compared RF Performance of 1.4 MHz-LTE and EVDO rev. A in Rural Environments at 450 MHz," *in 78th Vehicular Technology Conference (VTC Fall)*, Las Vegas, NV, 2013.

[78] B. Holfeld, S. Jaeckel, L. Thiele, T. Wirth, K. Scheppelmann, "Smart Grid Communications: LTE Outdoor Field Trials at 450 MHz," *in 81st Vechicalr Technology Conference (VCT Spring)*, Glasgow, UK, 2015.

[79] P.-S. Kildal, S.R. Best, "Further investigations of fundamental directivity limitations of small antennas with and without ground planes," *in IEEE Antennas and Propagation Society International Symposium (APSURSI)*, San Diego, 2008, pp. 1-4.

[80] C. Hagerling, C. Ide, C. Wietfeld, "Coverage and capacity analysis of wireless M2M technologies for smart distribution grid services," *in IEEE International Conference on Smart Grid Communications*, Venice, 2014, pp. 368-373.

[81] Z. M. Fadlulah, M. M. Fouda, N. Kato, A. Takeuchi, N. Iwasaki and Y. Nozaki, "Toward intelligent machine-to-machine communications in smart grid," *IEEE Communications Magazine*, vol. 49, no. 4, pp. 60-65, 2011.

[82] Electronic Communication Committee (ECC) Decision (05)02, “A harmonised frequency plan for the use of the band 169.4-169.8125 MHz,” Amended 8 November 2013.

[83] European Committee for Standardization, “EN 13757-4,” 2013.

[84] D. Li, B. Hu, "Advanced metering standard infrastructure for smart grid," *in China Intrenational Conference on Electricity Distribution (CICED)*, China, 2012.

[85] E. Higashi, Y. Iida, Y. Omura, "A Study of Antenna Efficiency Measurements by Wheeler Cap Method Applied to Planer Inverted-F Antenna (PIFA)," *in International Symposium on Signals, Systems and Electronics (ISSSE)*, Montreal, 2007, pp. 599-601.

[86] M. John, P. McEvoy and M. J. Ammann, "Evaluation of ABS enclosed printed monopole antenna supplied by Benetel Limited," Dublin Institute of Technology, Tech. Rep., Sep. 2007.

[87] Clayton R. Paul, *Introduction to Electromagnetic Compatibility*, Wiley-Interscience Publication, 1992.

[88] Mohit Arora, *The Art of Hardware Architecture: Design Methods and Techniques Digital Circuits*, Springer Science & Business Media, LLC 2012.

[89] M. Steer, *Microwave and RF Design: A Systems Approach*, 2nd edition. Edison, NJ: SciTech Publishing, 2013.

[90] M. Golio and J. Golio, Eds., *RF and Microwave Circuits, Measurements and Modeling*, 2nd edition. Boca Raton, FL: CRC Press, 2007.

[91] N.L. Bohannon, J.T. Bernhard, "Ground plane effects on planar inverted-F antennas," *in IEEE Antennas and Propagation Society International Symposium (APSURSI)*, Chicago, 2012.

[92] L. Cheng-Tse, W. Kin-Lu, "Internal WWAN Clamshell Mobile Phone Antenna Using a Current Trap for Reduced Ground Plane Effects," *IEEE Transactions on Antennas and Propagation*, vol. 57, Issue 10, pp. 3303-3308, 2009.

[93] Y. Lu, Y. Huang, H.T. Chattha, Y. Shen, "Technique for minimising the effects of ground plane on planar ultra-wideband monopole antennas," *IET Microwaves, Antennas & Propagation*, vol. 6, Issue 5, pp. 510-518, 2012.

[94] C.C. Chiau, C. Xiaodong, C. G. Parini, "Effect of antenna's positioning on a handset for a miniature dielectric-loaded folded half-loop antenna," *in 1st European Conference on Antennas and Propagation*, Nice, 2006.

[95] K. S. Sultan, H. H. Abdullah, E. A. Abdallah, E. A. Hashish, "Low SAR, compact and multiband antenna for mobile and wireless communication," *in Middle East Conference on Antennas and Propagation (MECAP)*, Cairo, Dec. 2012.

[96] M. K. Taher, "Small size multiband meander line antenna for wireless applications," *in Loughborough Antennas and Propagation Conference (LAPC)*, Loughborough, UK, March 2008, pp. 401-404.

[97] R. Hartman and Jack Berlekamp, "Fundamentals of Antenna Test and Evaluation," *in Microwave Systems New and Communications Tracking*, June 1988.

[98] J.S. Hollis, T.J. Lyon and L. Clayton, eds., *Microwave Antenna Measurements*, Scientific-Atlanta, Inc., 1985.

# Appendix A.

## LIST OF PUBLICATIONS

In this dissertation many of the ideas and designs have been published in various journals and international conferences. These publications are listed here in reverse chronological order.

### Journal Publications

[JP1] K. Yang, A. Loutridis, X. Bao, G. Ruvio and M. J. Ammann, "Printed Inverted-F Antenna with Reconfigurable Pattern and Polarization", *IEEE Transactions Antennas and Propagation Letters*; (In review).

[JP2] A. Loutridis, M. John and M. J. Ammann, "Folded Meandered Monopole for Emerging Smart Metering & M2M Applications in the Lower UHF Band," *IEEE Antenna & Propagation Magazine*; (In review).

[JP3] A. Loutridis, M. John and M. J. Ammann, "Folded Meander Line Antenna for Wireless M-Bus in the VHF and UHF Bands," *Electronics Letters IET*, vol. 51, no. 15, pp. 1138-1140, July 2015.

[JP4] A. Loutridis, M. John, M. J. Ammann, "A Dual Band LTE PIFA Antenna for M2M Applications," *Microwave and Optical Technology Letters*, vol. 57, no. 7, pp. 1655-1658, July 2015.

[JP5] A. Loutridis, M. John, M. J. Ammann, "Dual Band LTE Planar Inverted-F Antenna for M2M Applications," *Microwave and Optical Technology Letters*, vol. 22, no. 12, pp. 2925–2929, Dec 2013.

## Conference Proceedings

[CP1] A. Loutridis, K. Yang, M. John and M. J. Ammann, "Dual Band Printed Antenna for M2M Applications in ISM and GSM bands," *Loughborough Antennas & Propagation Conference (LAPC)*, Loughborough, UK. 2015; (Accepted).

[CP2] A. Loutridis, K. Yang, M. John and M. J. Ammann, "Compact Printed Spiral FM Antenna," *Progress in Electromagnetics Research Symposium, (PIERS)*, Prague, Czech Republic, July 2015.

[CP3] A. Loutridis, M. John and M. J. Ammann, "Printed Folded Meander Line Dual-Band Monopole for TV White Space and GSM," *European Conference of Antennas and Propagation (EuCAP)*, Hague, Netherlands, Feb. 2014, pp. 2848-2852.

[CP4] A. Loutridis, M. John, M. J. Ammann, G. Ruvio, "A Wideband Printed Inverted-F Antenna for M2M Applications in the Lower UHF Band," *Loughborough Antennas & Propagation Conference (LAPC)*, Loughborough, UK, Nov. 2013, pp. 242-245.

[CP5] A. Loutridis, M. John, G. Ruvio, M. J. Ammann, "A 2.45/5.8 GHz Folded Monopole Antenna for WLAN Applications," *Loughborough Antennas & Propagation Conference (LAPC)*, Loughborough, UK, Nov. 2012.